CRYSTAL GROWTH OF ALPHA–RHOMBOHEDRAL BORON

by

WEI GAO

B.S., East China University of Science and Technology, 2004

A THESIS

submitted in partial fulfillment of the requirements for the degree

MASTER OF SCIENCE

Department of Chemical Engineering
College of Engineering

KANSAS STATE UNIVERSITY
Manhattan, Kansas

2010

Approved by:

Major Professor
Dr. James H. Edgar

Copyright

WEI GAO

2010

Abstract

Pure boron exists in two main polymorphs, the common β-rhombohedral boron and the relatively rare α-rhombohedral boron. α-rhombohedral boron (α-B) possesses several extraordinary properties: self-healing from radiation damage and a high hole mobility. In addition, the ^{10}B isotope has a large thermal neutron capture cross section. Such properties make it an excellent candidate for novel electronic device, such as direct energy conversion devices (alphacells and betacells) and neutron detectors. However, research on the properties and applications of α-B has been limited due to the difficulty to produce high quality α-B crystals of significant size. The preparation of α-rhombohedral boron is challenging for several reasons: first, α-rhombohedral boron has a low thermodynamic stability; it is only stable below 1100°C, at higher temperature β-rhombohedral boron is the stable polymorph. In addition, at elevated temperatures, boron is highly reactive, which make it is difficult to produce pure boron crystals.

The primary goal of this research was to produce high quality α-B crystals of significant size. The main focus of this study was to explore the feasibility of producing α-B from a copper flux. Copper is a promising solvent for α-B crystal growth: the eutectic temperature of copper-boron is low, 996 °C, and the phase diagram of copper-boron is relatively simple, and there are not many intermediate boride-copper compounds. In addition, copper is easily removed from crystals by etching with concentrated nitric acid. Last but not least, copper is less expensive than other metal solvents such as platinum. Boron crystal growth from a platinum solvent and vapor-liquid-solid growth by chemical vapor deposition were also performed for comparison.

A series of crystals were grown over a range of initial boron concentrations (9.9 to 27.7 mole %) and cooling rates. Small irregular-shaped black crystals (>100μm) and well-faceted red crystals in various shapes, as large as 500 microns were produced. The crystals were characterized by optical microscopy, scanning electron microscopy, energy dispersive spectroscopy, x-ray diffraction analysis, and Raman spectroscopy. The correlation between experiment results and experimental parameters (source materials, the purity of growth atmosphere, and crucible materials, etc.) are reported. Suggestions about further investigation for α-B crystal growth are proposed.

Table of Contents

List of Figures

List of Tables

Acknowledgements

Dedication

I dedicate this paper to my parents for all their loving support.

献给我亲爱的父亲母亲。

CHAPTER 1 - Introduction

Boron is an old chemical acquaintance; it has long been known for its household and industrial use in the forms of borax and boric acid. Recently, with the development of nuclear and semiconductor technology, boron and boron-rich compounds have attracted increasing attention because of their exceptional properties, such as high melting temperatures, extreme hardness and low density, unique transport and mechanical properties, etc.[1] These extraordinary properties make boron-rich solids excellent candidates for novel semiconductor devices such as neutron detectors and beta cells.

Despite the prevalence of boron in many compounds, the properties of boron-rich compounds have rarely been studied due to the technological difficulties of producing high purity crystals of various polymorphs, the complexities of obtaining perfect single crystals of sizes required for scientific investigations, the insufficient insight into the crystalline structure and lattice defects of the various polymorphs, and the difficulties in unraveling the characteristic nature of interatomic bonds. [2]

α-rhombohedral boron (α-B), the objective of our research, is the simplest crystal modification in the family of the icosahedral boron-rich solids. Its unit cell has only one B_{12} icosahedron, the basic building block of all crystals rich in boron. Many other boron- rich solids are derived from α-B structure by adding two or three atom chains along the diagonal of the unit cell (e.g. icosahedral boron carbide, boron arsenide, and boron phosphide).

In previous studies, α-rhombohedral boron was mostly prepared by chemical vapor deposition, and solution growth using platinum as a solvent. However, the success of the earlier studies was limited; the purity and size of the crystals were unsatisfactory for the investigation of the electrical properties of α-B. The expense of these methods was high (only platinum was proved to be a successful solvent).

The primary goal of our research was to explore the possibilities of preparing high quality α-B from a copper flux. The experimental parameters and the crystal quality were correlated, the crystals produced were characterized by various techniques, including, optical microscopy, x-ray diffraction (XRD), scanning electron microscopy (SEM), energy dispersive spectroscopy (EDS) and Raman spectroscopy.

1.1 The Properties of Elemental Boron

Boron, a chemical element, symbol B, has an atomic weight of 10.811, and is in the group III of the periodic table. It has three valence electrons, but unlike other group III elements, it is nonmetallic in behavior. Boron is classified as a metalloid and is the only nonmetallic element which has fewer than four electrons in its outer shell. In the naturally occurring distribution, boron has two stable isotopes with atomic weights of 10 and 11. The ^{10}B isotope, which has a nature abundance of 18.8 % of the total boron, is an excellent absorber of thermal neutrons [3].

Table 1.1 is a summary of the atomic properties of boron. Three points should be emphasized. First, boron has high ionization energies (8.96eV, 23.98eV, and 37.75eV for first, second, and third ionization potentials). Second, boron has a small atomic radius, 0.87Å (the atomic radius of hydrogen is 0.53 Å). Third, the electronegativity of boron is high (2.0); carbon (2.5) and hydrogen (2.1) are all similar, resulting in extensive and unusual covalent chemistry [4]. These three features of the boron atom are the primary cause leading to the diverse and complex chemistry of boron/boron compounds; they can also explain the formation of the unique bonding and structures of icosahedral boron-rich solids.

Table 1.1 Atomic Properties of Boron [5] [6].

Oxidation states	4, 3, 2, 1(mildly acidic oxide)
Electronegativity	2.04 (Pauling scale)
Ionization energies	1st: 800.6 kJ·mol^{-1} 2nd: 2427.1 kJ·mol^{-1} 3rd: 3659.7 kJ·mol^{-1}
Atomic radius	90 pm
Covalent radius	84±3 pm
Ionic radius	0.23 Å (the third smallest of all elements)

1.1.1 Physical Properties of Elemental Boron

The literature shows considerable discrepancies in the physical properties of boron; this is due to differences between the samples used, in particular, differences in the impurities present and their concentrations. For example, the densities of crystalline boron was reported as 2.31g/cm^3 in reference [3], but was 2.50g/cm^3 in reference [1]. Table 1.2 is the summary of the physical properties of boron.

1.1.2 Chemical Properties of Elemental Boron

The chemical properties of boron are also greatly influenced by its crystallinity. Crystalline boron is reported to be quite stable to heat and oxidation even at relatively high temperatures (>500°C). It is slowly attacked and oxidized by hot concentrated nitric acid, and by mixtures of sodium dichromate and sulfuric acid. Hydrogen peroxide and ammonium persulfate also slowly oxidize crystalline boron. In contrast, these reagents react violently with amorphous boron [3].

Generally speaking, boron is barely reactive at room temperature; at high temperature, it reacts with almost all the element of the periodic table (see Table 1.3). Due to its strong reducing power, it also reacts with numerous compounds, and in the case of oxygenated or halogenated compounds, sometimes in a violent ways [7].

Because of its high reactivity at high temperature, the preparation of pure boron is extremely difficult: it attacks refractory compounds containing oxides, graphite, and refractory metals. Even under high vacuum or under a controlled atmosphere, it combines with traces of oxygen or nitrogen or with carbonaceous residues from the oils of the vacuum pumps. Due to its extreme hardness, pulverization of boron introduces impurities from the crushers and causes a superficial oxidation of the grains [7]. Thus the experimental study of the chemistry of boron is difficult; the findings from many studies are conflicting. For example, some scientists [3] claim that boron can be oxidized by nitric acid at room temperature, however, according to my own experience, it does not. In conclusion, numerous systematic and elaborate studies are needed to further refine the accuracy and correctness of the data in the field of boron chemistry.

Table 1.2 Physical Properties of Boron at 25°C except as noted) [3].

Property	Value	Reference
Density (g/cm^3)		
Crystalline	2.31 ,2.45 ,2.50	[3], [4],[1]
Amorphous	2.30 ,2.35	[3], [4]
Mohs hardness		
Crystalline	9.3	[3]
Melting Point (°C)		
Amorphous	2100	[3]
Crystalline	2180-2300	[4]
Boiling Point (°C)	2500	[3]
Resistivity (ohm-cm)		
Crystalline/Amorphous	1.7×10^6	[3]
Coefficient of thermal expansion (1/°C)		
Crystalline/Amorphous	8.3×10^{-6}	[3]
Heat of combustion (kcal/mole)		
Crystalline/Amorphous	302.0±3.4	[3]
Entropy(cal/(mole)(deg))		
Crystalline	1.403	[3]
Amorphous	1.564	[3]
Heat capacity (cal/(mole)(deg))		
Crystalline	2.65	[3]
Amorphous	2.86	[3]

Table 1.3 Chemical Properties of Elemental Boron [7].

Group Number	Elements	Reaction Temperature Range	Product	Notes
IVth B	Carbon	>1000°C	$B_{1\sim24}C$	Many reported forms of boron carbide later proved to be only mixtures or solid solutions. Only $B_{12}C_2$ and B_4C were well determined, whose structure are derived from α-rhombohedral boron.
	Silicon	>1400°C	SiB_3, SiB_6, SiB_{14}	
VIth B	Oxygen	Room temperature	B_2O_3	Boron combines with oxygen, sulfur and selenium but does not appear to react with tellurium.
	Sulfur	High temperature	B_2S_3, B_2S_5, B_2S_2	
	Selenium	High temperature	B_2Se_3, B_2Se_2, BSe	
VIIth B	Fluorine	Room temperature	BF_3	Boron trifluoride is very stable while the boron triiodide can be decomposed at lower temperature. Boron trifluoride and boron trichloride are gaseous at room temperature. Boron tribromide is liquid and boron triiodide is solid.
	Chlorine	400°C ~900°C	BCl_3	
	Bromine	400°C ~900°C	BBr_3	
	Iodine	400°C ~900°C	BI_3	
Metals	Boron combines with almost all metals. Borides are mostly obtained by directly mixing boron and metal at high temperatures. The existence of more than 200 metal borides has been reported, though half of them either do not exist or represent mixtures and solid solutions. The uncertainty as to the existence of a great number of borides and their composition is not difficult to understand considering the difficulties in synthesis, analysis, purification, single crystal growth, and in determining phase diagrams at high temperatures.			

1.2 Crystalline structure of Boron

Several different crystal structures of pure boron that have been proposed in the literature, but most of them proved to be borides or to be stabilized by a small concentration of impurities. Only α-rhombohedral boron and β-rhombohedral boron are established as pure boron crystalline forms. (For example, the existence of "tetragonal boron" as a modification for pure elemental boron or as a boron-rich nitride or carbide has been a subject of controversy. [2][8]

To explain the unusual structure of icosahedral boron, it is helpful to describe the exceptional chemical bonds formed with boron atoms. For most of the compounds formed by other elements, two electrons are shared between two atoms; however, boron can form chemical bonds in which a pair of electrons is equally shared among three atoms, as shown in Figure 1.1. [9]

Based on the three-atom bonding, boron can form icosahedra, twelve atom clusters with boron atoms positioned at each vertex. The highest electron density occurs at the center of an equilateral triangle which serves as one facet of the icosahedra (as shown in Figure 1.2 [10]). This icosahedral unit is the basic building block for icosahedral boron and its compounds.

a. Two center bond   **b. Three center bond**
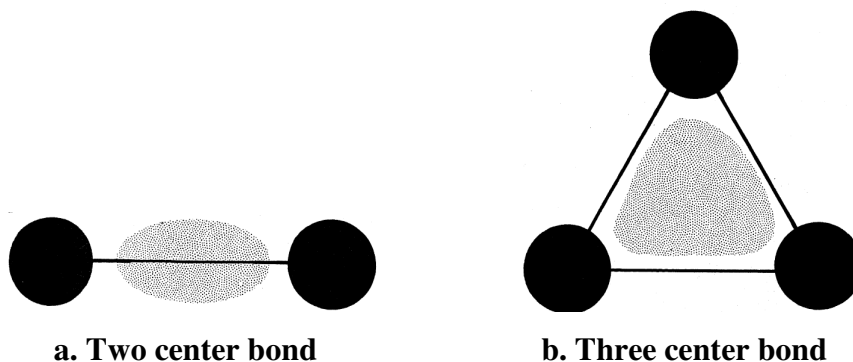
Figure 1.1 The colored regions roughly show the dominant parts of the electronic charge distributions of a (a) two center bond and a (b) three-center bond. Black filled circles represent boron atoms [9].

This three-atom bonding structure is unique to icosahedral boron-rich solids. The atoms lighter than boron, such as beryllium, do not have enough electrons available for forming intericosahedral covalent bonds [9]; atoms heavier than boron are also larger in size, and their bigger interatomic separations prevents the formation of stable three-center bonds. Therefore,

boron-rich solids possess some distinctive, perhaps unique physical and electronic properties which are the consequence of this atypical structure. [9]
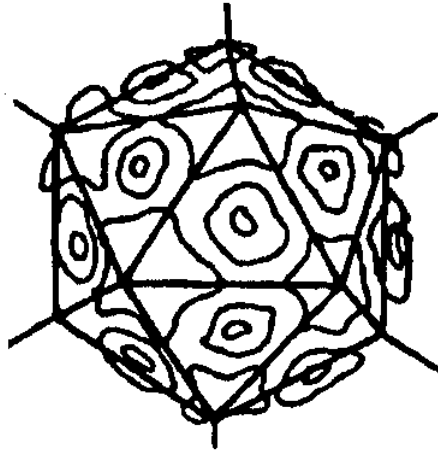
Figure 1.2 An icosahedron of boron is illustrated. Boron atoms sit at the vertex of the icosahedron, and the contours depict the accumulation of bonding charge on the icosahedron's triangular faces [10].

α-rhombohedral boron is the simplest boron polymorph, there are only 12 atoms in each unit cell. Boron atoms are located at each vertex of the icosahedra, and icosahedra are bound to their neighbors by six-two center bonds, forming a rhombohedral lattice, as illustrated in Figure 1.3 [11]. Compared to α-B, the structure of β-rhombohedral boron is much more complex (Figure 1-4); there are 105 atoms in each unit cell. The complex structure of β-B leads to its high concentration of structural disorder, e.g. high concentration of boron interstitials and vacancies. These crystal imperfections greatly diminish the carrier mobility of β-B, which is about $0.01 cm^2/V \cdot s$ [12]. In contrast, the mobility of α-rhombohedral boron is four orders of magnitudes higher ($100 cm^2/V \cdot S$) [12]. Actually, the electrical properties of β-B are similar to amorphous semiconductors even though it is a crystal [13]. Therefore, α-rhombohedral boron is more useful than β-rhombohedral boron as a semiconductor material for electronic device applications.
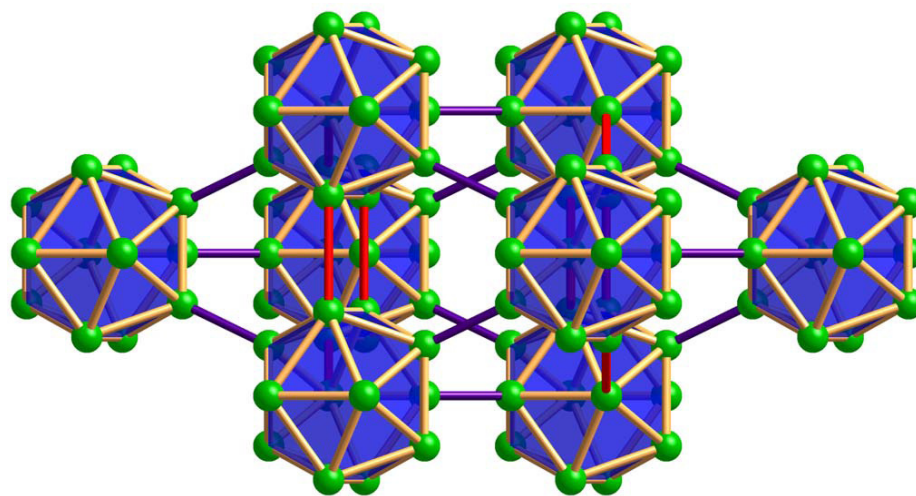
Figure 1.3 Structure of α-rhombohedral boron viewed along the rhombohedral (11) axis. Bond color scheme: 1.67 Å in purple; 1.75-1.81 Å in orange; 2.01 Å in red [11].
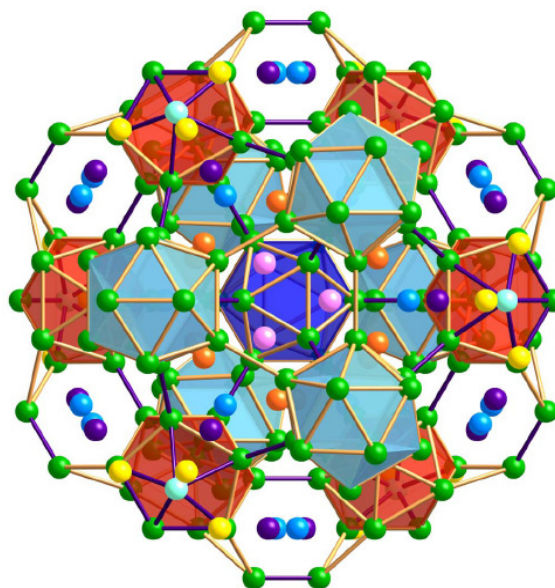
Figure 1.4 Structure of β-rhombohedral boron viewed along the rhombohedral (111) axis. In addition to boron icosahedra, this structure also contains isolated and paired boron atoms. Bond color scheme: 1.63-1.73 Å in purple; 1.73-1.92 Å in orange; partially occupied sites are shown in color: B13 (74.5% average occupancy) cyan; B16 (27.2%) pink; B17 (8.5%) yellow; B18 (6.6%) indigo; B19 (6.8%) blue; B20 (3.7%) orange. [11]

1.3 The Properties of Icosahedral Boron-Rich Solids

Icosahedral boron-rich solids have the same basic structure as α-rhombohedral boron (as illustrate in Figure 1.5 and 1.6). Their electrical properties range from a hopping-type semiconductor (boron carbide) to wide bandgap room temperature insulators (the boron pnictides B_6P and B_6As) [14].

These solids are stable refractory materials with melting temperatures up to 2400^oC-a thousand degrees greater than silicon's. [9]. As such, they are of interest for a variety of high temperature semiconductor applications. [14].

In this section, the unique self-healing ability of icosahedral boron-rich solids is explained. The properties of pure crystalline boron are summarized. Finally, two practical applications that exploit these exceptional properties are introduced.
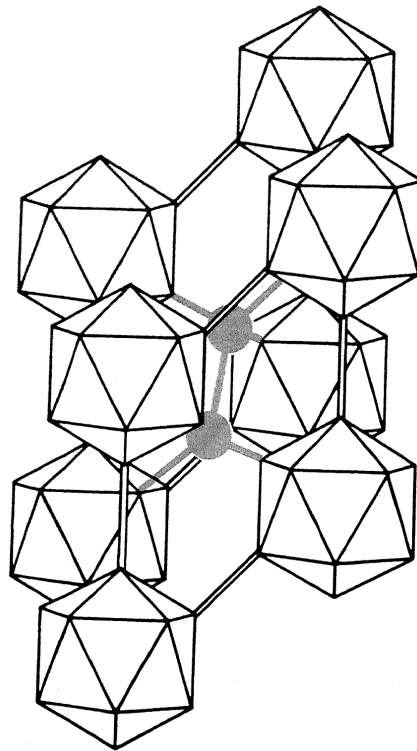
Figure 1.5 The structure of $B_{12}P_2$ and $B_{12}As_2$ is very similar to α-B, but has two atoms chains of phosphorus atoms or carbon atoms (grey) lying within the rhombus connected to six B12 icosahedra by two atom center bonds [9].
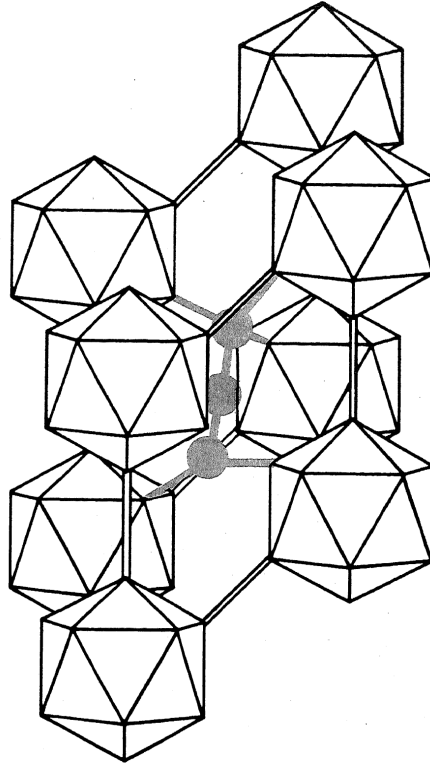
Figure 1.6 The structure of boron carbide: carbon atoms (grey) can occupy one end site(C-B-B), both end sites(C-B-C), or all of the sites(C-C-C) in the intericosahedral chain, as well as one of the sites within each icosahedron [9].

1.3.1 The self-healing ability of icosahedral boron- rich solids

Icosahedral boron-rich solids were observed to possess a self-healing ability from radiation damage. Several boron-rich solids (boron carbides, β-B [15-16], $B_{12}P_2$ and $B_{12}As_2$ [17]) were investigated by high resolution transmission electron microcopy during and after heavy bombardments (e.g. by 400 keV electrons). Damage such as clustering of defects and amorphization, which would be expected in most materials was not observed.

The absence of radiation damage in icosahedral boron-rich solids is ascribed to their exceptional structure. When an energetic particle e.g. electron, ion, or neutron, displaces a boron atom, a negatively charged degenerate icosahedra (with only eleven boron atoms) and a positively charged isolated boron ion is formed. In addition, the size of a boron cation is very small (which would aid its diffusion and thereby facilitate recombination) [10]. The attractive force between the icosahedra and the boron ion is so strong as to draw the boron ion back to

10

complete the icosahedra. This process is not thermally activated, as it can occur even at very low temperature (~12K).[18]

Before   After
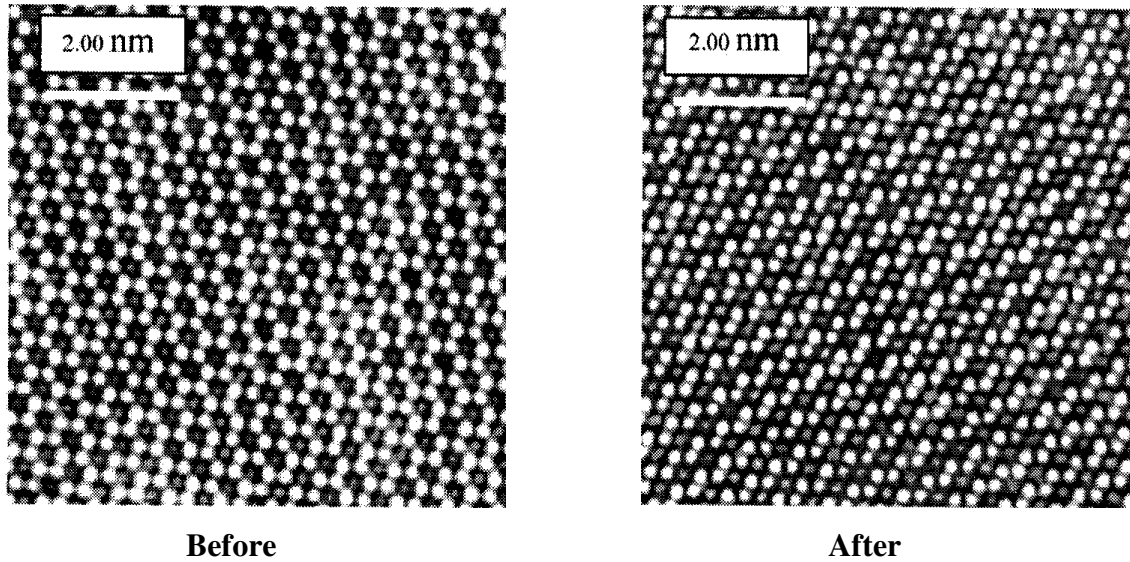
Figure 1.7 High-resolution transmission electron micrograph shows no damage to $B_{12}P_2$ after an intense bombardment (10^{18} electrons/cm^{2}s) by 400 keV electrons to a net dose of about 10^{23}electrons/cm^2. The bombardment is more intense than that from undiluted ^{90}Sr (10^{12}electrons/cm^{2}s). [10]

1.3.2 Miscellaneous properties of Rhombohedral Boron

Table 1.4 Structural parameters and electrical properties of α- and β-B as measured in experiments. Lattice parameters a_0 and α, number of atoms N_{atom}, atom density $ρ$, coordination number N_c, Debye temperature $θ_D$, and bulk modulus B_0. The bond length is presented as the minimum d_{min} and average d_{avg} for all the bonds. [19]

	α-boron	β-boron	Reference
a_0(Å)	5.057	10.145	[19]
A (°)	58.06	65.17	[19]
Space group	R3m	R3m	[12]
N_{atom}	12	105	[19]
$ρ(atoms/Å^3)$	0.1373	0.1278	[19]
N_c	5.50	6.40	[19]
d_{min}(Å)	1.71	1.62	[19]
d_{avg}(Å)	1.77	1.80	[19]
$θ_D$(K)	1430	1200-1300	[19]
B_0(GPa)	213-224	185-210	[19]
Structural analogues	$B_{13}P_2$, $B_{13}As_2$. boron carbide	$Ga_{1.5}B_{103}$, ScB_{28}, ZrB_{51},CrB_{41},SiB_{14}	[12]
Bandgap (eV)	2	1.5-1.6	[20][22][13]
Hall mobility(cm^2/V·S) at T=300K	~100	~10^{-2}	[12]
Resistivity(Ω·cm) at T=1000K	~10	~0.15	[21]

Table 1.5 Calculated electronic structures of α-rhombohedral boron [1]

	α-rhombohedral boron
Band gap (eV)	
Indirect:	1.70(Z→Γ)
Direct:	2.17(Γ)
	4.12(X)
	2.79(Z)
	3.53(A)
	4.12(D)
Bandwidths(eV)	
Upper VB	10.00
Middle VB	2.57
Lower VB	0.82
Effective mass (electron)	
CB edge	0.21(ΓX)
	1.10(ΓZ)
	0.56(ΓD)
	0.58(ΓA)
VB edge	-0.21(ZA)
	-1.63(Z Γ)
	-0.36(ΓD)
	-0.30(ΓA)

1.3.3 Application of icosahedral boron-rich solids

1.3.3.1 Neutron Detector

Neutron detectors are used to monitor neutron-emitting radioactive sources in and at reactors and accelerators. It can be also used for surveillance and detection of radioactive materials and as research tools [23].

The present generations of neutron detectors employing scintillation counters or ionization chambers to measure electronic ionization have low efficiencies, consume significant power, and are bulky. By contrast, a solid state boron-rich-solids-based device which exploits the exceptional neutron absorbing capacity of ^{10}B, the high melting temperature and the radiation tolerance of icosahedral boron solids could be more sensitive, more compact, long-lived, mobile, and operate with minimum power.

Figure 1.8 illustrates the concept design of a boron-rich-solids based neutron detector. Boron 10 is an excellent neutron absorber; it has a large thermal neutron capture cross section of ~3800 barns, in contrast to most elements which have values is typically less than 1 barn. When the boron-rich solids are bombarded with thermal (~25 meV) neutrons two reactions will happen [24]:

$(1)\ {}^{10}B + n \rightarrow {}^{7}Li\ (0.84\ MeV) + {}^{4}He(1.47\ MeV) + \gamma(0.48\ MeV)$ (94%)

$(2)\ {}^{10}B + n \rightarrow {}^{7}Li\ (1.02\ MeV) + {}^{4}He(1.78\ MeV)$ (6%)
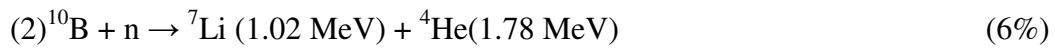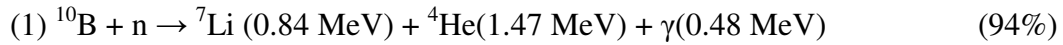
In both reactions high energy Li and He (alpha particles) ions are produced. If this process occurs in a semiconductor, for each neutron captured, a huge number (~1.5×10^{6}) of electron-hole pairs are created as the energetic ions pass through the material. This charge is large enough to be detected directly without further amplification. Thus a thermal neutron detector could be based on a boron-rich semiconductor Shottky, *pn*, or *pin* diodes.
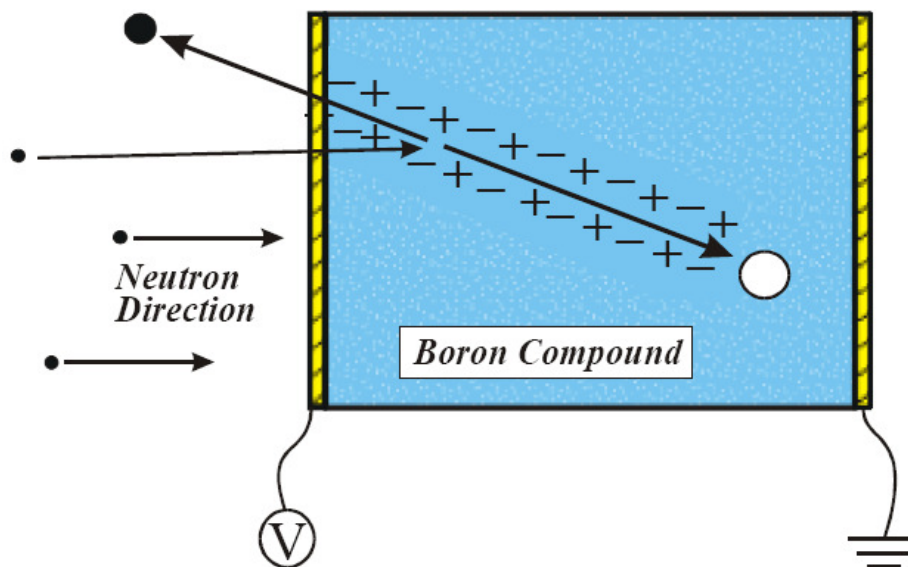
Figure 1.8 A Neutron Detector: A high resistivity boron-based semiconductor slab is fastened with metallic electrodes on opposing surfaces. A neutron interacts with ^{10}B, it produces Li and He ions that then create a cloud of electron-hole pairs. A voltage applied across the device drifts the free charges to their respective electrodes, which in turn induces a measurable current (or voltage pulse) in an externally attached circuit [25].

1.3.3.2 Beta Cell

The nuclear energy of some radioisotopes is primarily released in the form of beta particles which are energetic electrons that are emitted from a nucleus as a product of its decay. A beta cell is a device, which utilizes beta particles from radioisotopes by interacting with a semiconductor material, to produce electrical power.

The working mechanism of beta cell is illustrated in Figure 1.9; electrical power is created by combining a radioisotope (e.g. ^{90}Sr, ^{147}Pm, and ^{170}Tm) emitting beta particles to a semiconductor junction. The electron-hole pairs generated as the beta particles pass through the semiconductor are separated by the local electric field of a semiconductor junction, and the generated current is collected in the external circuit.

Compared with those of even excellent chemical sources (e.g. 10^4W-hr/kg of gasoline), the energy capacities of the radioactive source is huge (10^7 to 10^8 W-hr/kg of fuel), thus beta cells could be much smaller power suppliers than conventional chemical power sources such as batteries. Furthermore, because of the long half-life of some radioisotopes (e.g. the half-life of

^{90}Sr is 28 years), beta cells could supply power for decades. Beta cells can find numerous applications wherever high-energy-capacity, reliable power sources are needed, for example, remote sensors, cardiac pacemakers, laptop, spacecraft, etc.

Conventional semiconductors such as Si, Ge,GeAs, or CdTe have limited utility as beta cells because of their low radiation tolerance. The defects created by the incident high-energy beta particles within the semiconductors could scatter and trap the generated charge carriers. For example, in Rappaport *et al*'s study [26], the silicon beta cells fueled by ^{90}Sr were degraded over a few days as a result of accumulating damage. Thus, beta cells made of standard semiconductors can be used for only a short times or with very weak beta sources, such as ^{3}H or ^{147}Pm.

The degradation problem can potentially be alleviated by replacing conventional semiconductors with icosahedral boron-rich solids. Because of the self-healing ability of boron-rich semiconductors, high-energy beta particles emitting source such as ^{90}Sr or ^{170}Tm could be used. Because of the self-healing, the lifetimes of icosahedral boron based beta cells are limited by the rate of decay of the radioisotope energy source rather than by radiation damage to the semiconductor. Particularly, the relatively high charge carrier mobility of α-rhombohedral boron in the family of icosahedral boron-rich solids makes it more promising as a candidate for fabricating beta cells.
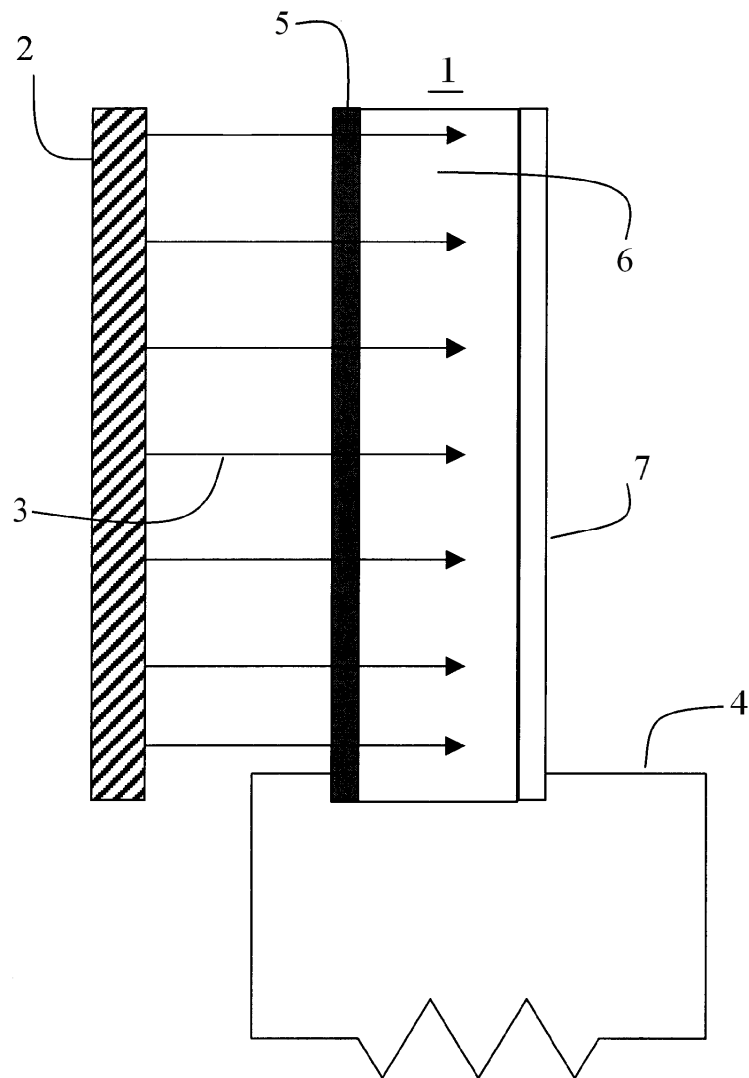
Figure 1.9 A Beta Cell: 1- Schottky-barrier junction device; 2-beta emitting radioisotope layer; 3-beta radiation; 4-means (for transmitting the produced electrical energy to a load); 5-metal contact (e.g. Au); 6-icosahedral boride semiconductor (e.g.-B); 7-metal contact [27].

CHAPTER 2 - Methods of Preparing α-rhombohedral Boron

The preparation of α-rhombohedral boron is challenging for several reasons: first, α-rhombohedral boron polymorph has low thermal stability; it is stable only below 1100°C; at higher temperatures β-rhombohedral boron is the stable polymorph. In addition, as mentioned in the Chapter One, at elevated temperatures, α-B is highly reactive: it reacts with trace concentrations of water, oxygen, nitrogen, and carbon, etc. to form compounds of high stability and inertness. It can also react with the refractories, such as graphite which are common crucible materials. Furthermore, the icosahedral framework of boron changes with small concentrations of impurities. For example, certain polymorphs of boron tended to be stabilized by carbon forming the tetragonal boron polymorph rather than rhombohedral boron. [2] [28]

The synthesis of α-rhombohedral boron was first reported in 1958 by McCarty *et al*. [29]. Since then there have been mainly two methods for its preparation of α-B: (1) the deposition of boron out of the vapor phase (chemical vapor deposition method); and (2) the precipitation of α-boron from metallic solutions forming low melting eutectics (solution growth method). The growth of α-B from the vapor phase can be achieved by reducing boron halogen (BX_3) or by decomposing diborane (B_2H_6). To grow α-B from a metal flux, only platinum has proved to be a successful solvent as reported with detailed experimental conditions and confirming analysis. In addition to these two main methods, α-B was prepared by the Vapor-Liquid-Solution (VLS) method which is a combination of chemical vapor deposition and solution growth method.

In spite of many attempts to prepare α-B, growing high quality crystals of large size and high purity for the investigation of its semiconductor properties has not been reported. This chapter reviews the literature on methods for preparing α-rhombohedral boron. In particular, it will explain why copper was chosen as the solvent in the past study.

2.1 α-rhombohedral boron preparations from the vapor phase

A typical Chemical Vapor Deposition (CVD) system can be used for preparing α-B from the vapor phase. In an evacuated or controlled atmosphere chamber, boron production takes place on the substrate which is resistively or inductively heated. Tantalum, silica, boron nitride and amorphous boron were reported as successful substrate choices [38].

Boron iodide, BI_3, decomposes to boron and iodine at 800°C. It is the least stable compound among the boron halides, thus, it is most widely used as the boron source in the method of direct thermal decomposition. For the reduction of boron halides with hydrogen, BBr_3 was most frequently applied, the reaction can occur as low as 600 °C [30]. BCl_3 and BF_3 were also employed as boron sources, but these reactants require higher temperatures. BI_3 was barely used in the hydrogen reduction method because of the instability of hydrogen iodide (HI).

2.1.1 Pyrolysis of Boron Triiodide

Both McCaty and Carpenter [30] and Amerger and Dietze [31] purified the BI_3 before using it as the boron source for producing α-B. They purified it by distillation in a glass column with the efficiency of 30 theoretical plates and by the zone melting method putting the samples in an evacuated glass tube, passed through the system of alternate heating and cooling units.

$$\text{Equation 2.1: } BI_3 \xleftarrow{\Delta} B + \frac{3}{2}I_2$$
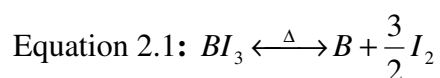
In McCarty and Carpenter's study in 1960 [30], the decomposition of BI_3 (eqation.2.1) occurred on a heated tantalum wire at an argon partial pressure of 0.1-1mm of Hg. Table 2.1 presents the experimental parameters of this study. At 1000°C, a 1.8mm thick deposit of boron was obtained on the surface of tantalum wire (0.0075mm diameter) in 4.5h. On breaking the wire, a cluster of red crystals surrounding the tantalum wire were clearly visible to the unaided eyes. In this sample, a wedge-shaped band of orange-colored boron in a fractured portion of the rod was formed. This band started as a narrow band at the tantalum core and expanded as it grew out to the surface, which, in the author's opinion, testified to the influence of tantalum upon the nature of the deposit: tantalum might act as a "getter" for impurities and thus promote the growth of α rhombohedral boron locally. [30]

X-ray powder diffraction photographs of the samples at 800°C, 900°C and 1000°C revealed that the samples had three major components: α-B, β-B and tantalum borides. Unexpectedly, the amount of tantalum contamination decreased with an increase in temperature: X-ray emission analysis of the sample at 800°C indicated the presence of approximately 78% tantalum but the 900°C sample had only a very small amount of tantalum boride in it (0.03%). This phenomenon contradicts the diffusion law (the diffusion rate increases with temperature) and the experience of Stern, *et al*. [32] and Laubengayer *et al*. [33]. McCarty and Carpenter [30] explained this phenomenon as the tantalum iodide was formed at lower temperature; at higher

19

temperature this compound would be volatile. Obviously, it is difficult to reconcile the various observations on the basis of diffusion law. The chemistry of the various phases that can form at the surface of tantalum may depend strongly on the particular halide used and the presence or absence of hydrogen [30].

Other scientists also conducted similar experiments on the growth of α-rhombohedral boron. Amberger and Dietze [34] found that from 850°C -1100°C, the temperature showed little influence on the formation of α-B, but the impurities in the system greatly influenced the growth of α-B (e.g. the impurity in the boron source, the contamination from the substrate). Among the boron crystals (α-B, β-B, tetragonal boron) produced in their experiments, α-B always had a high level of purity. They concluded that the α polymorphs of boron offers the least crystallographic vacancies to accommodate foreign atoms. Therefore, the more foreign atoms present, the smaller the probability that α-rhombohedral boron will form [34]. This conclusion by E.Amberger and W. Dietze [34] is attractive, since we observed a similar phenomenon in our own experiments, as disclosed in detail in a later chapter.

Table 2.1 Thermal decomposition of BI$_3$ on the tantalum rod (91.5cm long) [30].

Decomposition Temperature(°C)	BI$_3$ Temperature (°C)	Decomposition time (hr)	Deposit weight (g)	Yield (%)
800	0-~25	73.5	10.3	Not determined
900	20	23	11	43
1000	25	64.3	56.6	78

2.1.2 Pyrolysis of Boron Tribromide

As already mentioned above, the reduction of boron tribromide (Eq.2.2) can take place at a temperature as low as 600°C. R.Naslain et al [35]. conducted this reaction in an electrically heated quartz tube. The partial vapor pressure of BBr$_3$ was sustained at around 160 mmHg, and the boron was deposited directly on the wall of the quartz tube. Due to the low reaction temperature (700°C to 850°C), the yield of boron was low. Thus the unconverted BBr$_3$, which can be separated by fractional distillation, was recycled, and returned to the evaporator (a condenser used to collect the unconsumed BBr$_3$).

$$\text{Equation 2.2: } BBr_3 + \frac{3}{2}H_2 \xrightarrow{\Delta} B + 3HBr$$
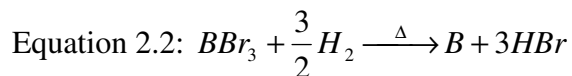
Over the temperature range of 600°C to 700°C, the crystal fraction was low. Above than 850°C, the rate of boron deposition became significant, but the quartz tube (silica) started to react with the boron. Therefore, temperatures from 700°C to 850°C were chosen as a compromise, as they permitted an appreciable yield of boron deposition while avoiding noticeable contamination by the reactor tube material (silica).

During their experiment, the only factor which seemed to influence the appearance of β-boron was the residence time τ, the time spent by the boron deposits in the reduction zone. There was a critical time τ_c. When $\tau < \tau_c$, the boron deposits were in the form of granules which were α-B only, completely free of β-boron, and no detectable reaction between boron and silica took place. When $\tau > \tau_c$, the product was a compact powder containing both the α and β modifications, and a superficial corrosion of the wall of the chamber was detected after many deposition experiments. The critical time τ_c depended upon the geometry of the reaction chamber and the temperature-the higher the temperature, the lower τ_c was [35]. (Table 2.2). The influence of the experimental parameters upon the boron structure is summarized in Table 2.3.

The boron crystals were small, essentially fine powder. Compositional analysis by titration gave 99%-99.5% boron. X-ray fluorescence analysis detected only bromine as a definite impurity. Heating in high vacuum (10^{-6} torr) didn't remove the trace amounts of bromine, suggesting that bromine was chemically bonded to boron. Based on their observation that β-boron was produced over the entire temperature range, R Naslain *et al*. [35] proposed that β-rhombohedral boron is the only thermodynamically stable variety, for ordinary pressure at all temperatures up to the melting point of boron.

Talley et al. [36] and Bean *et al*. [37] also conducted experiments with boron tribromide reduction with hydrogen. Although their goals were not to prepare α-B, both groups observed its formation. Their experimental parameters are presented in table 2.4. [38] Amberger *et al*. [34] found the formation of α-B in the hydrogen reduction of BCl_3. From 950°C to1050°C, α-rhombohedral boron was deposited on the tantalum filament mostly in the form of fine crystals, with β-rhombohedral boron as a byproduct, when the substrate temperature exceeded 1050°C; β-B predominated in the deposited material.

Table 2.2 Experimental value of τ_c for a reactor of 30mm diameter and for a hot zone of 60mm length. [35]

Reduction temperature (°C)	P_{BBr3} (mm Hg)	Deposition rate(mg/h)	τ_c (h)
850	150	250	10
750	160	150	13
700	160	120	15
675	160	80	25

2.1.3 Pyrolysis of Diborane

Robb and Landauer[39] studied the low pressure vapor deposition of boron by the thermal decomposition of B_2H_6. Their study included investigating methods for purifying diborane. The purest boron crystals were produced from carefully distilled diborane. In this case, the boron purities of 99.8 to 99.99 percent were consistently obtained. They also attempted to purify diborane by passing it through a 4A. molecular sieve. However, methane (CH_4) and carbon monoxide (CO) were not completely removed by this method, and approximately 0.1% carbon was contained in the boron made from this gas.

Most of the deposition experiments were conducted at temperatures below 1000°C, and consistently produced α-rhombohedral boron. Although the total pressure in the decomposition chamber ranged as high as 10mm Hg, the pressure close by the substrate was barely above 100μmHg. Boron rods 8 inches long and up to 3/8 to 1/2 inch in diameter were grown, and the crystalline deposit containing α-B was obtained at the deposition rate of 0.5g/h·cm.

Table 2.3 Experimental parameters used for BBr$_3$ low-temperature reduction in hydrogen [35].

Nature of the deposit	Reduction temperature (°C)	P_{BBr3} (mm Hg)	Length of the hot zone (cm)	τ_c (h)	τ (h)	Rate (mg/h)
α	750	160	6	13	12	150
β	800-850	170	12	10	40	250

Table 2.4 Experimental parameters in Talley et al and Bean et al's investigation [38]

	Talley et al.	Bean and Medcalf
Substrate material	W+1% ThO$_2$	B-boron
Substrate size	d=0.025mm l=5cm	D=1.6mm
Substrate temperature	1200°C	1000°C
Hydrogen stream volumetric flow rate	500ml/min	970ml/min
Vaporizer temperature(rate of evaporation of BBr$_3$)	25°C	60ml/min
BBr$_3$ concentration in hydrogen	8-10M%	20M%
Deposition rate of boron	0.01g/h	2-3g/h

2.2 α-rhombohedral Boron Preparation by Vapor Liquid Solid Method (VLS)

VLS is a modified chemical vapor deposition (CVD) method. For α-B preparation, the substrates were seeded with platinum or gold particles to promote the nucleation of boron from the vapor phase (which is usually boron halide).

In this mechanism, the role of the metal particle is to form a liquid alloy droplet of relatively low melting point. The liquid alloy (e.g. platinum-boron alloy) acts as a preferred site for absorbing the boron atoms from the vapor phase, or perhaps more likely, as a catalyst for the chemical process involved. [40] The boron dissolves into the liquid and crystallizes, with a very low concentration of platinum in the solid solution at the interface between solid boron and the liquid alloy. By a continuation of this process, the boron-metal alloy droplet becomes displaced from the substrate and rides atop the growing whisker [41], as shown in Figure 2.1
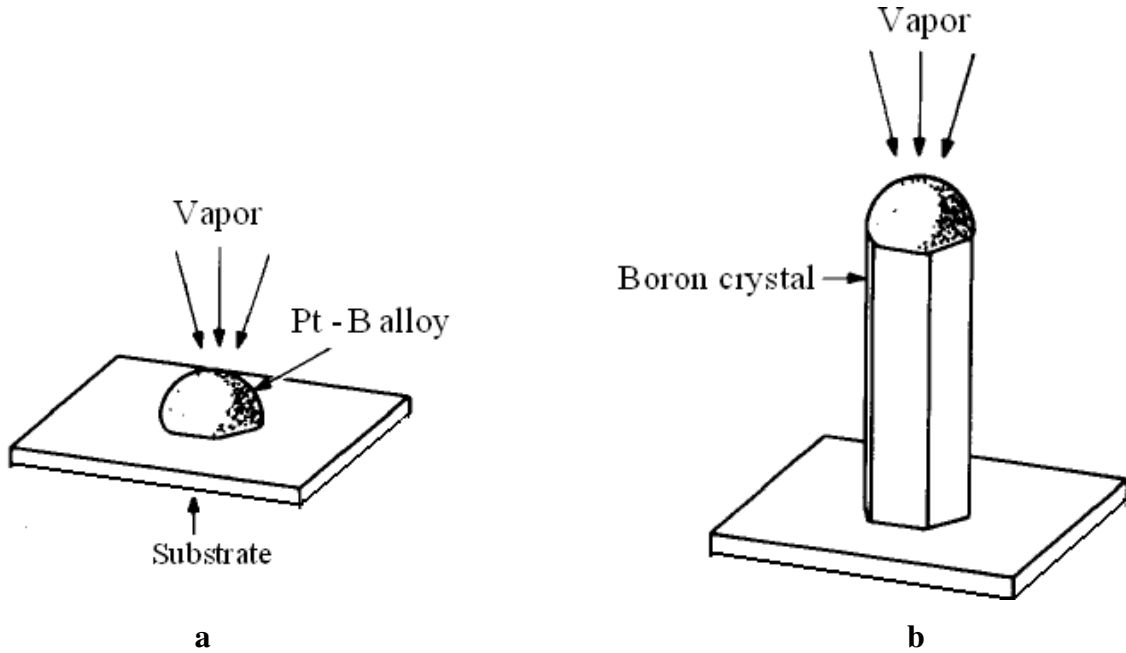
Figure 2.1 Growth of α-B by VLS. a. Initial condition with liquid platinum droplet on substrate. b. Growing crystal with liquid platinum droplet on the tip [40].

α-B whiskers were grown by Starik and Ellis [41] by the Vapor Liquid Solid method using platinum as liquid forming agent. The transport process was the reduction of BCl_3 with hydrogen at around 1000°C in a fused silica open tube; amorphous boron and fused silica were employed as substrates. The hydrogen flow rate was maintained at 1.5 liters/min. When the substrate reached the growth temperature, a small flow (1.4cc/min) of BCl_3 was introduced into the hydrogen. Both twisted and straight crystal whiskers were produced in the size range of about 2 mm long and 25μm in cross section. These crystals were red, translucent with spherical terminations; electron beam microprobe analysis confirmed that the termination consisted mainly of platinum. Five crystals were studied by polarizing microscope with a Weissenber goniometer, the results were recorded in table 2.4.

As illustrated in Table 2.5, the growth direction of the straight crystals was determined as $\langle \overline{4}401 \rangle$ (hexagonal indexing). For the kinked whisker, sample 2, if the growth direction of the base is assigned as $[\overline{4}401]$, the growth direction of the peak is $[\overline{4}041]$. These directions make an angle of about 70° with one another, as well as the c axis of α-B, and both lie in the plane $(0\overline{1}14)$. The reason for this unusual growth direction remains unknown.

24

Table 2.5 Experimental parameters in Talley et al and Bean et al's investigation [38]

Specimen number	Description	Extinction angle degrees	Growth direction(hexagonal indices)
1	Straight		$\langle \bar{4}401\rangle$
2	Kinked at an angle of 70°		$[\bar{4}401]$ main segment $[\bar{4}041]$ tip segment
3	Straight	71	$\langle \bar{4}401\rangle$
4	Kinked	72	$\langle \bar{4}401\rangle$ main segment
5	Straight with small branching crystal	71	$\langle \bar{4}401\rangle$ main segment

2.3 α-Rhombohedral Boron Growth from Metallic Solution

Although α-B crystals of decent purity (99%-99.5%) can be produced by the chemical vapor deposition method, the size (<1mm in cross section) of the crystals are not large enough for definitive electrical and optical measurements to establish its semiconductor and transport properties. Thus other ways to obtain α-rhombohedral boron crystals were sought.

The precipitation of solid material from a liquid solution is a classic method for crystal growth. In this method, first a single liquid phase is formed containing the solvent (molten metal) and the solute (boron). Then precipitation occurs because of the decreasing solubility of a solute in a solvent which is generally realized by slowly cooling the system. Crystals randomly nucleate, then grew by diffusion of the solute to the crystal interface.

There are several advantages to the solution growth methods. (1) It is a relatively low temperature process, which depends on the solubility of the material in a given solvent, not on the melting point of the material itself. Thus, the goal was to prevent the formation of β-B by using a solvent which can dissolve boron at temperature lower than 1100 ^{o}C. (2) The successful growth of crystals is not as dependent on variables such as minor temperature transients and disturbance as with other methods of growth (e.g. melt growth or sublimation-recondensation growth) which depend on direct solidification from the melt or vapor. (3) Compared to VLS and

CVD methods, solution growth method is simple to operate, thus it requires less operator attention during an experiment.

For a metal to be considered as a good solvent for solution growth of boron crystals, several requirements have to be met [42]:

(1) A measurable solubility (not less than 1%) of crystal components in the solvent and change in solubility with temperature;

(2) A low melting point and a low volatility at the highest working temperature;

(3) Lack of interaction between the dissolved substance and the solvent with formation of solid phases or formation of phases whose stability is lower than of the dissolved substance;

(4) No formation of a solid solution by the dissolved substance and the solvent;

(5) Low degree of interaction with the material of the crucible;

(6) Low viscosity(less than 10 cp).

(8) Low toxicity.

It is hard to find a solvent which can meet all the above requirements, thus, a compromise is always made with respect to the ideal solvent properties.

To date, only platinum has proven to be a feasible solvent for α-B crystal growth. Although other boron-metal combination (boron -silver, boron -copper, boron –gold, etc.) [43, 44] were also reported as successful system for α-B growth, usually the red color of the crystal was the only evidence to support the existence of α-B. The red color by itself is not sufficient to prove the formation of α-B crystals (this will be shown in a later chapter).

In this section, the α-B crystal growth from platinum solvent will be described. The results of the investigation on several other boron-metal systems will be presented. Finally, I will explain why we chose copper as the solvent in our study.

2.3.1 Solution growth of α-B from a platinum flux

F.Horn [45] was the first scientist who successfully prepared α-rhombohedral boron from platinum solution in 1959. In his study, he identified the eutectic temperature of boron-platinum as 825°±5°C, the eutectic composition was approximately 50 atom percent boron, and the platinum boride PtB or Pt_2B_2 previously reported in 1951[46] were not found in his experiments.

To grow α-B crystals, a 50-50 at % commercial platinum and zone-refined boron were first melted together at 1200°C to form an alloy. The first melt was allowed to freeze then the surface and sides of the alloy-bar was grounded away to remove the slags which were frequently precipitated from the initial melt. The alloy was transferred to a hot pressed boron nitride crucible having a conically bottom. After melting the alloy under vacuum, the crucible was slowly lowered through an induction coil at the rate of 0.04mm/min.When reaching the eutectic temperature, the alloy was abruptly cooled. A polished section through such a solidified melt indicates black boron crystals in the bottom tip. And translucent, red crystals were distributed around the bottom tip of the alloy. The red crystals were recovered by crushing the platinum-boron matrix [45] or by electrolytic etching away the platinum in concentrated hydrochloric acid [44].

The recovered crystals were small, the largest being tenths of millimeters. X-ray diffraction confirmed that the red crystals were α-rhombohedral boron crystals, and the x-ray diffraction pattern of the black materials which was crystallizing in the tip of the ingot showed some similarity to the pattern of the β-rhombohedral polymorph. Results suggested there may be a number of intermediate structures between the complex and simple rhombohedral forms [45].

The phase behavior of platinum and boron are in marked disagreement between different reports in the literature. Wald and Rosenberg [47] observed very different phase behavior than Horn. They found that the compounds Pt_3B and PtB_2 were formed at 825°C and 890°C by peritectic reactions, and Pt_3B_2 was congruently melting with a flat maximum at 940°C but decomposed eutectoidally into Pt_2B and boron at~600°C to 650°C.

Further investigations on Pt-B system were conducted by many other scientists [48]. The most complete platinum-boron phase diagram (figure 2.2) was later developed by Wald in 1970[43]. He pointed out that the pattern of the Pt-B phase diagram was greatly influenced by the foreign impurities, for instance, less than 0.1% of Si can prevent the formation of Pt_3B but result in the emergence of a metastable Pt_2B-Pt eutectic.
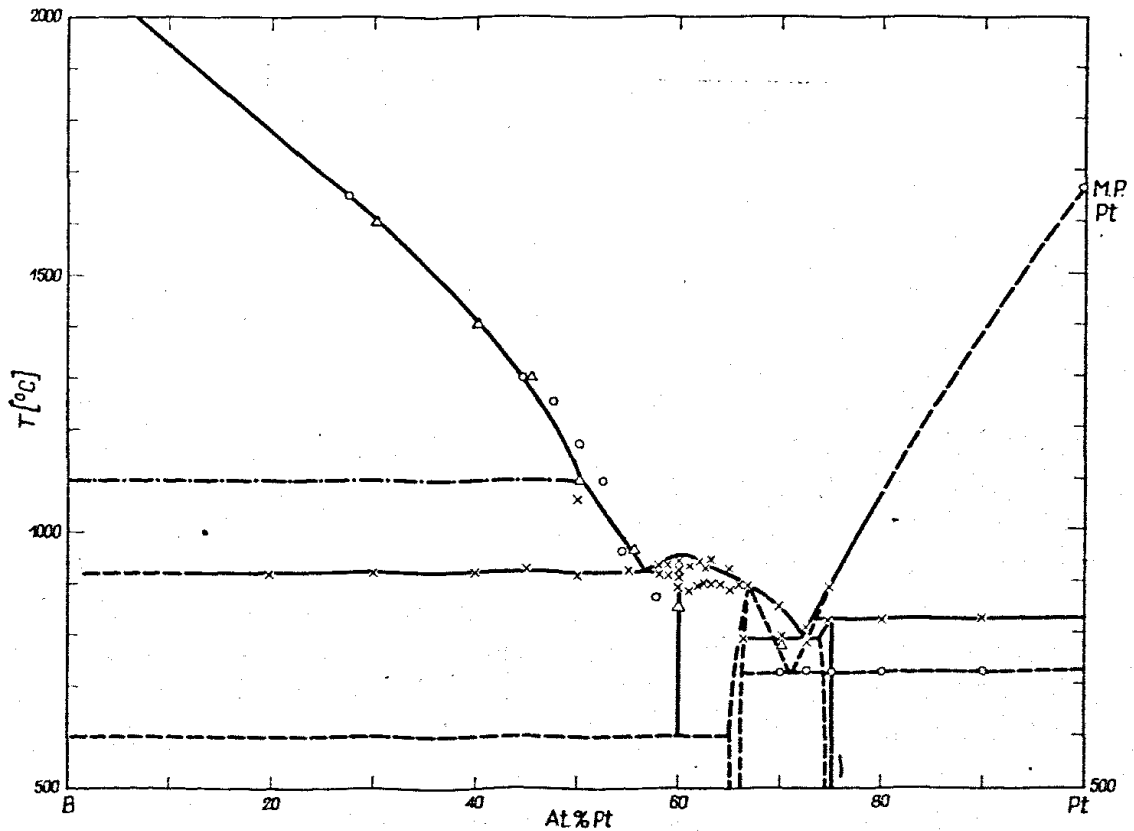
Figure 2.2. Phase diagram of the platinum-boron-system

O- Horn ;

Δ- Niemyski and Zawadzki;

×-Wald and Rosenberg ;

·-Wald; data on metastable eutectic. Impurities of ≤ 0.1 at% Si caused inhibition of Pt_3B

formation and reproducible establishment of metastable Pt_2B-Pt eutectic [43].

2.3.2 Born-metal binary systems

Several researchers have sought solvents other than platinum for the growth of α-rhombohedral boron, and their findings are summarized in Table 2.6.

Table 2.6 several metal-boron binary system

Boron-Metal system	Problems for growing α-B	Note
B-Ag	Formation of compound (AgB$_2$) [49] Low solubility (less than 1%) [44]	The formation of AgB$_2$ is in controversy:W.Obrowski *et. al* reported its formation in 1961[49], while F. Wald claimed AgB$_2$ was absent in his study [44]
C-Au	Formation of compound (AuB$_2$) [49] Low solubility(less than 1%) [44]	(1)The formation of AuB$_2$ was in dispute. [49][44] (2)In the VLS method, boron dissolves in a molten gold droplet almost instantaneously[50]
B-Cu	Formation of compound (CuB$_{22}$, CuB$_{24}$)	The formation of copper boride is in dispute[43,44][51-54]
B-Ga	Low solubility(less than 1%)[43]	
B-Ge	Low solubility(less than 1%)[43]	
B-Ni	Formation of compound(Ni$_2$B) [43]	
B-Pb	The loss of the solvent. Low solubility(less than 1%)[43]	
B-Sn	Low solubility(less than 1%)[43]	

2.3.3 Why copper was selected as the solvent in this study

In this investigation, the main focus was to grow α-rhombohedral boron by the solution growth method, employing copper as the solvent.

According to the phase diagram [55] of the boron-copper system, copper is a suitable solvent for the solution growth of boron crystal. First, the eutectic temperature is relatively low,

996 °C, lower than the maximum temperature (about 1100 °C) at which α-B is thermodynamically stable. Second, there are no intermediate phase boride-copper compounds although there is some dispute about this. In addition, copper is easily etched from the boron crystals with concentrated nitric acid. The last but not least factor is that copper is less expensive compared with other reported solvents such as platinum. The features of copper and platinum as solvent, for the growth of α-B are compared in Table 2.7.
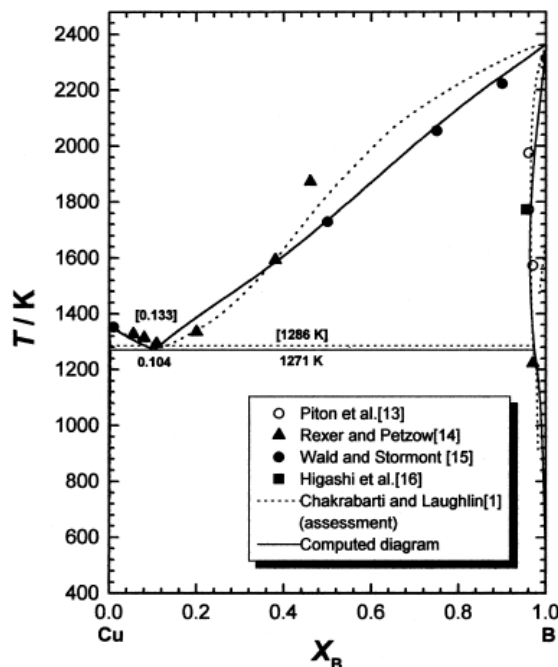
Figure 2.3 Phase diagram of boron-copper system [55].

Table 2.7 Comparison of copper and platinum as solvent for crystal growth of α-B.

	Eutectic temperature (°C)	Eutectic composition (at % B)	Phase diagram	Others
Copper	~996	~10.4	Simple(Figure 2.3)	Copper can be easily removed by concentrated nitric acid
Platinum	~825	~50	Complex(Figure 2.2)	Platinum only can be removed by electrolyzing or Crushing

30

In fact, Wald [43] reported that the eutectic in the copper boron system showed red boron, and an alloy with 90 at %B clearly showed red boron inclusions in an entirely unchanged microstructure after annealing for 21 days at 1000 °C [43]. But further characterization of the crystals were absent in his study.

In this study, a systematic investigation of α-rhombohedral boron crystal growth from copper solvent was conducted. We will study the influence of the relationship between the experimental parameters such as highest temperature, cooing rate, initial composition, and purity of the system with the results of the crystal growth. Various characterizations were also conducted on the crystals which were grown from copper solvent.

CHAPTER 3 - Experimental

3.1 Solution Growth of α-B from a Copper Flux

3.1.1 Setup

For the solution growth of boron crystals, a high temperature tube furnace (Figure 3.2) with molybdenum disilicide heating elements which is capable of reaching temperature up to 1500 °C was used. The system for removing the impurities (e.g. oxygen, water vapor) was comprised of vacuum pumps and a gas manifold. The mechanical pump was capable of pulling a vacuum to 10^{-4} torr, and then the diffusion pump could further reduce the pressure to as low as 10^{-6} torr. The crucibles and the reactor tube materials are given in Table 3.2. A schematic of the crystal growth system is given in Figure 3.1.

The most readily available polymorph of boron is β rhombohedral boron, thus, it was used as the source material for α-B crystal growth. Detail information of the source materials employed in our experiment is indicated in table 3.1
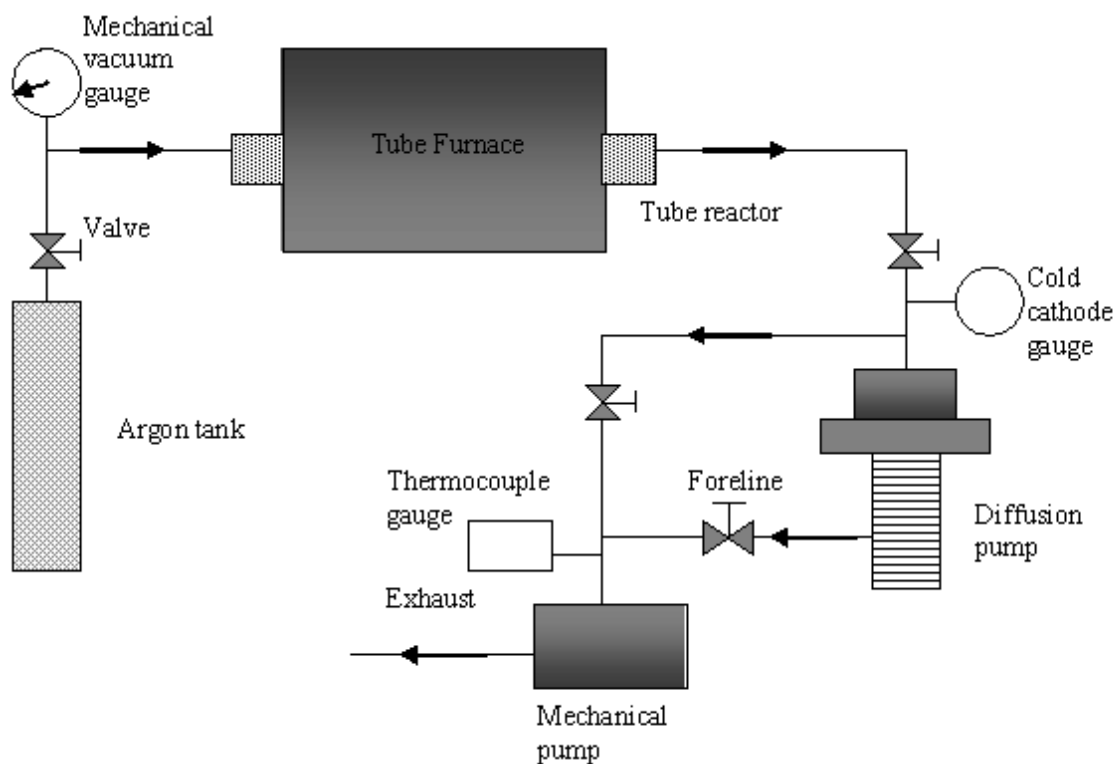
Figure 3.1 Schematic of the solution growth system (Copper-Boron).
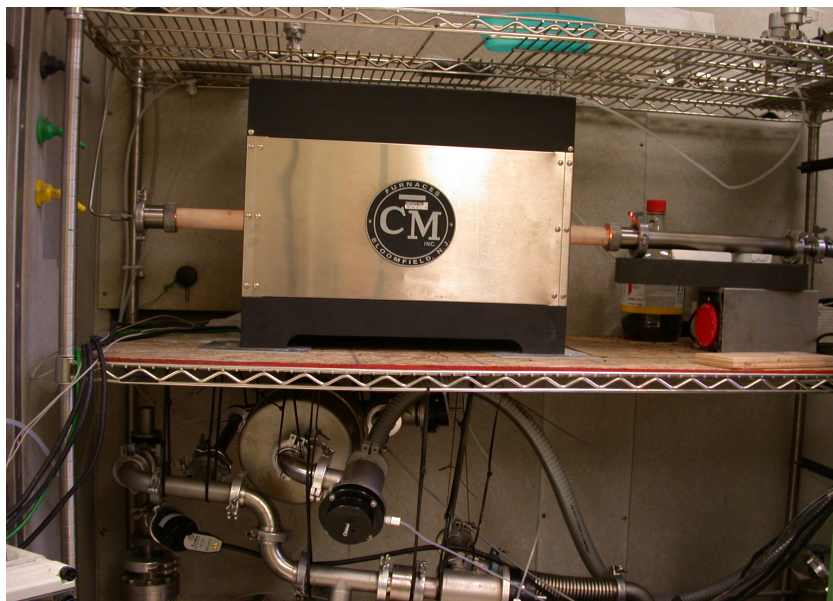
Figure 3.2 The high temperature tube furnace employed in solution growth of boron crystals.

Table 3.1 Purity and form of the β-rhombohedral boron employed in the copper-boron solution crystal growth experiments.

Name of the material	Purity (mol %)	Company	Forms	Notes
Boron	94%-96%	Cerac .Inc	Fine powder	Nature abundance
Boron	99.5%	Cerac .Inc	Particles (the largest one is ~0.5 cm in dimension)	Nature abundance
Boron	99.9999%	Ceradyne,Inc	Particles (the largest one is ~0.25 cm in dimension)	^{11}B isotope: 99 mol%, ^{10}B isotope 1 mol%
Copper shot	99.99%	Cerac.Inc	0.5 mm in diameter and 0.6 mm in length.	

Figure 3.3 Alumina tube reactor.

Figure 3.4 Alumina crucible (before use).
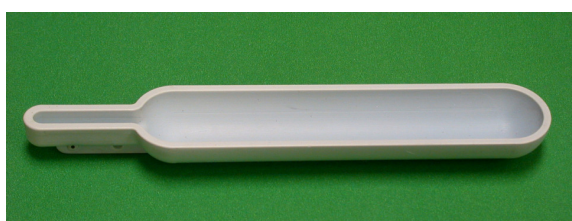
Figure 3.5 pBN coated boron nitride crucible.

Table 3.2 Reactor tube and crucible materials.

Parts	Name of the material
Tube Reactor	Alumina (Al_2O_3) (Figure 3.3)
	Mullite ($3Al_2O_3$-$2SiO_2$)
Crucible	Alumina (Al_2O_3) (Figure 3.4)
	pBN coated graphite (Figure 3.5)

3.1.2 Experimental Procedure

In a typical experiment, ~1g (0.0925mol) of boron and ~25g (0.3934mol) of copper, which approximated the eutectic composition of copper and boron system, were measured and put into the crucible. After loading them into the reactor, the system was evacuated by the mechanical pump to a pressure of 10^{-4} torr, and then purged with argon for two or three times to remove residual oxygen and water vapor. After purging, the system was evacuated to 10^{-4} torr again, and then connected to the diffusion pump, pumped overnight until a vacuum of 10^{-6} torr

was reached. The system was filled with argon until the pressure of the system attained 800 torr, the pressure of the crystal growth experiments.

The system was heated to 1350°C to form the copper and boron solution. After holding the system at 1350°C for 5 hours, the temperature was reduced to 1100°C in half an hour. To induce boron crystal precipitation, the temperature was slowly reduced from 1100 ^{0}C to 996^{0}C in 90 hours. The boron crystals were assumed to grow in this temperature range. The experiments were stopped by reducing from 996° C to room temperature by turning off the furnace.

The initial boron concentration was selected around the eutectic composition (boron mole fraction from 0.099 to 0.28), the temperature range for crystal growth was also near the eutectic point. Various cooling rates were employed (1°C/hr, 5°C /hr, 10°C /hr, 225°C/hr).

A mass balance was conducted on the copper and boron before and after the crystal growth. The total mass loss was about 2 grams in a typical experiment. The main reason for mass loss was the evaporation of copper. A layer of shiny copper was often observed on the inner wall of the reactor tube after the crystal growth.

Boron crystals were isolated by etching away the copper with nitric acid. The crystals were very small, (hundred of microns in dimension) and in large number. Powder x-ray diffraction analysis was conducted on the small crystals to determine their composition and boron polymorph. Scanning electron microscopy, optical microscopy, and elemental analysis were conducted on the samples embedded in the copper matrix and after being removed from the copper. Raman analysis was carried out on the boron crystals embedded in the copper matrix.

Table 3.3 the initial boron concentration.

Run No	Boron(g)	Copper(g)	Total Weight(g)	Boron(mol)	Copper(mol)	Sample Holder	Mol%	Wt%
1	0.746	24.224	24.97	0.0690	0.3812	Al_2O_3	0.1533	0.0299
2	0.74	24.31	25.05	0.0684	0.3826	Al_2O_3	0.1518	0.0295
3	0.731	24.269	25	0.0676	0.3819	Al_2O_3	0.1504	0.0292
4	0.732	24.3823	25.1143	0.0677	0.3837	Al_2O_3	0.1500	0.0291
5	0.389	20.908	21.297	0.0360	0.3290	BN	0.0986	0.0183
6	0.392	20.582	20.974	0.0363	0.3239	BN	0.1007	0.0187
7	0.8163	19.5447	20.361	0.0755	0.3076	BN	0.1971	0.0401
8	0.8117	18.3241	19.1358	0.0751	0.2884	BN	0.2066	0.0424
9	1.5302	23.4723	25.0025	0.1415	0.3694	BN	0.2770	0.0612
10	1.0348	24.5326	25.5674	0.0957	0.3861	BN	0.1987	0.0405
11	1.0108	24.546	25.5568	0.0935	0.3863	BN	0.1949	0.0396
12	0.7785	24.5024	25.2809	0.0720	0.3856	BN	0.1574	0.0308
13	0.778	22.76	23.538	0.0720	0.3582	BN	0.1673	0.0331
14	0.8051	24.5121	25.3172	0.0745	0.3857	BN	0.1618	0.0318
15	1.0376	24.1957	25.2333	0.0960	0.3808	BN	0.2013	0.0411
16	1.17431	25.6422	26.81651	0.1086	0.4035	BN	0.2121	0.0438
17	2.082	49.754	51.836	0.1926	0.7830	BN	0.1974	0.0402
18	1	24.017	25.017	0.0925	0.3779	BN	0.1966	0.0400
19	1.0997	25.6463	26.746	0.1017	0.4036	BN	0.2013	0.0411
20	1.026	25.6327	26.6587	0.0949	0.4034	BN	0.1905	0.0385
21	1.2403	26.945	28.1853	0.1147	0.4240	BN	0.2129	0.0440
22	1.0157	25.4342	26.4499	0.0940	0.4002	BN	0.1901	0.0384
23	1.2378	25.4886	26.7264	0.1145	0.4011	BN	0.2221	0.0463

3.2 Solution Growth of α-B from a Platinum Flux.

The experiments of Horn [45] who successfully grew α-B from a platinum flux were repeated here to compare the features of copper and platinum as the solvent for α-B crystal growth.

The melting point of platinum is 1768.3°C. To form a liquid phase of platinum, a high temperature furnace with a graphite heating element (Figure 3.6 and Figure 3.7) was employed in our experiment. This resistively heated graphite furnace is capable of attaining a temperature as high as 2000°C. The main components of the crystal growth system included the graphite furnace combined with an automated temperature and pressure control system, a cooling system and a vacuum system.

In this experiment, three samples were prepared, the purity of the boron and platinum source materials are summarized in Table 3.4, for both source materials. For the crystal growth experiments, samples were prepared with an initial boron concentration around 50 at %, as shown in Table 3.5. Boron and platinum were loaded into the hot pressed boron nitride crucible and then put into the reactor.

Figure 3.6 The resistively heated graphite reactor.

Table 3.4 The source materials for preparing α-B from a platinum flux.

Name of the material	Purity (mol %)	Company
Boron (zone refined)	99.9999%	Ceradyne,Inc
Platinum	4N	ESPI
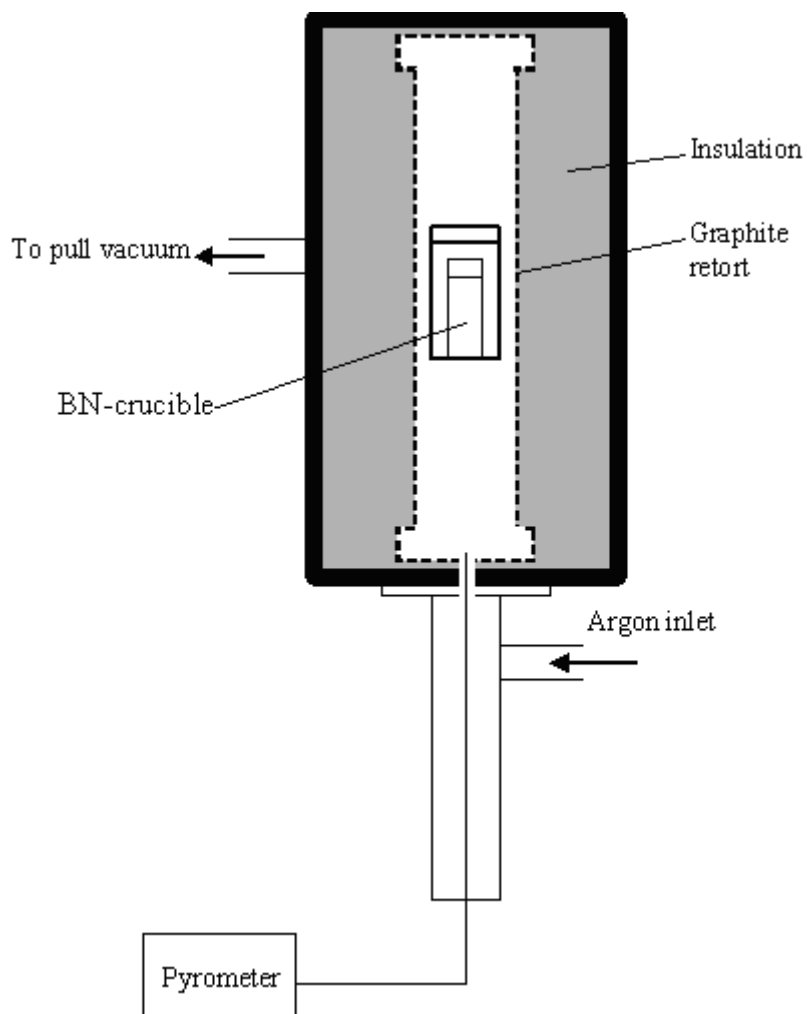
Figure 3.7 Schematic of the graphite furnace for preparing α-B from a platinum flux.

Table 3.5 Initial mass, moles and mole % of boron and platinum.

Sample No		Weight (g)	Mole	Mol%
1	Boron	0.0126	0.001165	50.18%
	Platinum	0.2257	0.001157	49.82%
2	Boron	0.0165	0.001526	47.37%
	Platinum	0.3308	0.001696	52.63%
3	Boron	0.04181	0.004896	48.96%
	Platinum	0.9551	0.003960	39.60%

The procedure for boron-platinum solution growth experiments was similar to that of the boron-copper system. First, the system was evacuated to 10^{-4} torr with a mechanical vacuum pump, and then purged with argon for two or three times. Then, the system was evacuated again, and the diffusion pump started, reducing the pressure in the boron-platinum system to 10^{-5} torr. The boron crystal growth from a platinum flux was in an argon ambient at a pressure of 800 torr. To form a liquid platinum phase, the temperature was increased to around 1800°C since the melting point of pure platinum is 1768.3 °C, and held for 5 hours. Next the temperature was reduced to 900°C, and held for 30 hours.

An interaction between crucible materials (hot-pressed boron nitride) and the platinum-boron melt was observed. To avoid this, an experiment at a lower temperature (1200 °C) for longer time (one week) was conducted.

The resulting boron-platinum alloys were analyzed by optical microscopy, scanning electron microcopy, and energy dispersive spectroscopy. Raman analysis was conducted on the crystals precipitated on the surface of boron-platinum alloy. X-ray diffraction analysis was conducted after the platinum-boron alloy was crushed into powders.

3.3 Chemical Vapor Deposition (CVD) method and Vapor-Liquid-Solid (VLS) Growth of α-B with diborane (B_2H_6)

Diborane can decompose to boron at 700°C [38], and also contains "three-center-two-electron" bonds [31], thus it qualifies as a good potential reactant for preparing α-rhombohedral boron. However, there have been few studies on growing α- B from diborane [39], possibly because in the past it was difficult to obtain pure, carbon free diborane [31] at the time of 1960s and 1970s study .In order to contribute more data on producing α-B from diborane, we conducted a series of experiments to determine feasible conditions.

The apparatus for preparing α-B from diborane was a typical chemical vapor deposition system, as indicated in Figure 3.8 and Figure 3.9. The source materials employed are listed in Table 3.6.

Table 3.6 The source materials for preparing α-B with CVD method.

Name	Purity	Company
H_2	99.9995%	Linweld
B_2H_6	99.995%	Matheson Tri-Gas

The diborane was transported to the reactor by hydrogen. The diborane decomposition and resulting boron decomposition takes place in a quartz chamber, on the substrate heated by conducting to an inductively heated susceptor.

Tantalum, silicon, spinel and boron nitride were used as the substrate materials. As indicated in Table 3.7, the silicon substrates seeded with platinum particles were investigated at 800ºC, 900ºC, and 1000ºC to search for an optimal growth temperature. To investigate the effect of metal particles, we compare the difference of substrates with/without seeding metal particles at the same growth condition. The influence of substrate and seed materials was also investigated.

Table 3.7 Experimental Parameter of CVD Investigation.

Run No	H$_2$ Flow (slm)	B$_2$H$_6$ (sccm)	B$_2$H$_6$ (mol %)	Maximum Temperature (ºC)	Substrate	Duration (min)
1	2	50	2.50%	900	Si+Pt seed	45
2	2	50	2.50%	900	Si only	45
3	2	40	2.00%	800	Si+Pt seed	90
4	2	40	2.00%	800	Spinel only	90
5	2	50	2.50%	1000	Si+Pt Seed	60
6	2	50	2.50%	1000	BN+Pt Seed	60
7	2	50	2.50%	1000	Si+Au Seed	60
8	2	50	2.50%	1000	Si+Pt Seed	60
9	2	50	2.50%	1000	Ta+Pt Seed	60
10	2	50	2.50%	1000	Ta only	60
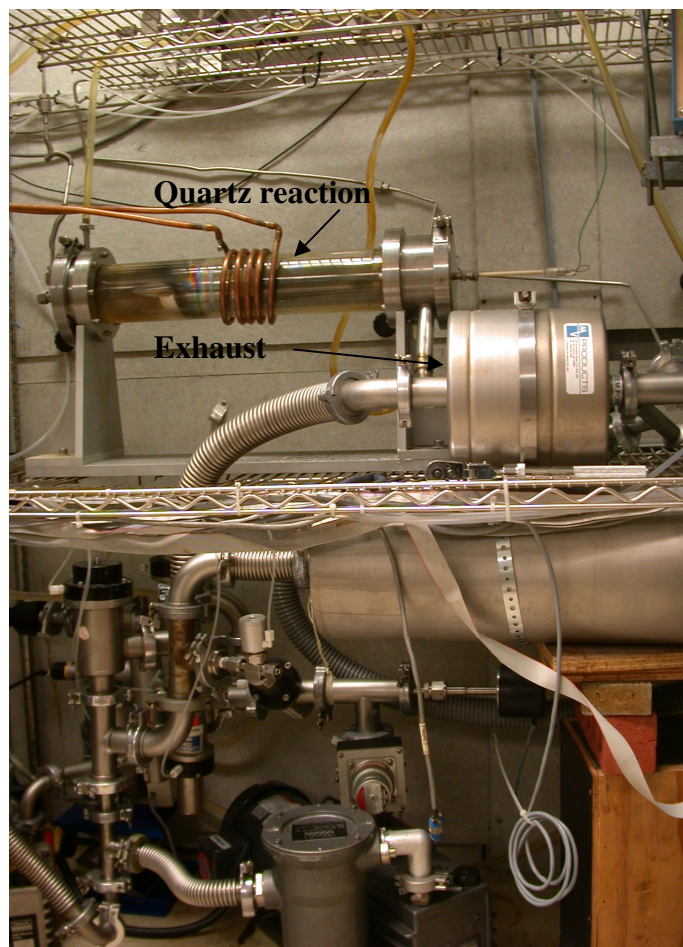
Figure 3.8 The chemical vapor deposition (CVD) system for preparing boron films and needles.
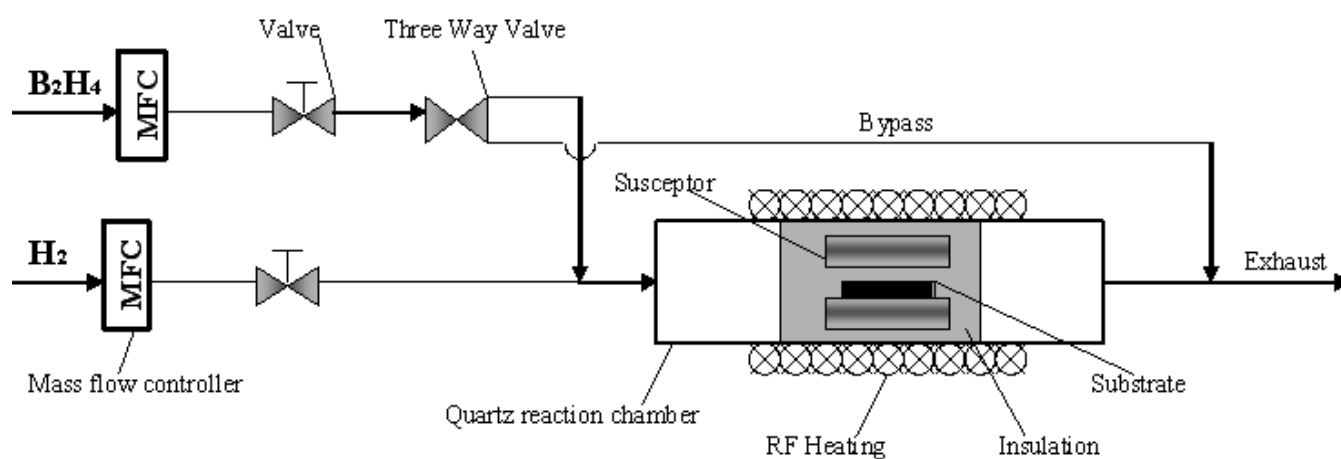
Figure 3.9 A schematic of the CVD system for depositing boron films and needles.

3.4 Characterization Techniques

Various analytical techniques including: optical microscopy, scanning electron microscopy (SEM), energy dispersive spectroscopy (EDS), x-ray diffraction (XRD) and Raman spectroscopy were applied in our investigation to identify the surface morphology, elemental concentration, and structure of the samples. In this section the principles and function of each technique are introduced.

3.4.1 Scanning Electron microscopy and Energy dispersive spectroscopy

Scanning Electron Microscopy (SEM) combined with Energy Dispersive Spectroscopy (EDS) was applied to characterize the morphology, topography, and composition of our samples.
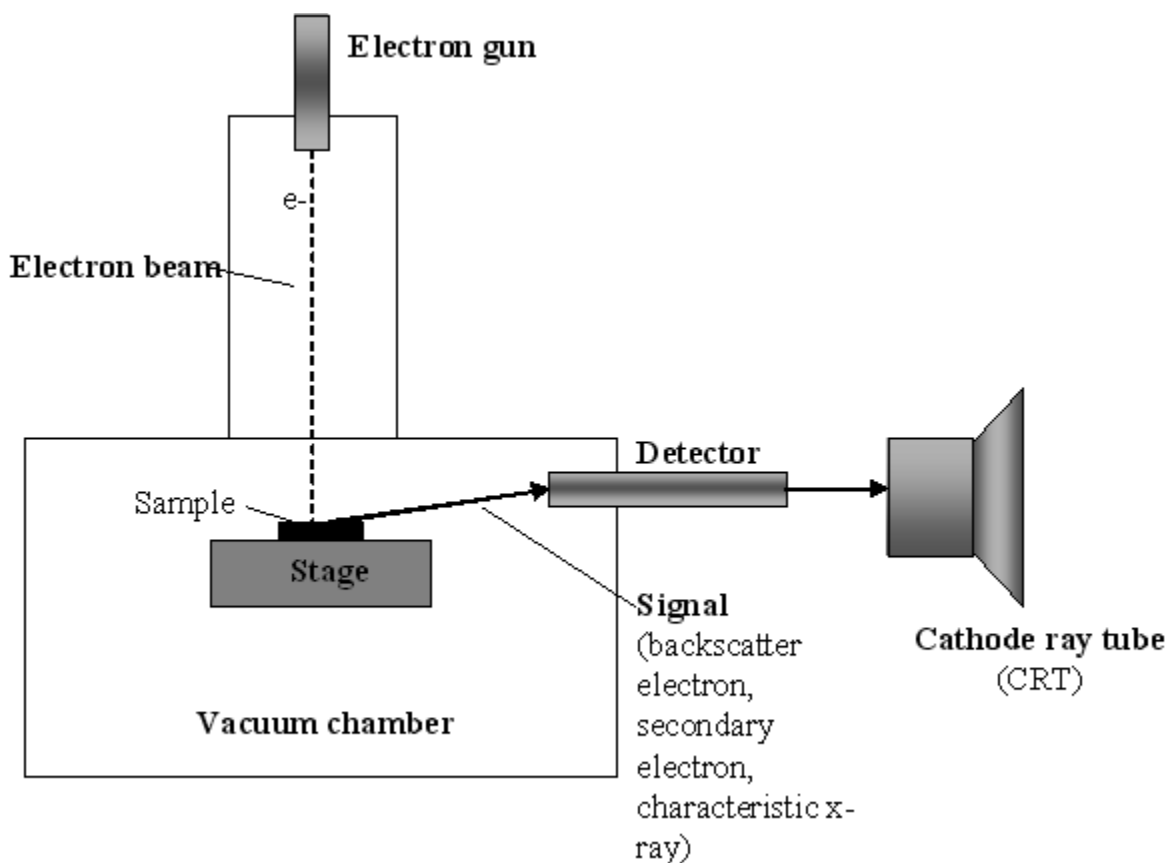
Figure 3.10 Schematic of SEM/EDS system [57].

SEM/EDS works by bombarding the surface of the sample with a finely focused electron beam.The electron interact with the atoms of the sample and produce various signals including the secondary electrons, back-scattered electrons (BSE), characteristic x-rays, and other photons

of various energies. These signals are collected and analyzed by the detectors revealing the information of the sample. [56] A schematic of a SEM/EDS system is given in Figure 3.10 [57].

Secondary electrons and backscattered electrons are used for imaging the samples: secondary electrons are most valuable for showing morphology and topography on samples; backscattered electrons are most valuable for illustrating contrasts in composition in multiphase samples. Characteristic x-rays are produced by inelastic collisions of the incident electrons with electrons in discrete orbitals (shells) of atoms in the sample. As the excited electrons of the sample atoms return to lower energy states, they yield X-rays that are of a fixed wavelength which is the "fingerprint" for an elements, thus the composition of the samples could be determined.

The SEM/EDS analysis was conducted in the Department of Entomology at Kansas State University. This SEM/EDS equipment has a backscatter detector, secondary electron detector, absorbed electron (environmental) detector, and a cold stage unit. One can examine non-coated specimens without concern for charging because the system can be operated under low vacuum. Additionally, the SEM has an Oxford INCA microanalytic system for x-ray microanalysis of specimens. [58]

3.4.2 Raman spectroscopy

Raman spectroscopy was applied as a tool to determine the polymorph of the boron samples. It is a spectroscopic technique used to study the vibrational, rotational, and other low frequency modes in a system. It depends on inelastic scattering, or Raman scattering, of monochromatic light, usually from a laser in the visible, near infrared, or near ultraviolet range. [59]

When light is scattered from a solid, most photons are elastically scattered. The scattered photons have the same energy (frequency) and, therefore, wavelength, as the incident photons. However, a small fraction of light (approximately 1 in 10^7 photons) is scattered at optical frequencies different from, and usually lower than, the frequency of the incident photons. The process leading to this inelastic scatter is termed the Raman Effect. Raman scattering can occur with a change in vibrational, rotational or electronic energy of a molecule. The energy change of vibrationl mode could reveal the information of the solid structure, and environment: atomic mass, bond order, molecular substituents, molecular geometry and hydrogen bonding all influence the vibrational force constant which, in turn dictates the vibrational energy. [59]

Raman measurements provide a means of probing the lattice dynamics of disordered solids thus giving insight into the structure, bonding and nature of the disorder. Raman peaks of well-defined phonons in single crystal semiconductors are very sharp. Asymmetrical peak broadening and a shift to lower frequencies occur in the spectra of polycrystalline and amorphous semiconductors. This is caused by the disorder introduced in their structure.

In our investigation, Raman measurements were carried out using a Renishaw InVia spectrometer using 488-nm line of Ar+ ion laser as the excitation source. The laser beam was focused on the sample surface using a 50× optical lens and the laser power was about 20mW. All measurements were made in backscattering geometry with unpolarized detection. These measurements were performed by our collaborators at the University of Bristol, UK.

The Raman pattern of α-rhombohedral boron and β-rhombohedral boron were indicated in Figure 3.11[60] and Figure 3.12. [61]
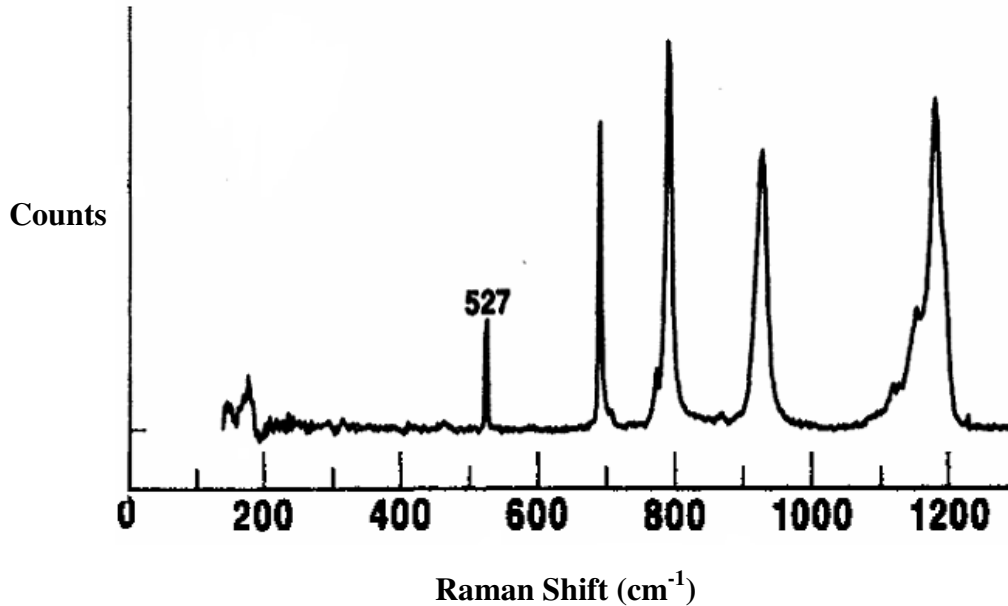
Figure 3.11 Background-corrected Raman spectra of α-rhombohedral boron. [60]
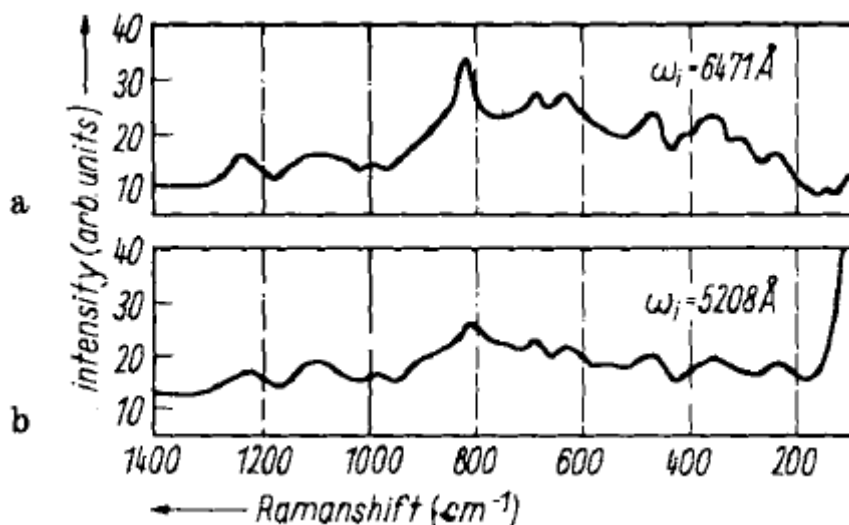
Figure 3.12 Unpolarized Raman spectra of β-rhombohedral boron taken with (a) 6471 Å , (b) 5208 Å excitation. [61]

3.4.3 X-Ray Diffraction

X-ray powder diffraction (XRD) was employed in our investigation to identify the chemical composition, polymorphs, and crystallographic structure of the samples. It is a rapid analytical technique primarily used for phase identification of a crystalline material and provides the information of unit cell dimensions.

The x-ray beams are generated by a cathode ray tube, filtered to produce monochromatic radiation, collimated to concentrate, and then directed toward to the sample (crystalline materials). X-ray diffraction occurs only when the interaction of the incident rays with the sample satisfy Bragg's Law as given in equation 3.1: (also illustrated in Figure 3.11) [62]
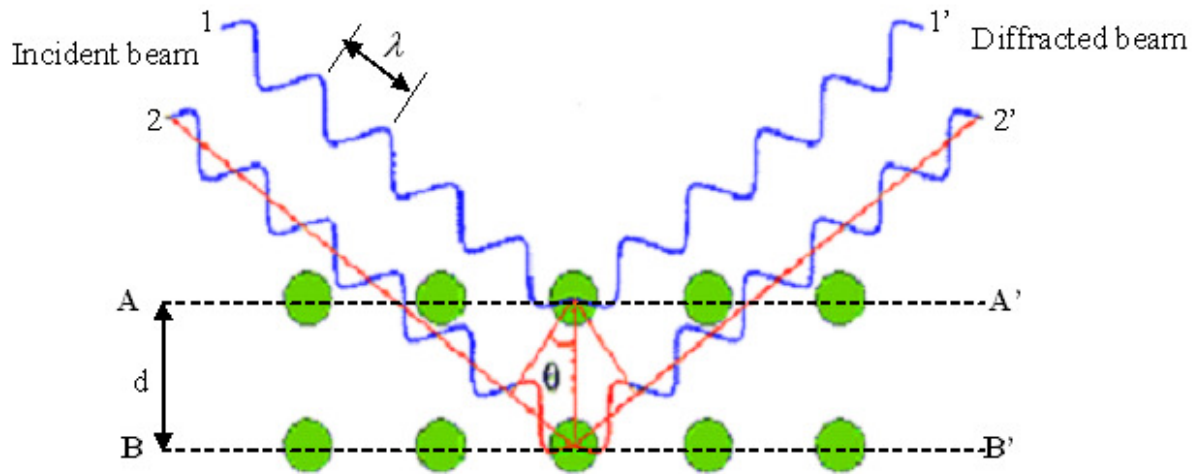
Figure 3.13 Diffraction of x-rays by planes of atoms (A-A' and B-B'): At the Bragg angle θ, the reflected rays are in phase and reinforce one another, X-ray diffraction occurs. [62]

Equation 3.1: $n\lambda = 2d \sin\theta$

λ- Wavelength of electromagnetic radiation

θ- Diffraction angle

d- The lattice spacing (d) of a crystalline sample

n- An integer, the order of diffraction

In the technique of powder x-ray diffraction, the sample consists of many fine and randomly oriented particles; each particle is a crystal and in large numbers with random orientations, this ensures that some particles are properly oriented such that every possible set of crystallographic plane will be available for diffraction. [63]

By scanning the sample through a range of 2θ angles (e.g. 5-70 for boron), all possible diffraction directions of the lattice could be collected. These diffracted x-rays are then detected, processed and counted. Plotting the angular positions (2θ) and intensities of resultant diffracted peaks, a characteristic pattern which reveals the sample's composition and crystallographic structure can be produced. [63]

CHAPTER 4 - Results and Discussion

4.1 The Copper-Boron System

Black crystals were always observed at the upper surface of the solid copper-boron alloy bar after crystal growth. After etching away the copper matrix with concentrated nitric acid, two kinds of crystals were always detected: transparent red crystals which were frequently absent on the surface of the copper-boron alloy bar, and black crystals. Since the characteristic color of α-rhombohedral boron is red (actually, some researchers claimed the production of α-rhombohedral boron based only on the evidence of the red color [43]), a sequence of experiments was conducted to find the optimal experimental condition for producing red boron crystals. Over a range of experiment variables, a series of large (up to ~500µm), well-faceted, transparent, red crystals in various shapes were successfully grown on the surface of the copper matrix. In this chapter, the correlation between the experimental process parameters and results are summarized. The results of various instrumental analyses are presented. Finally, the contradictions between the results from different characterization methods are considered.

4.1.1 The influence of various experimental parameters.

Figure 4.1 is a typical optical image of the isolated crystals: the yield of red crystals was much less than the yield of black crystals. For most of experiments, the red crystals were larger than the black crystals (Figure 4.2 and Figure 4.3), the black crystals were usually irregular in shape (Figure 4.4), in rare cases, the black crystals were rhombus shape (Figure 4.5). Through a systematic search of the experiment conditions for producing α-B, a number of well faceted, transparent red crystals in triangle, rhombus, pentagon, and hexagon shape were formed on the surface of the copper-boron alloy. The largest dimension of these crystals was about 500µm (Figure 4.6 to Figure 4.15). The experimental factors which influence the formation of red boron crystals are summarized in the following paragraphs.

(1) *The minimum system pressure (vacuum level).* If the pressure of the system was higher than 10^{-4} torr, no red crystals were obtained on the surface of the copper boron alloy, and the surface of the alloy was dark and smoky (Figure 4.16, 4.17). After etching the smoky dark bar by nitric acid, a few red crystals were observed, but the yield was low (Figure 4.18).

(2) ***The purity of the starting material (as shown in Table 4.1):*** The boron sources with low purity (94%-96%) were tried in preliminary experiments. Heavy slags formed on the surface of the alloy (Figure 4.19, 4.20), and no red crystals were observed. After etching away the copper matrix by concentrated nitric acid, some red crystals combined with the cotton-like black impurities (the structure of the black impurities was completely different than crystalline boron) were observed (Figure 4.21).

For the initial experiments with 99.5% purity boron, the boron was crushed with a ceramic mortar and pestle. This contaminated the boron with grindings, thus, no red crystals were formed on the surface of the copper-boron alloy bar, and after etching the samples with nitric acid, some insoluble cloudy white impurities were always found (Figure 4.22). These impurities were very inert; they were not dissolved by soaking in 0.5% hydrofluoric acid over night.

(3) ***The highest temperature*** (for forming the boron and copper solution). If the temperature was too high (e.g.>1500ºC), the boron obviously interacted with the crucible (Figure 4.24), if too low (<1000°C), the boron poorly dissolved into the copper even after 7 hours (Figure 4.25). (Table 4.2):

(4)***The total annealing time*** (the time for forming a boron and copper solution plus the time for crystal growth): the longer the annealing time, the more uniform was the composition of the boron-copper solution, and the larger the crystals produced. The effect of temperature was also supplemented in Table 4.3

(5) ***The materials of the crucible, and the reactor*** (Table 4.4): In our preliminary experiments, when alumina (Al_2O_3) (Figure 4.23) and mullite ($3Al_2O_3$-$2SiO_2$) were used as the material of the crucible and tube reactor respectively, significant interactions between the crucible and the copper-boron alloy were observed. Removing the surface of the alloy bar by concentrated nitric acid, some red, translucent, pyramid-shape crystals were observed (Figure 4.27, 4.28). Elemental analysis indicated that these crystals contained copper, silicon and oxygen (Table 4.5). More characterization (XRD, neutron activation analysis, etc) was attempted on these crystals; however, they disappeared after dissolving the alloy bar in concentrated acid for 12 hours. This phenomenon further proved that these red crystals couldn't be α-rhombohedral boron. Thus, it seems questionable to claim the formation of α-rhombohedral boron only based on the color of the crystals. [43] A simple test is to attempt to etch the crystals by nitric acid.

Surprisingly, the initial concentration of boron did not influence the crystal growth much. Some relatively large boron particles were always incompletely dissolved (Figure 4.25); some even kept their original morphology. To form the copper-boron solution, Wald [45] annealed the copper and boron at 1000°C for at least 21 days, thus it is possible that the diffusion rate of boron in copper is quite small due to the low growth temperature. A uniform copper and boron solution failed to form, instead, the solution was always locally supersaturated.

Figure 4.1 Optical micrograph (reflected white light 50 ×); this is a typical etched sample with representative amounts of black and red crystals in copper-born solution growth experiments. For all experiment conditions studied in our research, the number of black crystals always greatly outnumbered the number of red crystals. (In some cases, there were even fewer red crystals as for example in Figure 4.18).
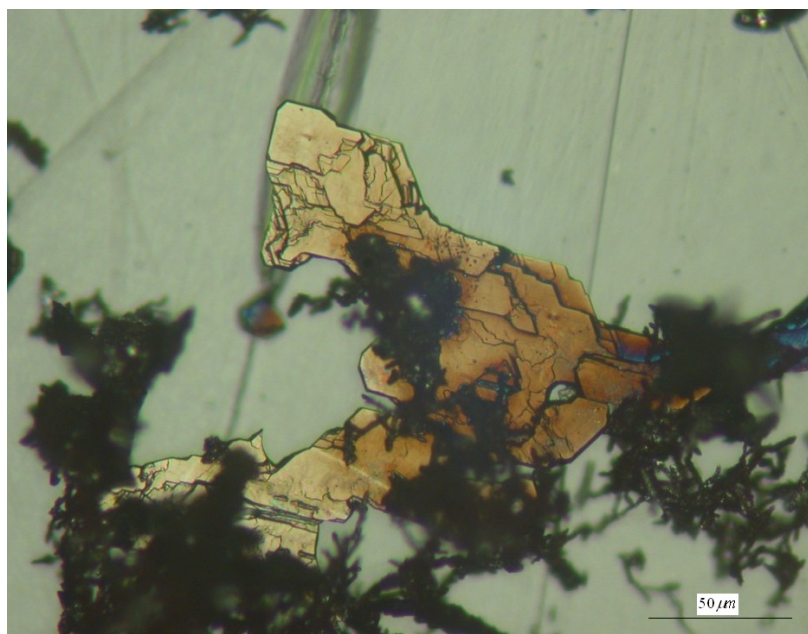
Figure 4.2 Optical micrograph (reflected white light 400 ×); a red crystal fragment was surrounded by many smaller black crystals. In copper-boron solution growth experiment, the size of red crystals was usually larger than the black crystals, and the black crystals were irregularly shaped.
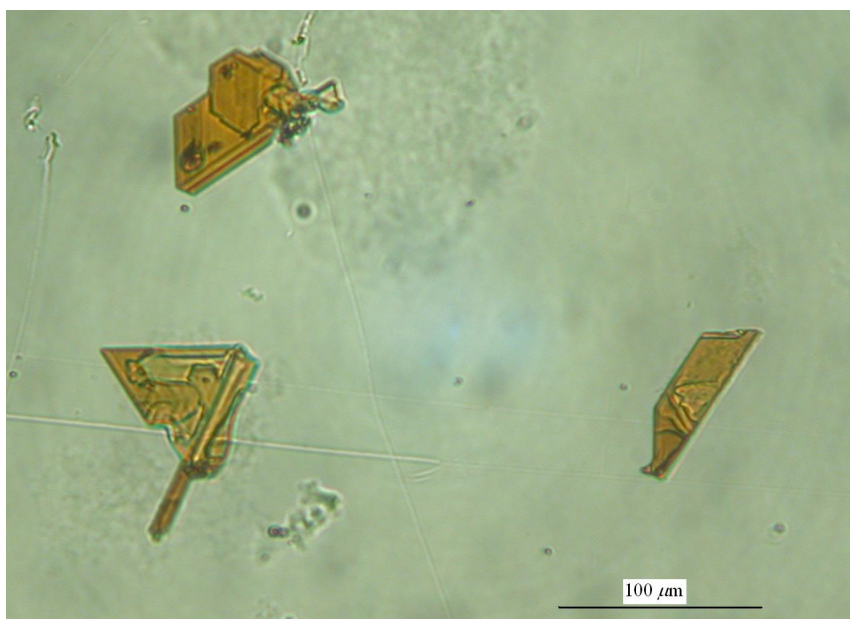
Figure 4.3 Optical micrograph (reflected white light 200 ×); the typical morphology of red boron crystals in copper-boron solution growth experiment, after etching way the copper matrix.
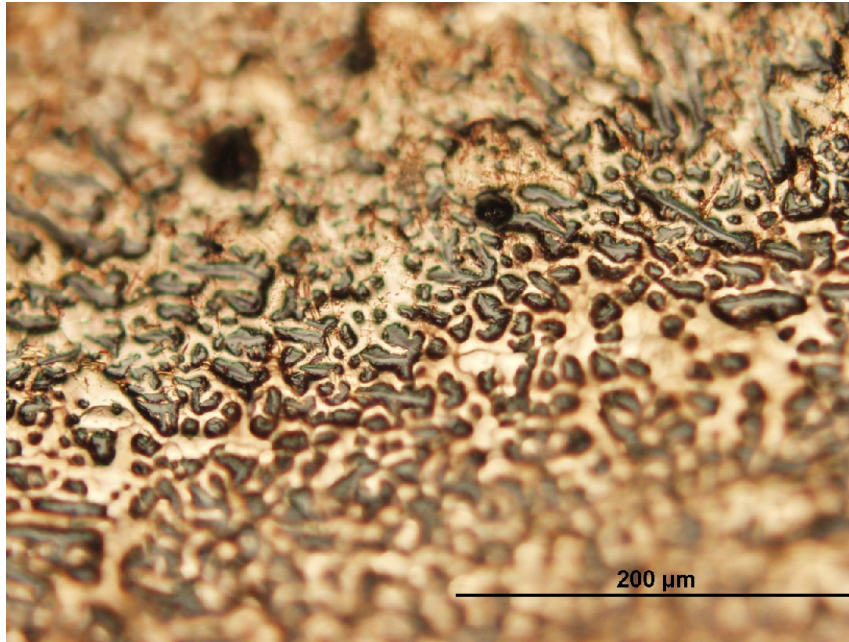
Figure 4.4 Optical micrograph (reflected white light 200 ×): in most of the copper-boron solution growth experiments, black crystals were observed on the surface of the copper-boron alloy. Frequently, the black crystals were irregular in shape, in rare cases; they were rhombus shape as indicated in the next figure.

Figure 4.5 Optical micrograph (reflected white light 200 ×); a black boron crystal in shape of rhombus embedded in the copper matrix (found on the surface of the same piece of alloy of Figure 4.4). The maximum dimension of this crystal is about 100μm.

Figure 4.6 to Figure 4.15 were taken from the samples prepared by the copper-boron solution growth experiments from runs No 9-18. In these experiments, red crystals were observed on the surface of the copper-boron alloy bars. The common experimental parameters were: the minimum system pressure: 10^{-6} torr, the highest temperature: 1350ºC; the starting materials: 99.5% boron particles and 99.99% copper short. The initial concentration of copper-boron was near the eutectic concentration (10.4 at. % boron, 89.6 at. % copper). The difference between the experiments was the annealing time. In the long-annealing time experiment (e.g. 90 hours), more pentagon and hexagon red crystals tended to appear. In the short annealing time experiment (e.g. 10 hours), most of the red crystals were in the shapes of rhombus, pentagon and hexagon red crystals were barely observed. The number of large size crystal (>300µm), as the crystal indicated in Figure 4.15, was higher in the long annealing time experiment. The relationship of annealing time and experiment results were also presented in Table 4.3.

Figure 4.6 Optical micrograph (reflected white light 200 ×); two red boron crystals in the shape of a rhombus embedded in the copper matrix. The maximum dimensions of these crystals was about 200µm. (Copper-boron solution growth, annealed at 1350°C for 5 hours then reduced temperature by turning off the furnace).

Figure 4.7 Optical micrograph (Transmitted polarized light 50×) of the crystals isolated from the copper matrix by nitric acid. This red crystal was originally surrounded by the black crystals. Some small pieces of black crystals remain. The largest dimension of this red rhombus crystal is about 250 μm. (Copper-boron solution growth, annealed at 1350°C for 5 hours then reduced temperature by turning off the furnace).

Figure 4.8 Optical micrograph (reflected white light 200 ×); a red pentagon shaped boron crystal embedded in the copper matrix. The maximum dimension of this crystal is about 300μm. (Copper-boron solution growth experiment, annealed at 1350°C for 5 hours, then the temperature was reduced from 1100°C to 960°C in 90 hours).
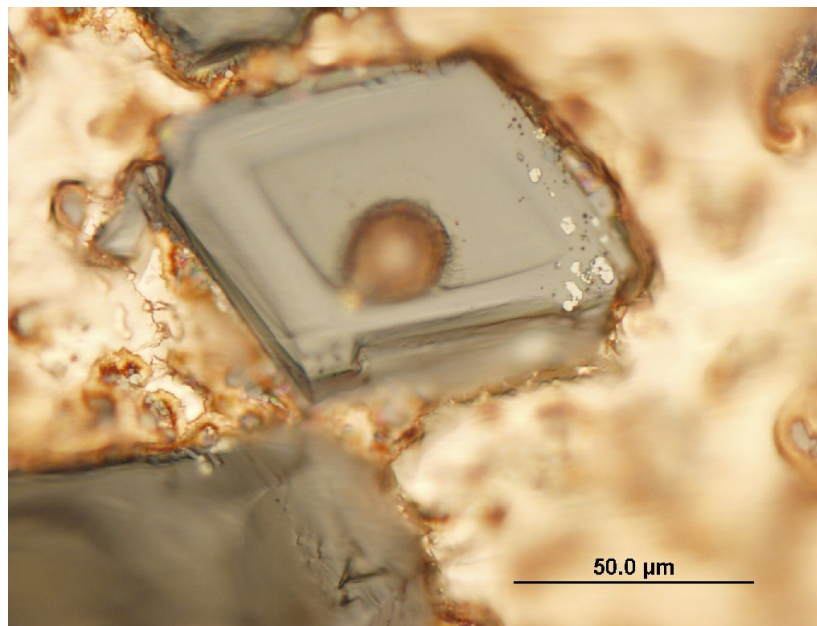
Figure 4.9 Optical micrograph (reflected white light 200 ×); a red boron crystal in the shape of pentagon embedded in the copper matrix. The maximum dimension of this crystal is about 250µm. (Copper-boron solution growth experiment, annealed at 1350°C for 5 hours, the reduced the temperature from 1100°C to 960°C in 90 hours).
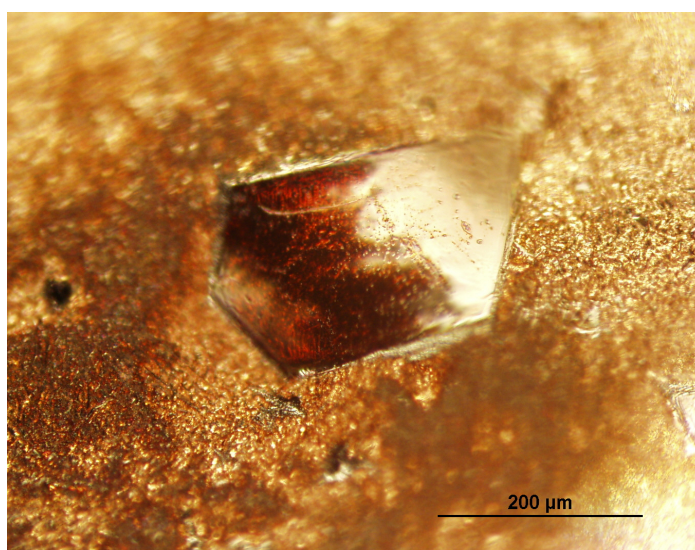
Figure 4.10 Optical micrograph (reflected white light 200 ×); a red boron crystal in the shape of pentagon embedded in the copper matrix. The maximum dimension of this crystal is around 400µm (Copper-boron solution growth experiment, annealed at 1350°C for 5 hours, the reduced the temperature from 1100°C to 960°C in 90 hours).
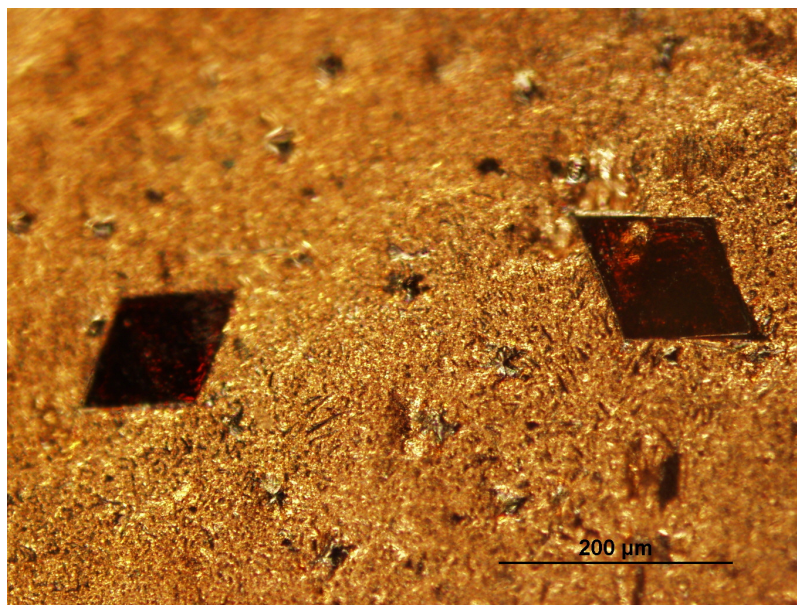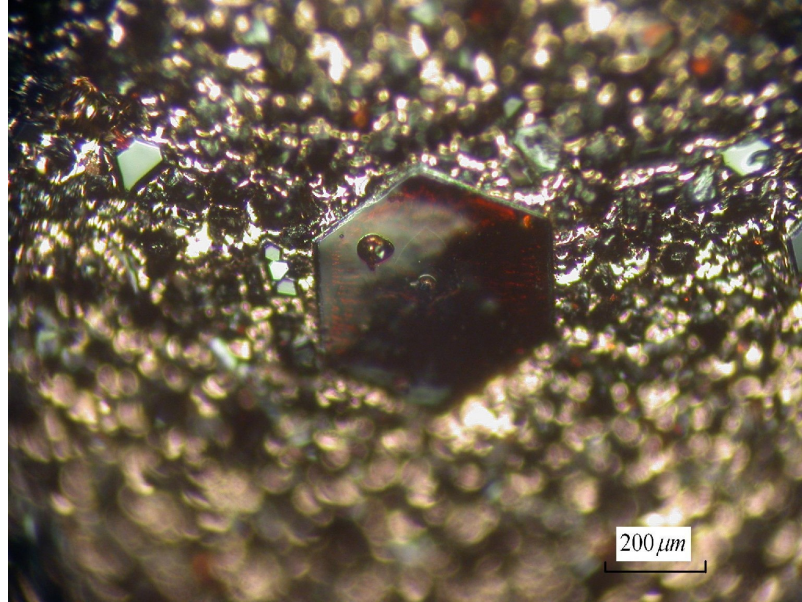
Figure 4.11 Optical micrograph (reflected white light 200 ×); a red boron crystal in the shape of hexagon embedded in the copper matrix. The maximum dimension of this crystal is around 500 μm (Copper-boron solution growth experiment, annealed at 1350°C for 5 hours, the reduced the temperature from 1100°C to 960°C in 90 hours).
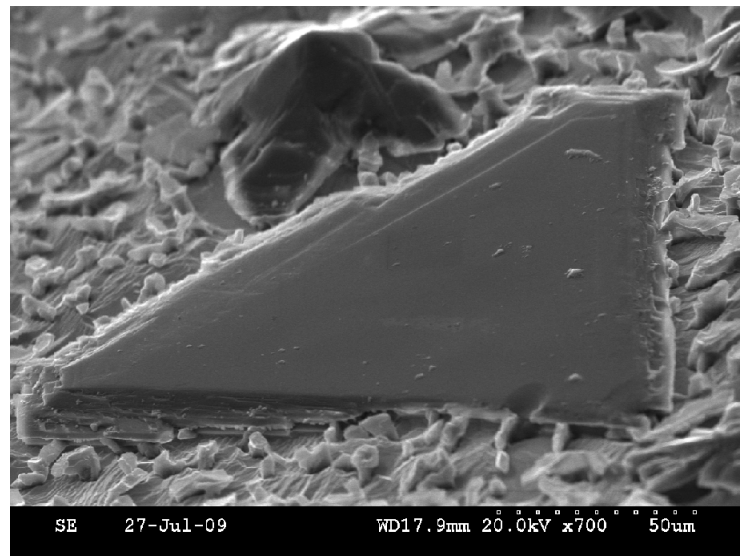
Figure 4.12 SEM (scanning electron microcopy) image of a triangle shaped red boron crystal embedded in cooper matrix which was briefly etched, the largest dimension of this crystal is about 190μm(Copper-boron solution growth, annealed at 1350°C for 5 hours then reduced temperature by turning off the furnace).
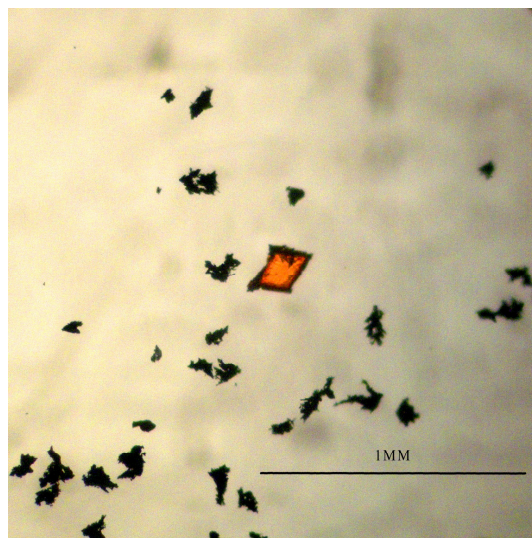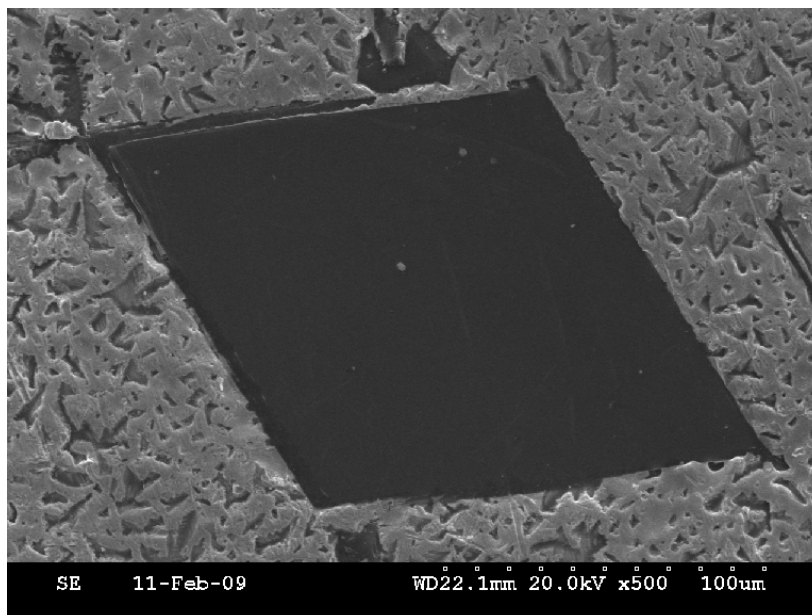
Figure 4.13 SEM image of a red rhombus boron crystal embedded in the unetched copper matrix, the largest dimension of this crystal is about 200µm. (Copper-boron solution growth, annealed at 1350°C for 5 hours then the temperature was reduced by turning off the furnace).
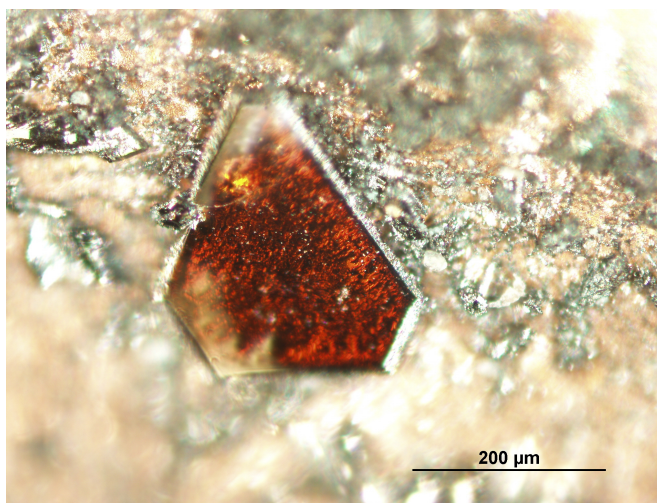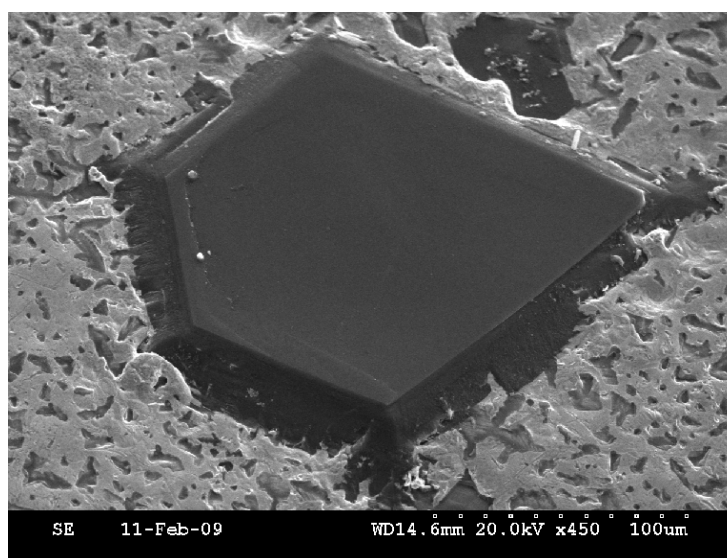

Figure 4.14 SEM image of a red pentagon shaped boron crystal embedded in the unetched copper matrix, the largest dimension of this crystal is about 180µm. (Copper-boron solution growth experiment, annealed at 1350°C for 5 hours, then the temperature was reduced from 1100°C to 960°C in 90 hours).
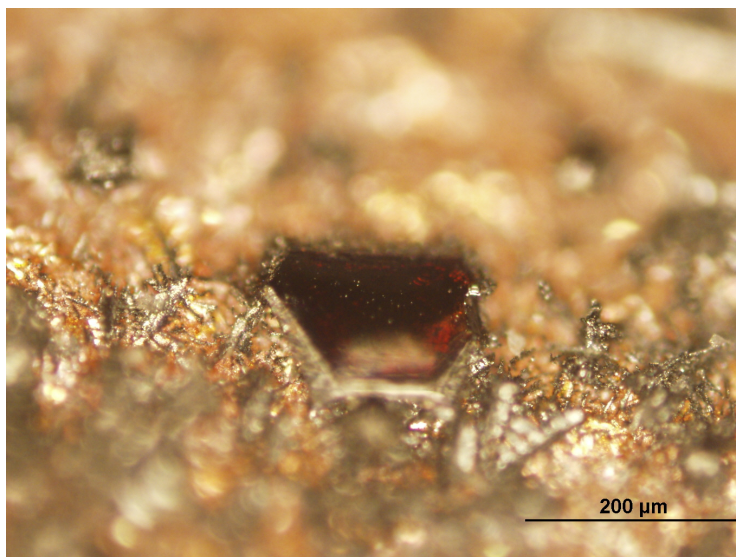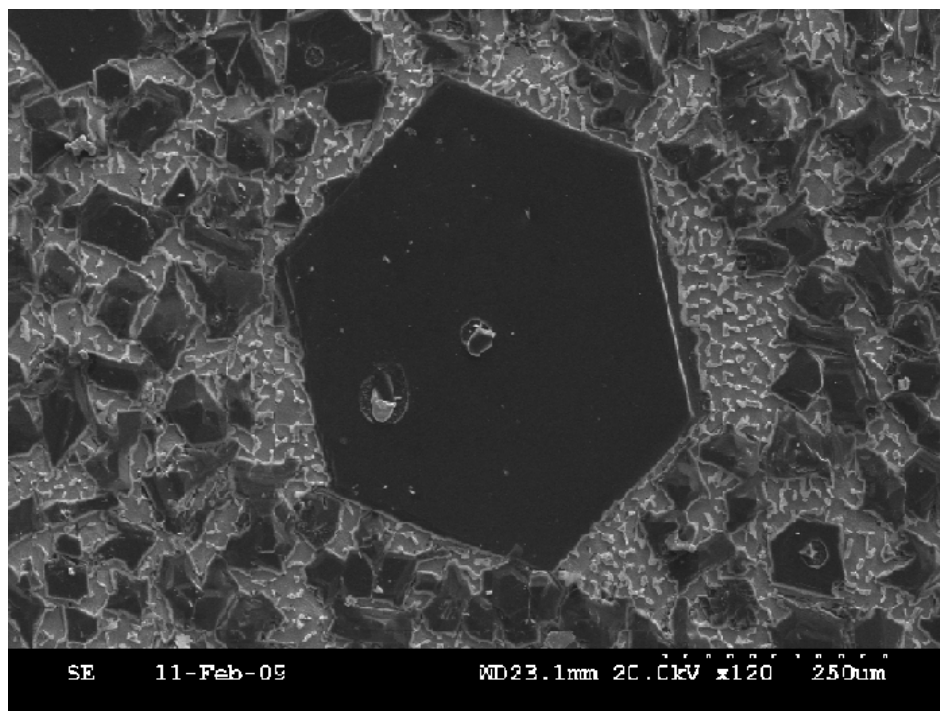
Figure 4.15 SEM image of a red hexagon shaped boron crystal, embedded in the unetched copper matrix; the largest dimension of this crystal is about 500μm. (Copper-boron solution growth experiment, annealed at 1350°C for 5 hours, then the temperature was reduced from 1100°C to 960°C in 90 hours).


Figure 4.16 A dark and smoky copper-boron alloy bar, the minimum system pressure for preparing this sample was higher than 10^{-4} torr, thus more impurities from the atmosphere (H_2O, O_2) were introduced.
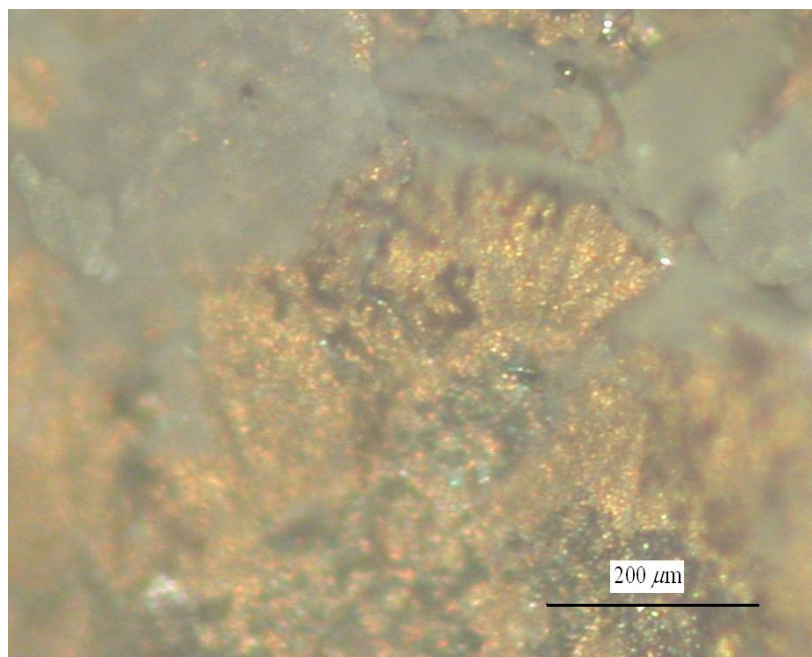
Figure 4.17 An optical micrograph of the same surface of the copper-boron alloy bar in Figure 4.16 at 100× magnification (white reflected light); no red crystals were observed.
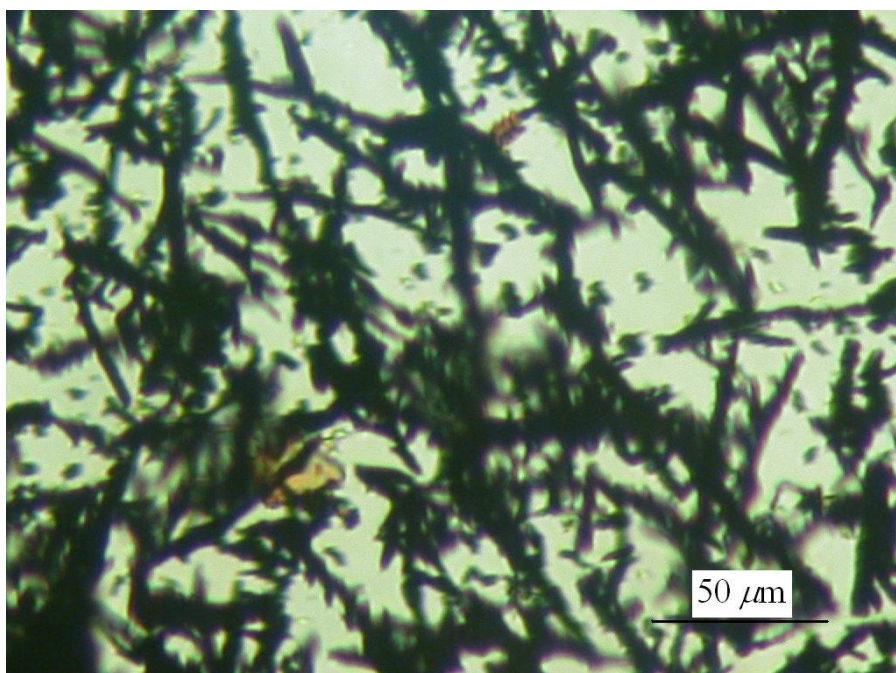
Figure 4.18 Optical micrograph (reflected white light 400×): after etching the cooper-boron bar in figure 4.16. Only a few red crystals were observed.

Figure 4.19 A copper boron-alloy bar with a dull surface, produced with low purity boron powder (94%-96%), no red crystals were observed on the surface of this alloy bar.
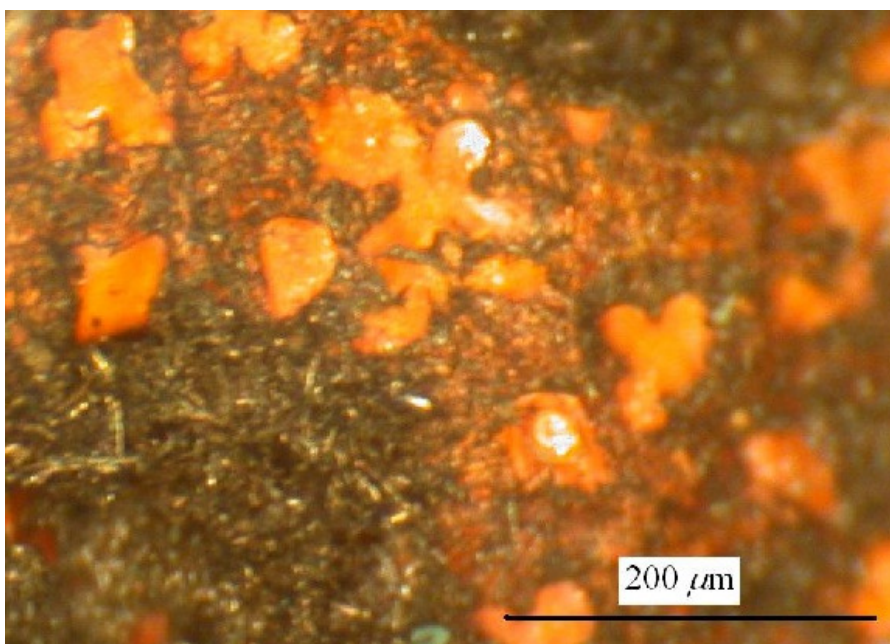
Figure 4.20 Optical micrograph of the surface of the copper-boron alloy bar in figure 4.19 at 200× magnification (reflected white light). No red crystals were found.
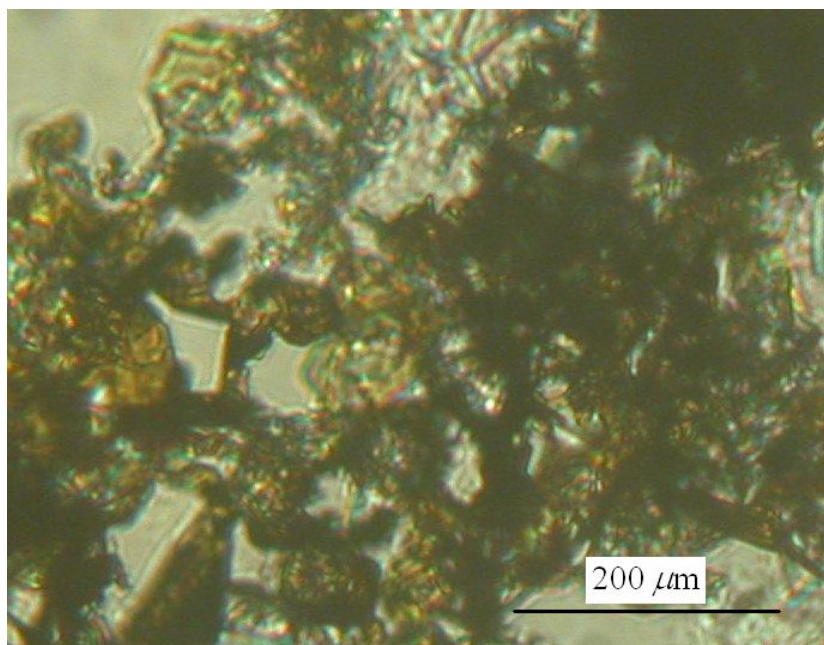
Figure 4.21 Optical micrograph (reflected white light 200×): after etching the cooper-boron bar in Figure 4.19, red crystals was found, as showed in the upper right corner of this figure some cotton-like black impurities was formed.
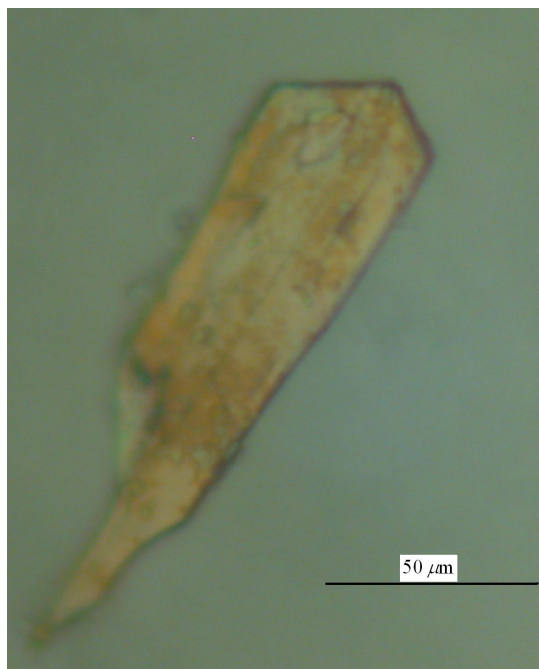
Figure 4.22 Optical micrograph (reflected white light, 400×) after etching the cooper-boron bar prepared by the boron particles which were crushed by ceramic mortar, this crystal was surrounded by white cloudy gel-like impurities.

a

b

Figure 4.23 top picture indicated an Al$_2$O$_3$ crucible before the experiment, the bottom picture is the Al$_2$O$_3$ crucible after a copper boron solution growth experiment (annealing copper-boron at 1350ºC for 5 hours, then reducing the temperature by turning off the furnace).

Figure 4.24 This copper-boron alloy was posed upside-down to expose the surface in contact with the pBN crucible; the copper-boron melt interacted with the crucible materials after annealing at 1500ºC for 5 hours. The white slag on the surface of the bar is the crucible material (boron nitride).
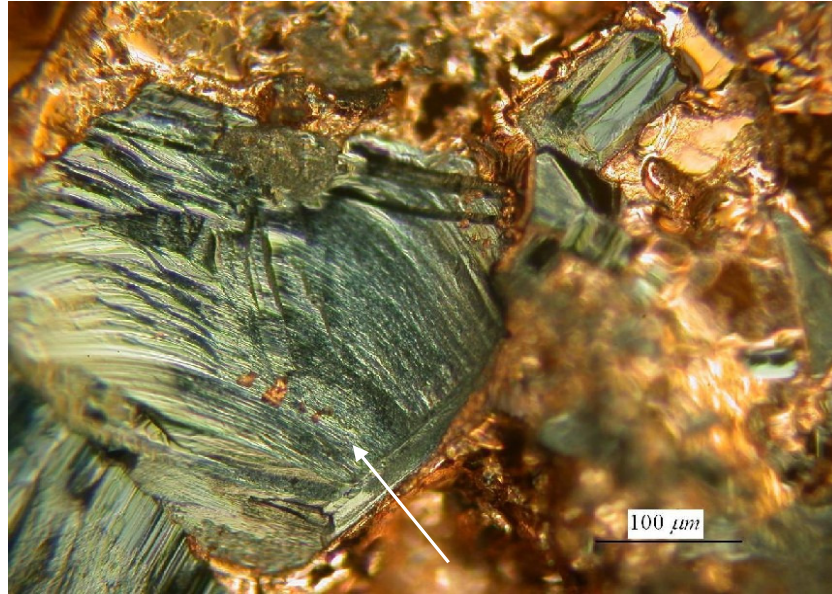
Figure 4.25 Optical micrograph (reflected white light 25×). In the copper-boron solution growth experiments, there were always observed some large particles of source materials (β-rhombohedral B) incompletely dissolved (as indicated by the arrow).
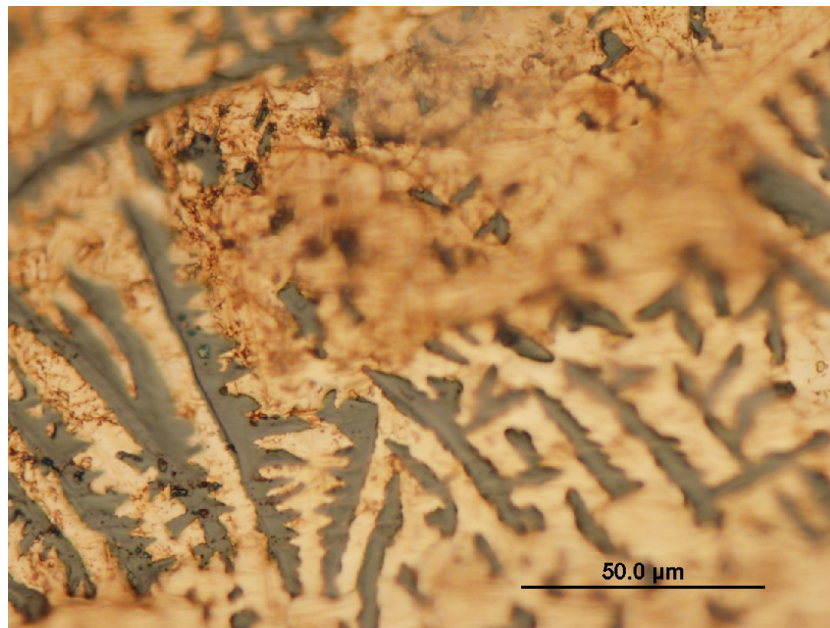
Figure 4.26 Optical micrograph (reflected white light 200×) dentric structure on the surface of copper-boron alloy (annealing copper-boron at 1000°C for 90 hours, reducing the temperature by turning off the furnace).
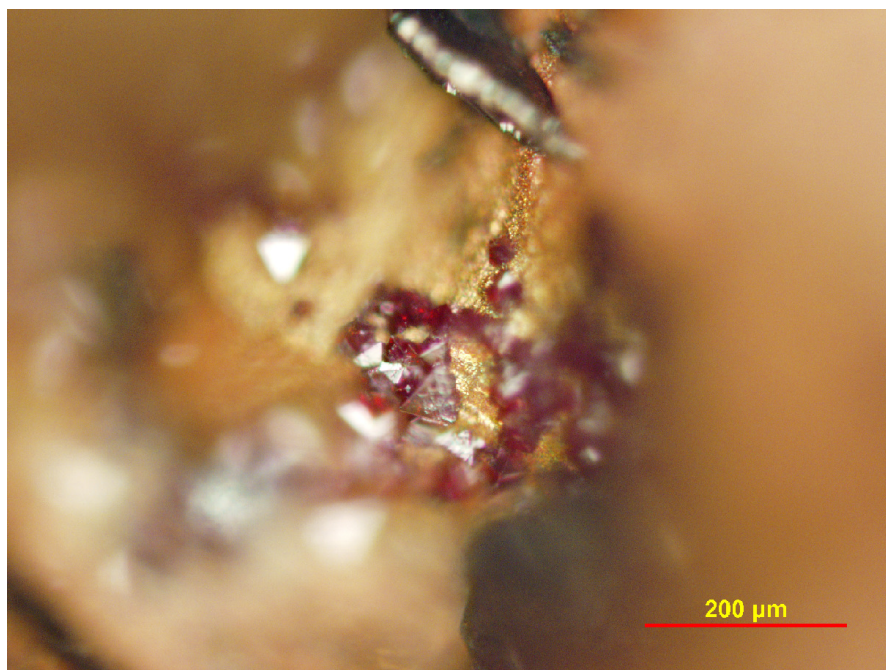
Figure 4.27 Optical micrograph (200×, reflected light) of red translucent crystal with pyramid shape. The copper-boron alloy was loaded in the Al₂O₃ crucible, elemental analysis indicated that these red crystals contained copper, silicon and oxygen (Table 4.5).
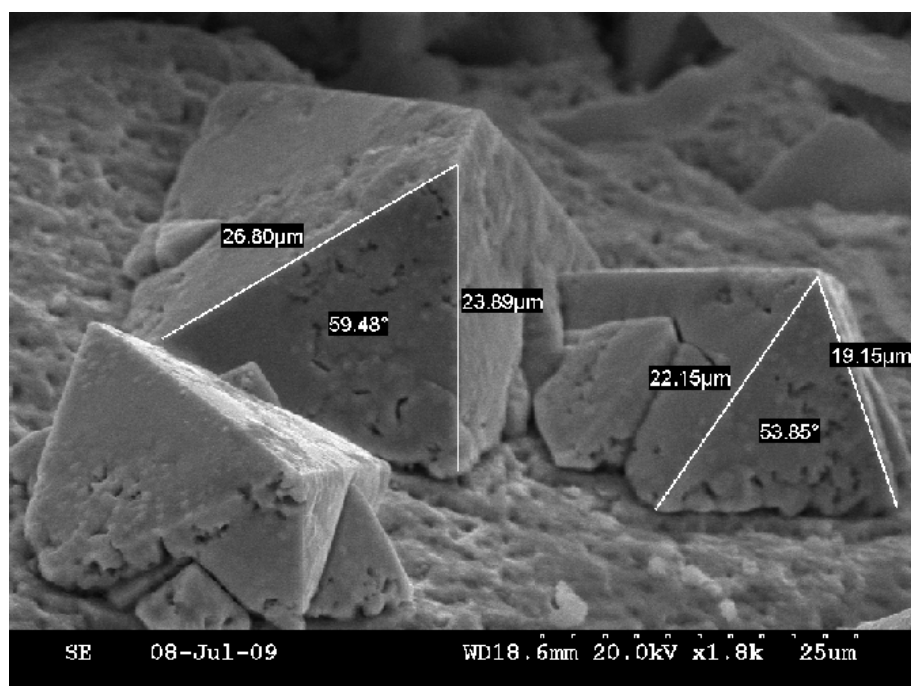
Figure 4.28 The Scanning Electron Microscopy (SEM) image of the same red translucent crystals in figure 4.27.

Table 4.1 The influence of the purity of β-rhombohedral boron employed in the Cu-B solution growth.

Source material	Purity (mol %)	Note
Boron (powder)	94%-96%	No red crystals were observed
Boron (the largest grain dimension is about 0.5cm)	99.5%	Red crystals were observed
Boron	99.9999%	Red crystals were observed
Copper short	99.99%	

Table 4.2 The highest temperature used to dissolve boron into copper.

Highest temperature (ºC)	Duration time at highest temperature (hr)	Results
1000	5,7,8	More than one third of boron didn't dissolve into copper.
1350	5,8,12	Most of the boron dissolved in 5 hours, still some of the larger boron particles remained even after 12 hours. No obvious interaction of the reactants and pBN crucible was observed with the first several experiments, but the crucible needed to be change after about 5 runs, because it was gradually "etched" by the copper-boron melt after each experiments (as indicated in figure 4.29).
1500	5	Significant interaction between the melt and the crucible occurred.
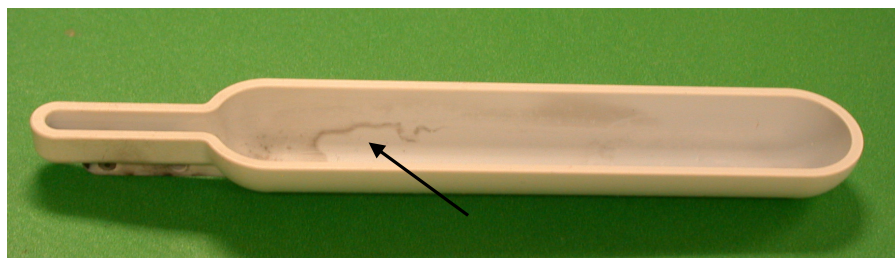
Figure 4.29 As indicated by the arrow, the pBN coated boron nitride crystal was slighted "etched" after a copper-boron solution growth experiment.

Table 4.3 Temperature profile and cooling rate for growing crystal.

Temperature range for crystal growth	Temperature profile	Results
1100°C to 960°C	Reduce from 1100°C -960°C in 90 hours then turning off the furnace	Some red crystals were observed on the surface of the copper-boron alloy
1000 °C	Hold the temperature at 1000°C for 90°C hours, and then reduce to room temperature by tuning off the furnace.	Small black crystals (~50 μm in dimension) were usually obtained, dentritic structure was mostly observed under this temperature profile (Figure 4.26). Occasionally, red rhombus crystals were also observed.
1000°C to room temperature (~25°C)	Hold at 1000°C for 10 hours then reduced to room temperature by turning off the furnace.	Boron was not dissolved into copper completely.
1350°C to room temperature (~25°C)	First hold the system at 1350°C for 5 hours then turn off the furnace	Red crystals were observed. Most of them were rhombus shaped and small in size (<300μm).

Note: Once turned off, the system cools from ~1000°C to room temperature (~25°C) in around 6 hours.

Table 4.4 Reactor and the tube materials.

Parts	Material	Notes
Tube Reactor	Alumina(Al_2O_3)	No obvious contamination was detected
	Mullite($3Al_2O_3$-$2SiO_2$)	Unsuitable for boron crystal growth due to the decomposition of $3Al_2O_3$-$2SiO_2$ at high temperature (T>1300 °C).
Crucible	Alumina(Al_2O_3)	Highly reactive with boron during crystal growth.
	pBN coated graphite	Slightly attacked by the solution but can be used for more than 5 times.

4.1.2 Analytical Results

4.1.2.1 The results of elemental analysis (by EDS, from k-electron shells)

Elemental analysis was conducted on the samples by Energy Dispersive Spectroscopy (EDS). The analysis of Table 4.5 and Table 4.6 were conducted on a piece of copper-boron alloy sample which was loaded in alumina crucible (Al_2O_3) and grew in a mullite ($3Al_2O_3$-$2SiO_2$) reactor tube. In Table 4.5, the composition of pyramid- shaped, translucent, red crystals was studied. As mentioned in the last section, these crystals appeared after etching the surface of the copper-boron alloy with concentrated nitric acid. In Table 4.6, pyramid-shaped red crystals disappeared after etching the alloy bar in concentrated nitric acid over night, leaving some rod shaped black crystals. Clearly, considerable contamination was introduced (silicon, aluminum and oxygen) into the alloy from the crucible and reactor materials.

The sample in Table 4.7 is a piece of copper boron alloy, prepared in pBN coated graphite crucible and alumina reactor tube. However, the vacuum level for preparing this sample not high (~9×10^{-4}), and only black crystals were observed on the surface of this sample. The contamination of silicon, aluminum was greatly reduced but the contamination of oxygen and carbon was significant. Comparing the composition of this sample to a different area, (1) in the upper side of the alloy bar, the concentration of boron is higher than that of in the down side of the bar, probably due to the relatively low density of boron compared to copper, after boron was dissolved, it aggregated on the surface of the solution;(2) on the same side of the alloy bar, the distribution of boron is not even. This probably due to the low diffusion rate of boron in copper, thus the copper-boron solvent was locally supersaturated or under saturated.

66

Table 4.5 The element analysis results on the red, translucent pyramid shape crystals (sample Cu-B-082908, run No 2).
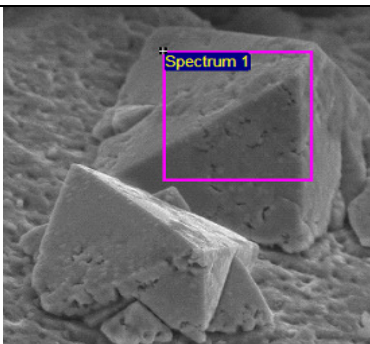
Element	Atomic%	Detected Area	Note
O	43.5		The pyramid shape crystals are translucent and red; however, they dissolve in nitric acid over night, further proved that it could not be α-B
Si	2.2		
Cu	54.4		
Totals	100.0		

Table 4.6 the element analysis results of a piece of black materials (a mixture of black crystal, red crystal and impurities) after etching away the copper matrix of the sample Cu-B-082908.

Element	Atomic%	Detected Area	Note
B	40.4		This piece of copper-boron alloy was formed in an alumina crucible in a mullite reactor tube. Significant contamination was detected with EDS. Because of this contamination, the crucible and reactor tube were changed to pNB coated graphite and alumina respectively.
C	53.7		
O	3.9		
Al	1.1		
Si	0.1		
Cu	0.8		
Totals	100.0		

Table 4.7 The elemental analysis results of various spots in the same piece of copper-boron alloy (Sample Cu-B-020409, run No. 19).
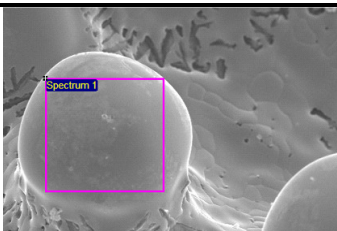
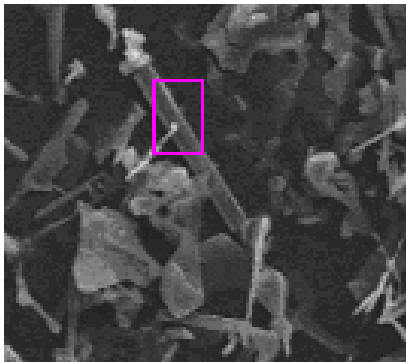|	Element	Atomic%	Detected Area	Note
Spot 1	B	95.14		The crucible materials was pBN coated graphite and the tube reactor materials was alumina.
	Cu	4.86		
	Totals	100		
Spot 2	C	22.22		This sample was prepared by annealing copper-boron at 1350°C for 5 hours, and reducing the temperature from 1100°C to 960°C over 90 hours. The minimum pressure for preparing this sample was a little bit high ($\sim 9 \times 10^{-4}$ torr), only black crystals were observed on the surface of this copper-boron alloy.
	Cu	77.78		
	Totals	100		
Spot 3	B	86.80		
	O	4.23		
	Cu	8.98		
	Totals	100		
Spot 4	B	86.95		
	O	11.99		Spot 1 to Spot 4 are on the upper side of the copper-boron alloy.
	Cu	1.05		
	Totals	100		
Spot 5	Cu	100		Spot 5 and Spot 6 are on the under side of the alloy, which was contact with the crucible.
	Totals	100		
Spot 6	C	10.02		
	Cu	89.98		
	Totals	100		

Table 4.8 The element analysis results of various spots in the same piece of copper-boron alloy (sample Cu-B-120908, run No. 10).
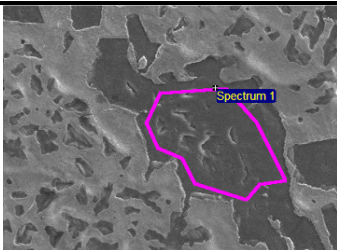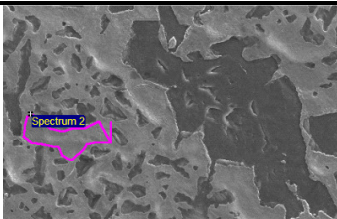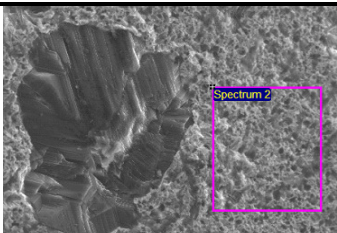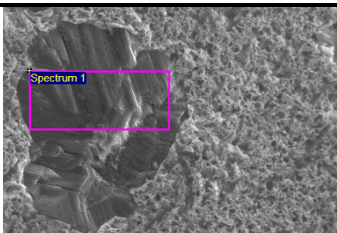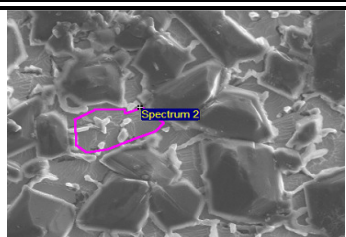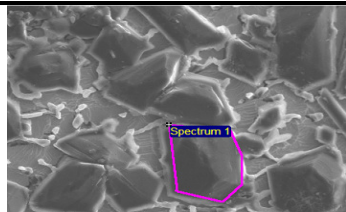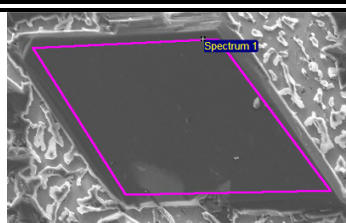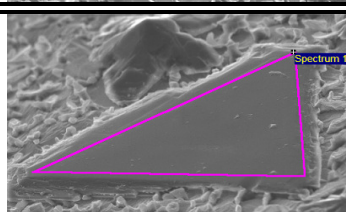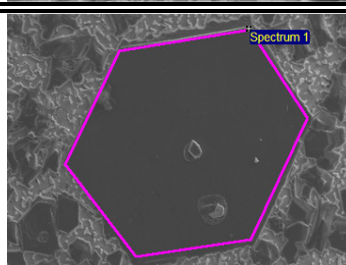
	Element	Atomic%	Detected Area	Note
Spot 1	B	84.00		Experiment condition: purity:99.9% boron, 99.99% copper; pNB coated graphite crucible; Al_2O_3 reactor tube; 10^{-6} torr minimum pressure; dissolved copper boron at 1350°C for 5 hours, reduced the temperature from 1100°C to 960ºC in 90 hours for boron precipitation.
	Cu	16.00		
	Totals: 100			
Spot 2	B	99.43		
	Cu	0.57		
	Totals: 100	**CuB$_{174}$**		
Spot 3	B	99.38		All the elemental analysis was conducted on the free surface of the alloy. The analysis result of spot 1 indicates that even at the "blank" area, the boron concentration was high. At spot 2, there is a piece of black crystal, possibly incompletely dissolved β-boron.
	Cu	0.62		
	Totals: 100	**CuB$_{160}$**		
Spot 4	B	99.26		
	Cu	0.74		
	B	99.26		
	Totals: 100	**CuB$_{134}$**		
Spot 5	B	99.56		The crystals at spot 3 to 6 were transparent well-faceted, red boron crystals. Further characterization is reported in the next section.
	Cu	0.44		
	Totals: 100	**CuB$_{226}$**		
Spot 6	B	99.46		"CuB$_x$" indicates the atomic ratio of boron to copper
	Cu	0.54		
	Totals: 100	**CuB$_{184}$**		

Table 4.8 collects the results of elemental analysis of a copper-boron alloy with well-faceted, transparent red crystals in various shapes. The impurities present and their concentrations were much lower than the sample characterized in the Table 4.7. The atomic ratio of boron to copper was also indicated in this table, and the concentration of copper in the boron is negligible. Consider that these crystals were embedded in the copper ingot when EDS was conducted; it was possible that the copper signal was due to the electron beam penetrating the boron crystal. Table 4.9 summarized the results of elemental analysis of a series of red crystals in different samples, especially, for red crystal #4 which was a small crystal that grew on top of a big red crystal (Figure 4.30). The concentration of boron is almost two times higher than red crystal #1 which is a thin rhombohedral boron crystal (Figure 4.31 and Figure 4.32), this data can be served as a supporting evidence of our proposition-the copper signal is due to the penetration of electron beam through boron crystal.

Table 4.9 The ratio of boron in various red boron crystals. (The crystals were collected from different copper-boron alloys which were prepared under different conditions).

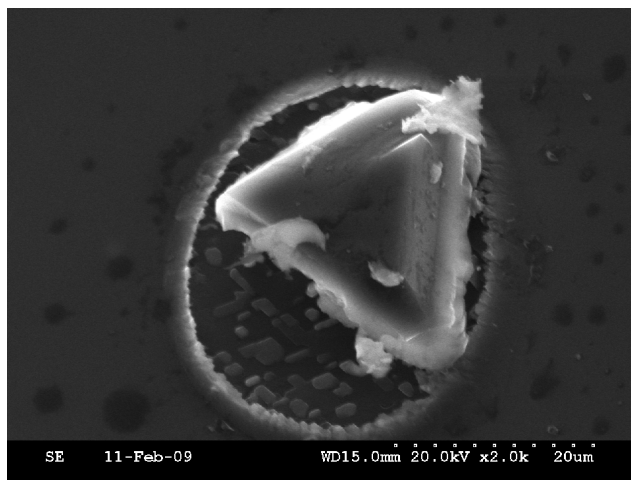| Red Crystal	Elements	Weight%	Atomic%	Cu/Boron(atomic number ratio)
1	B	94.00	98.93	$CuB_{92.5}$
	Cu	6.00	1.07	
2	B	93.11	97.81	$CuB_{117.8}$
	Cu	4.62	0.83	
3	B	96.71	99.42	$CuB_{171.4}$
	Cu	3.29	0.58	
4	B	97.67	99.60	CuB_{249}
	Cu	2.33	0.40	
5	B	96.47	99.37	$CuB_{171.3}$
	Cu	3.30	0.58	
6	B	96.95	99.47	$CuB_{187.7}$
	Cu	3.05	0.53	
7	B	96.37	99.36	CuB_{155}
	Cu	3.63	0.64	

Figure 4.30 SEM image of a triangle-shaped small red crystal grew on top of another crystal.
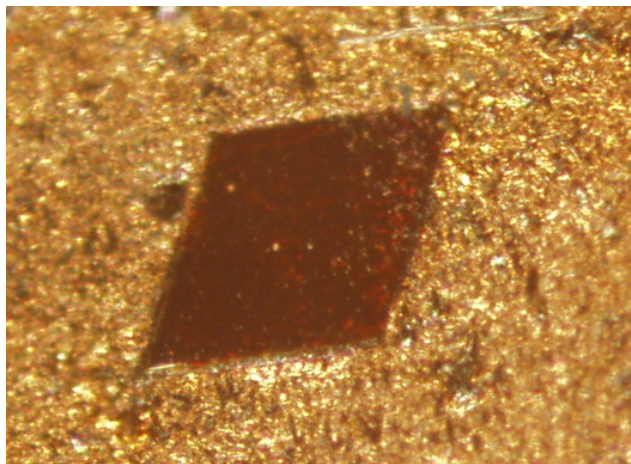
Figure 4.31 Optical Micrograph of a rhombus-shaped red boron crystal, the pattern from the copper matrix can be seen through this crystal.
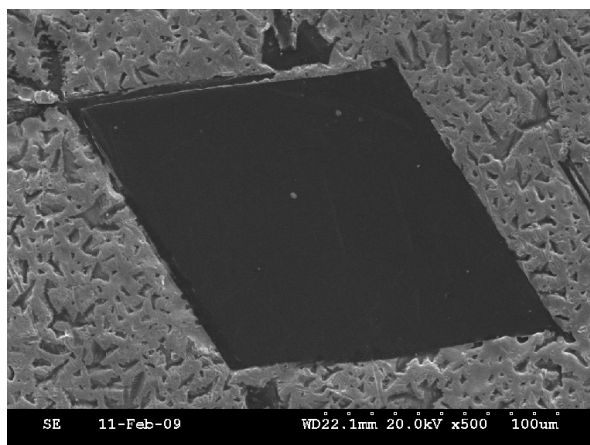
Figure 4.32 SEM image of the same rhombus-shaped red crystal as indicated in figure 4.29.

71

4.1.2.2 The results of Raman analysis

Figure 4.33 shows a typical Raman spectrum taken from the red boron crystals grown from copper solvent. The Raman spectrum exhibits a narrow band at 528 cm^{-1}, which has been reported for alpha-rhombohedral boron (α-B) crystals [60] [64] [65]. This mode has been attributed to the rigid rotation of boron icosahedra and has E_g symmetry [65]. Broad features at 694 and 930 cm^{-1} are related to the vibrational modes of the icosahedra and have A_g symmetry [64, 65]. Additional features with frequencies at ~375, ~820, ~973, and ~1065 cm^{-1} are also observed, indicating the existence of other phases or impurities. A plausible candidate will be beta-rhombohedral boron (see e.g. Richter *et al.* [61]). However, a more detailed study has to be carried out in order to fully understand the observed optical properties and the growth mechanism.
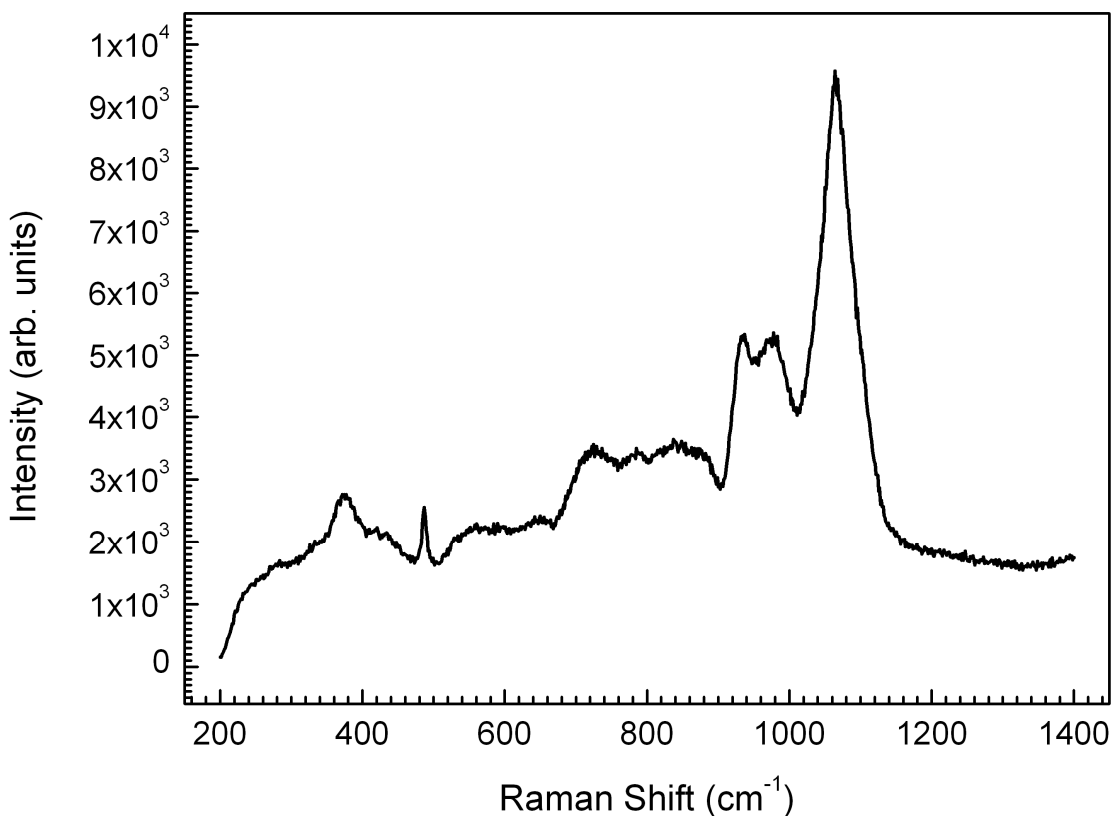
Figure 4.33 Raman spectra of a red boron crystal grown from a boron-copper solution (growth condition: 99.9% boron, 99.99% copper; pBN coated graphite crucible; Al$_2$O$_3$ reactor tube; 10^{-6} torr minimum pressure; dissolved copper boron at 1350°C for 5 hours, then reduced the temperature from 1100°C to 960°C in 90 hours for boron precipitation).
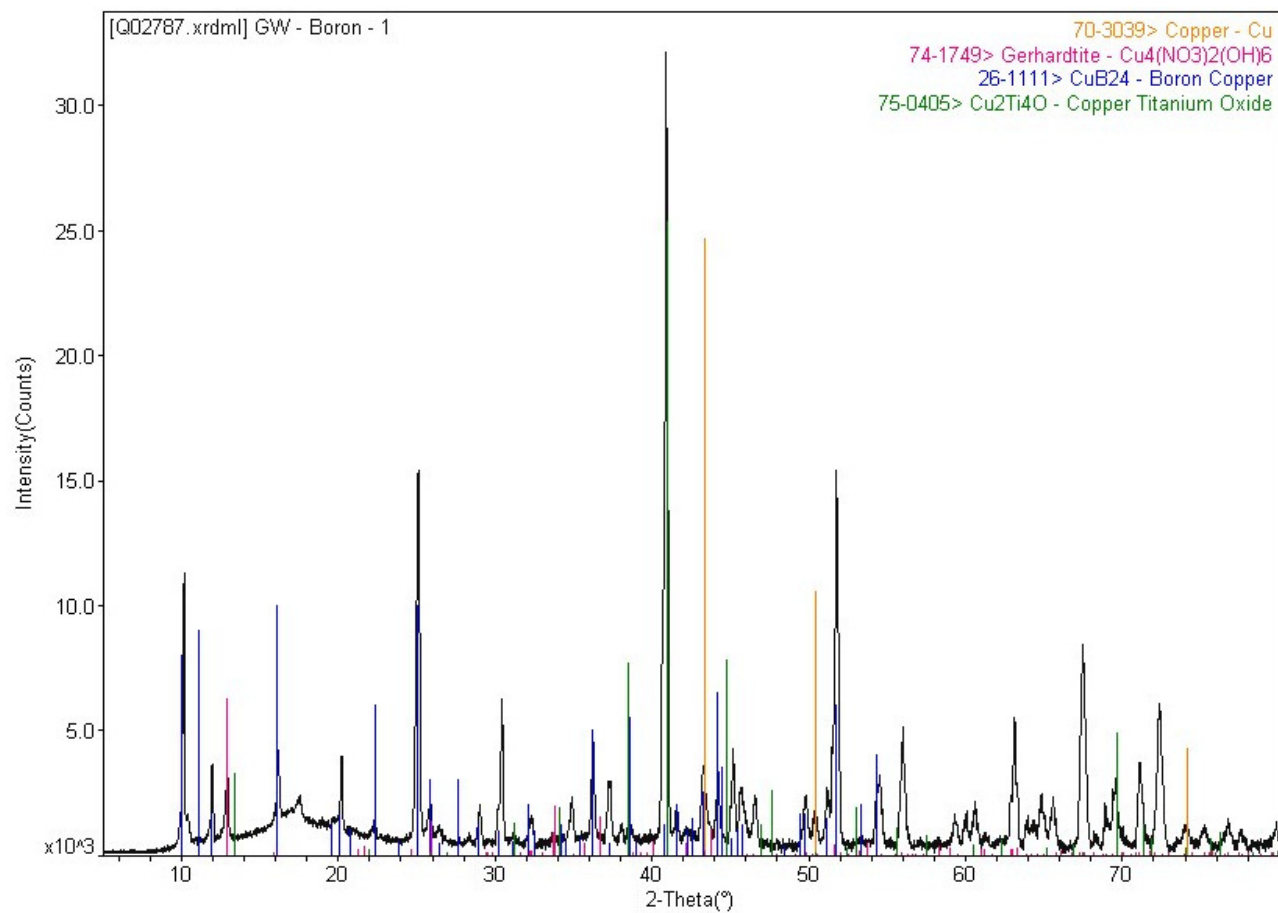
Figure 4.34 XRD pattern of the boron crystals prepared by solution growth with copper (The sample for XRD analysis was prepared by etching away the copper matrix, in this sample red boron crystals were observed on the surface of the copper-boron alloy, the growth condition for this sample is the same as indicated below Figure 4.33).

73
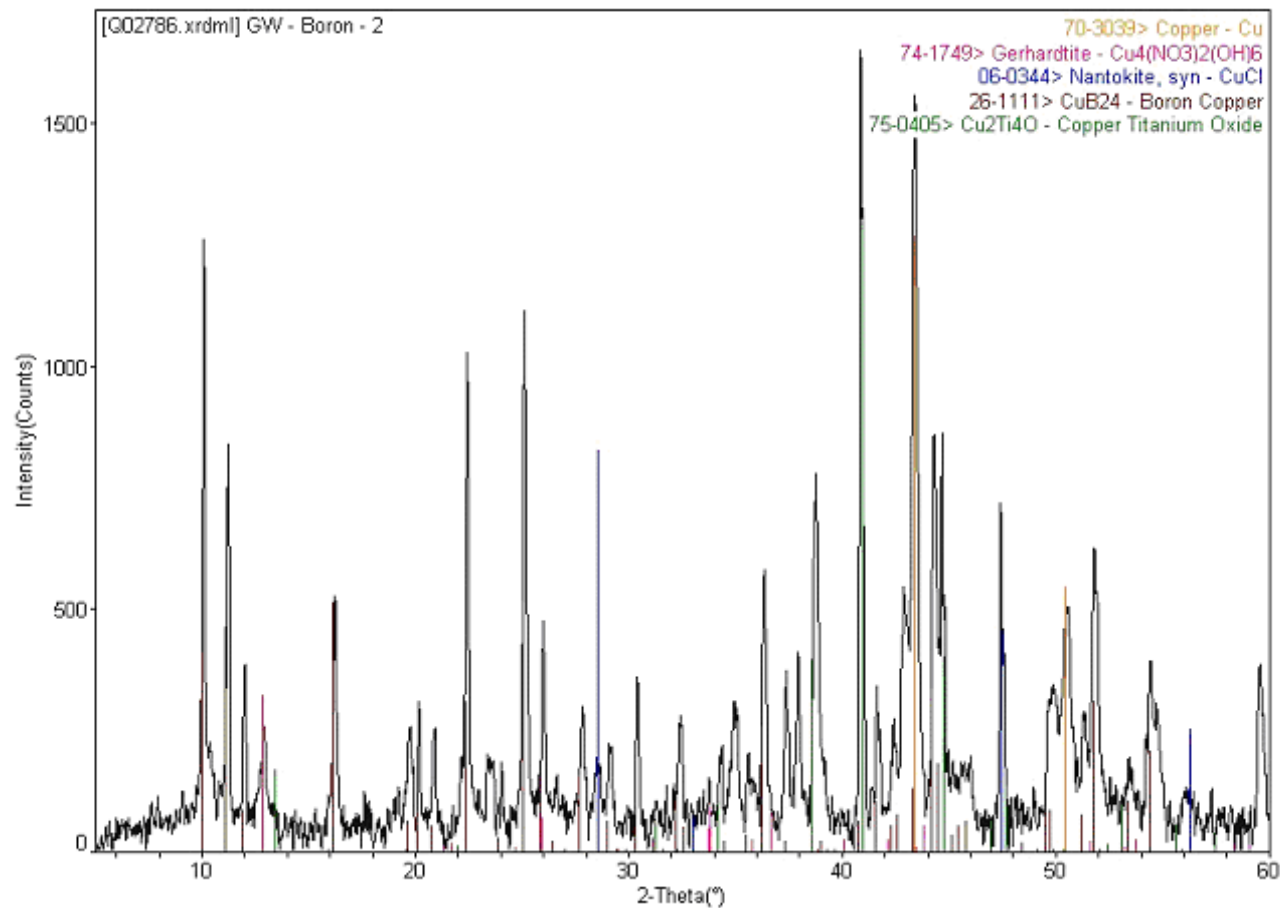
Figure 4.35 XRD pattern of the boron crystals prepared by solution growth with copper(This sample was produced by annealing copper-boron at 1350°C for 5 hours, and reducing the temperature from 1100°C to 960°C for 90 hours. The minimum pressure for preparing this sample was a little bit high (~9×10^{-4} torr), only black crystals were observed on the surface of this copper-boron alloy).

The presence of α-B or even β-B could not be confirmed by x-ray diffraction (Figure 4.34, Figure 4.35). Depending on the samples, the patterns most closely match those reported for copper borides $Cu_{4.5}B_{105}$ or CuB_{24}.

4.1.3 Conclusion and Future Work of Solution Growth from a copper Flux

The results of the boron-rich crystal growth from a copper-boron flux appear to be conflicting: the optical micrograph and Raman spectroscopy, indicate the existence of α-B, elemental analysis indicate that the red crystals were pure boron. However, the pattern of x-ray diffraction could not confirm the formation of α-B, instead, copper boride (CuB_{24}) was produced.

As summarized in Chapter 2, the formation of copper boride from a copper-boron flux has been controversial. More research groups have reported the formation of copper boride than have concluded that copper boride is not produced from a boron-copper solution. Based on the results of our research, several conclusions can be made.

(1) Copper boride was the main product: Copper boride was produced from the copper boron flux, and based on the evidence of micrograph and X-ray diffraction analysis, the yield of copper boride was large (the number of black crystals was much larger than the number of red boron crystal), and the signal of copper boride are strongest.

(2) α-B was formed: based on the results of elemental analysis, Raman spectroscopy, and the color of the crystals, α-B was produced. The absence of α-B in x-Ray diffraction analysis is probably due to the low atomic number of boron [7], in addition the amount of α-B is small, thus the signal of x-ray diffraction of α-B is weak compared with copper boride. In fact, Wald [44] also reported the similar phenomena in his study: α-B was appeared in the micrographs, but the appearance of α-B couldn't be confirmed by X-ray diffraction analysis.

(3) The phase diagram for Cu-B is not a simple eutectic. Some researchers [43] [51] concluded that the Cu-B diagram is a simple eutectic type because they didn't produced any copper boride in their research. However, based on the results of our experiments copper boride can be formed at certain a certain range of boron-copper ratio.

(4) The growth of α-B is greatly influenced by the impurity concentrations: depending on the results of elemental analysis, for the low purity samples (low purity source material, low purity atmosphere, contamination of crucible) fewer or no red crystals were produced.

To further investigate the α-rhombohedral boron crystal growth condition and growth mechanism, an annealing experiment would be useful: anneal copper and boron around their eutectic composition and temperature for a longer time (e.g. 2 month). The longest annealing time of our experiments was about 100 hours; in contrast, Wald [44] annealed his sample for at least 21 days. By comparing the yield of red crystals at different annealing time, it may be possible to determine if the low yield of red boron crystals is due to slow kinetics or thermodynamic limitations.

4.2 The Platinum-Boron System

4.2.1 The results of various characterization methods

Three experiments were conducted to prepare α-B from a platinum flux. For the first experiment, boron and platinum was melted at ~1800 °C for 5 hours to form a liquid phase, and then annealed at 900°C for 30 hours to precipitate α-B crystals.

A significant amount of slags were observed (Figure 4.36) in the first experiment. When examined under higher magnification by SEM (Figure 4.37 and Figure 4.38), three material shapes were observed: prisms, sharp narrow needles, and fine irregular deposits. Table 4.10 presents the elemental analysis of the crystals: the main elements detected were boron and oxygen. The minimum pressure for this experiment was relatively high (~10^{-4} torr) thus the oxygen may have originated growth atmosphere. Another source of contamination was the sample holder which is a customer-machined hot-pressed boron nitride crucible, there was loosen boron nitride particles in the crucible and trace of various impurities introduced by the machine.

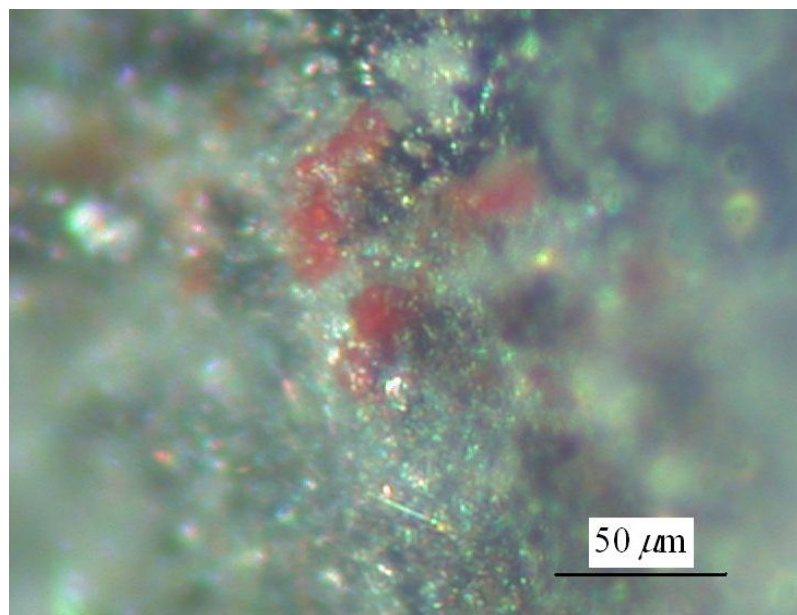**Figure 4.36 Optical Micrograph (200×, reflected white light), the white and black particles are slags, the red crystal-like spots remained unknown. (Platinum-boron solution growth, Sample #1, minimum pressure ~10^{-4} torr, annealing at 1800 for 5 hours, then annealing at 900 for 30 hours.)**
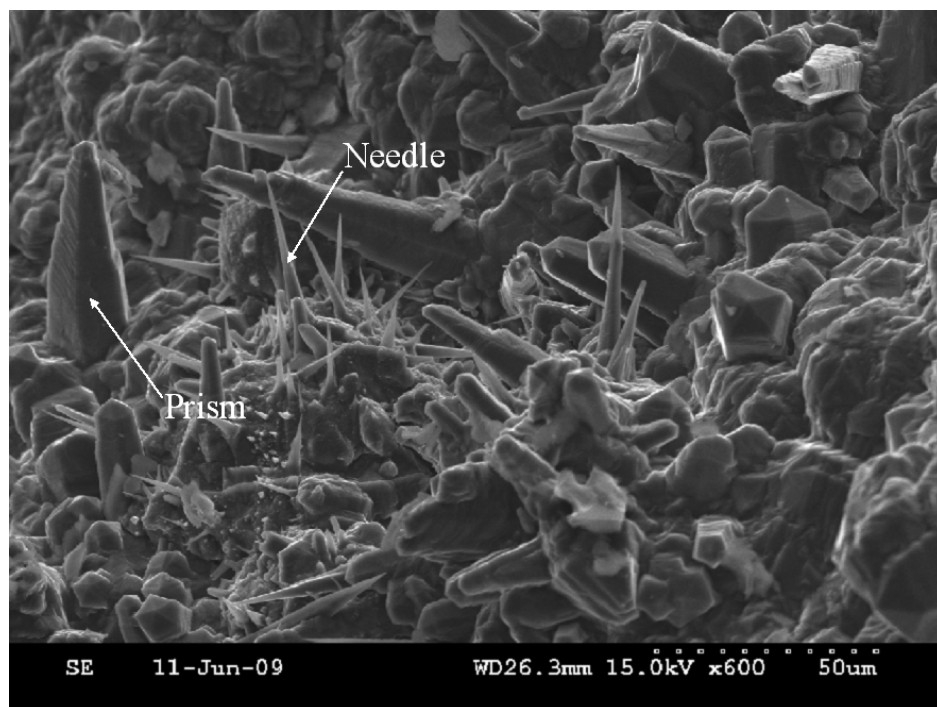

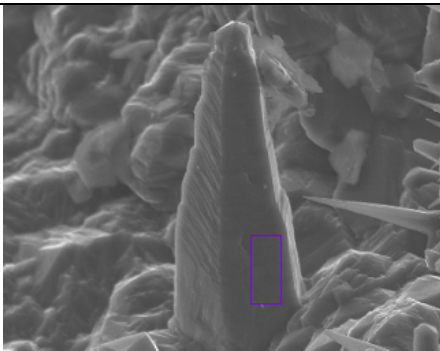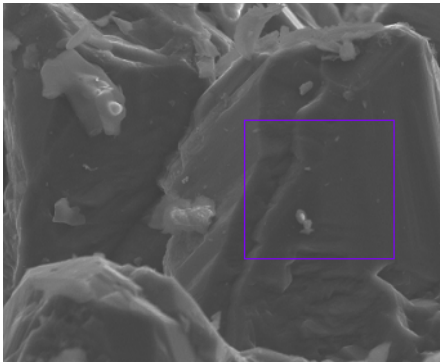**Figure 4.37 SEM image of the platinum-boron solution growth Sample #1.**
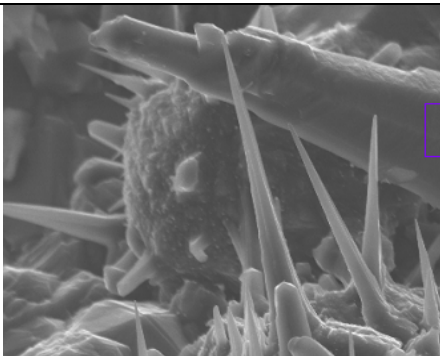
Figure 4.38 SEM image of the platinum-boron solution growth Sample #1 (different area).

The sample was cleaned in concentrated nitric acid and hydrochloric acid. This removed some but not all of the slags. Some of the slags were very stubborn, which can not be etched away by either HCl or HNO_3. Then this sample was annealed at 900°C for another 30 hours. This sample is identified as Pt-B Sample #2. The surface of the re-annealed sample was dull; it seemed that the grain size of the slags was smaller and more uniform. And the red spots which were observed after the initial run couldn't be found anymore.

The elemental analysis indicates that the surface of the sample was covered with boron nitride crystals which probably due to the interaction of the melt with the crucible. Since the second run was operated at low temperature, it was possible that both boron oxide and boron nitride were formed at the first run, but the amount of boron oxide was much more than boron nitride (and probably, the boron nitride was covered by boron oxide). Thus only boron oxide was detected by EDS. However, boron oxide were removed by the acid, while boron nitride remained, thus in the second run of our experiment the boron nitride crystal was grown.

78

Table 4.10 Elemental analysis on the different spot of Pt-B Sample #1.

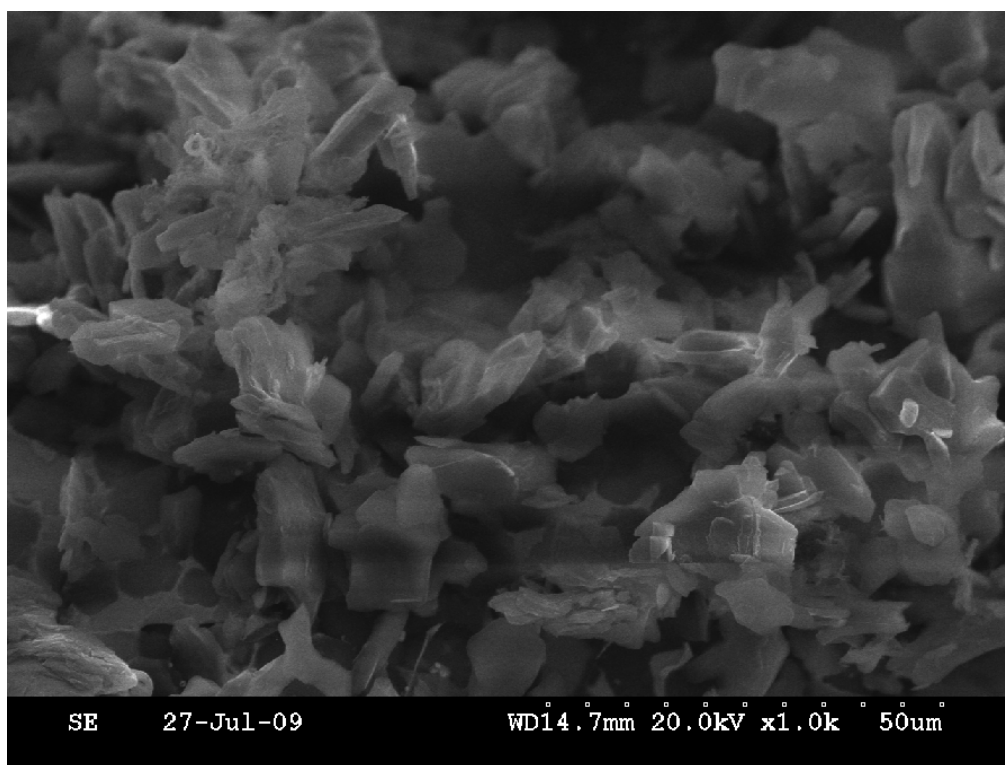| Spot	Element	Atomic%	
	B	97.09	
	O	2.91	
	Totals	100	
	B	97.18	
	O	2.77	
	Si	0.02	
	Ca	0.02	
	Totals	100	
	B	97.94	
	O	2.06	
	Totals	100	

Figure 4.39 SEM image of Pt-B Sample #2. This sample was prepared by annealed the etched Sample#1 at 900°C for another 30 hours.
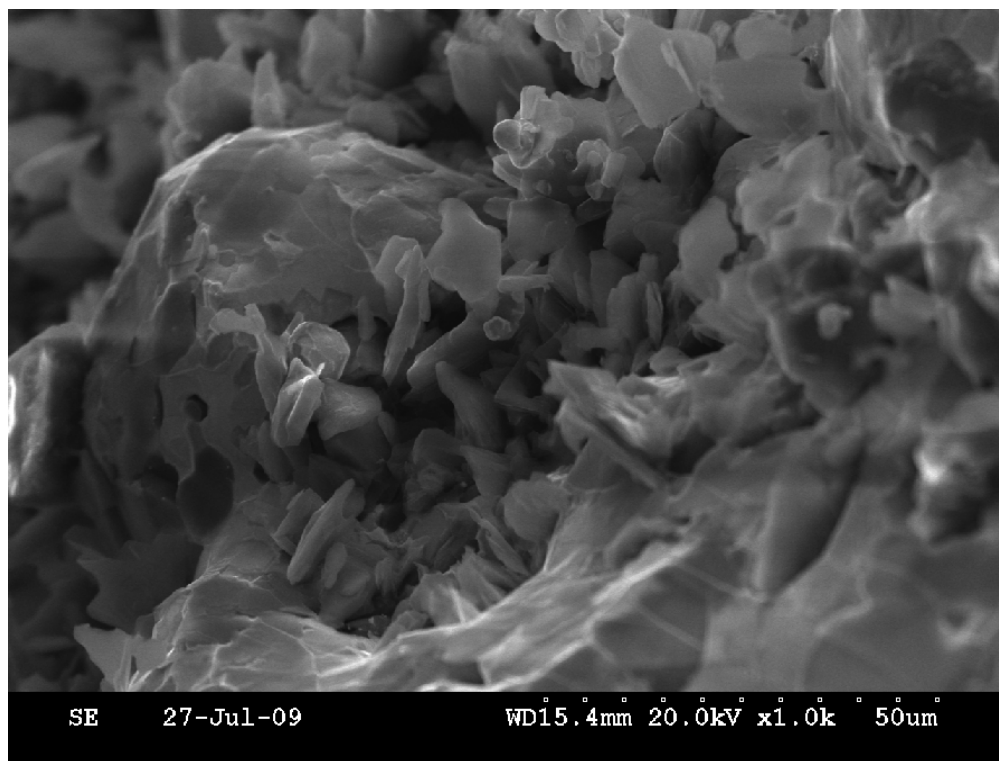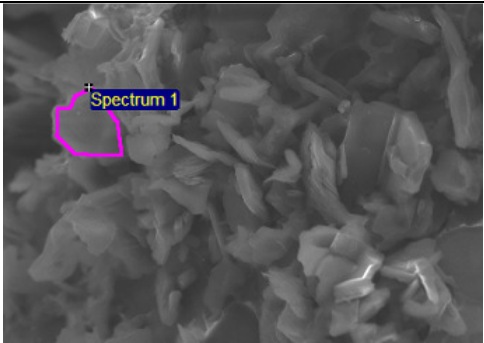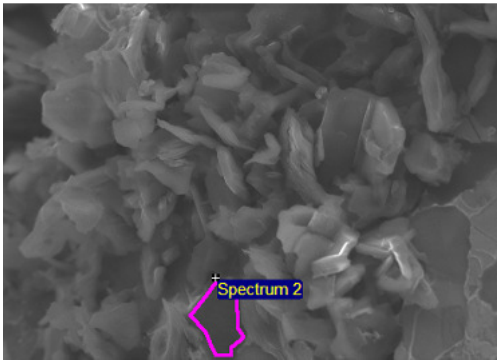
Figure 4.40 SEM image of Pt-B Sample #2(different area).

Table 4.11 Elemental analysis on the different spot of the Pt-B Sample #2.

Spot	Element	Atomic %	
1	B	43.95	
	N	55.93	
	Pt	0.12	
	Totals	100	
2	B	47.48	
	N	51.44	
	Pt	1.08	
	Totals	100	

This sample was also analyzed by x-ray diffraction. And the resulting pattern is in Figure 4.41. The XRD pattern indicates that β-rhombohedral boron, platinum boride and boron nitride were present. No α-B was detected. As mentioned before, the source of boron nitride is the crucible material; according to the phase diagram of Pt-B, the formation of platinum boride is expectable; and β-rhombohedral boron could come from the source material: the diffusion rate of boron in platinum was low, even the total annealing time was 65 hours, lots of source materials (β-B) were incompletely dissolved.
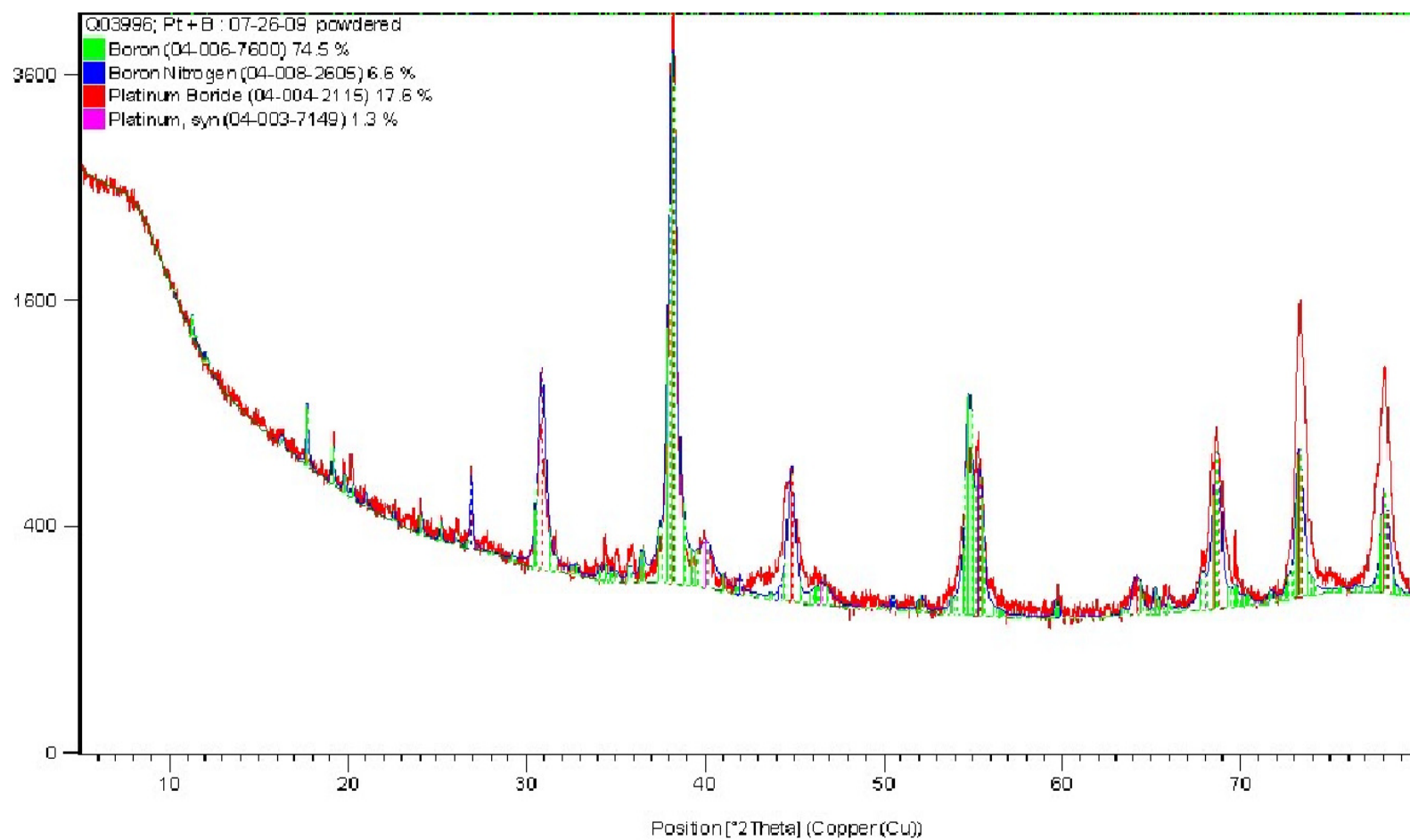
Figure 4.41 Figure 4.41 X-ray diffraction of Pt-B Sample #2. As indicated in the upper left corner of this figure, the strength of the signals is: beta boron>boron nitride> platinum boride.

In the third experiment, 48.96 mol % boron and 39.60 mol % platinum were loaded in the graphite furnace. This experiments were operated at lower temperature (annealed at 1200°C, seven days) to reduce the interaction of the crucible materials and the melt, in addition, the hot pressed boron nitride crucible was soaked in ultra sonic cleaner with water, acetone, and ethanol each for one hour to removed the impurity and the loosen boron nitride particles.

The sample prepared in the third run was a shiny platinum ball embedded with black crystals (Figure 4.42). This suggests that the contamination on this sample was less compared with the sample in first and second run. The results of elemental analysis are presented in Table 4.12. It is obvious that the contamination of oxygen was still considerable; however, the interaction of the melt between the crucible was greatly reduced.

Figure 4.42 . The SEM image of the Pt-B Sample #3, the bright area is metal, and the dark spots are boron areas.

Figure 4.43 SEM image of Pt-B Sample #3: the boron area under 1000× magnification.
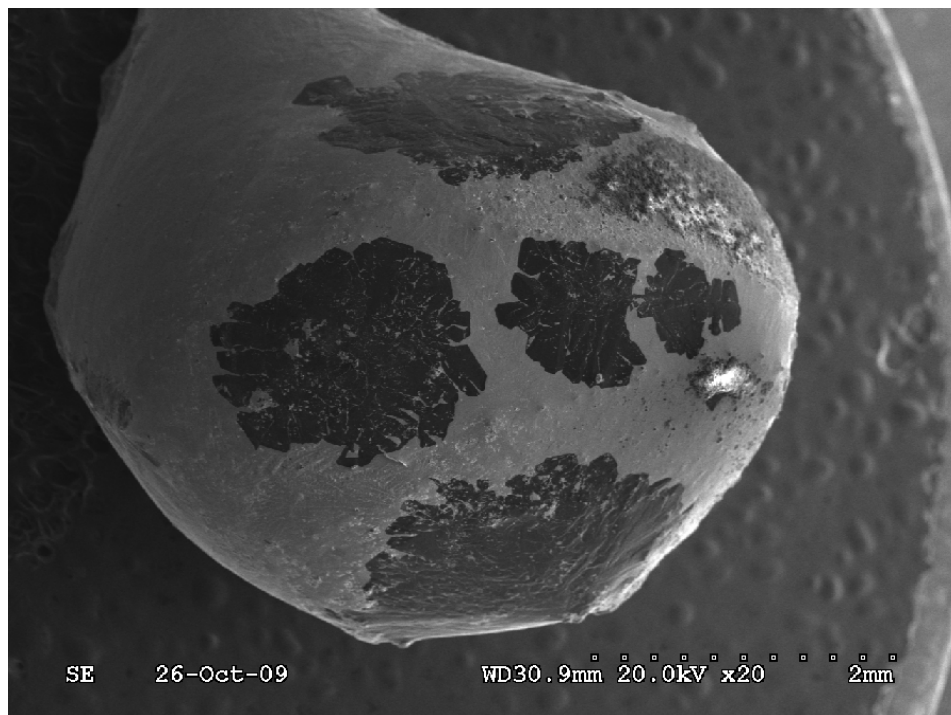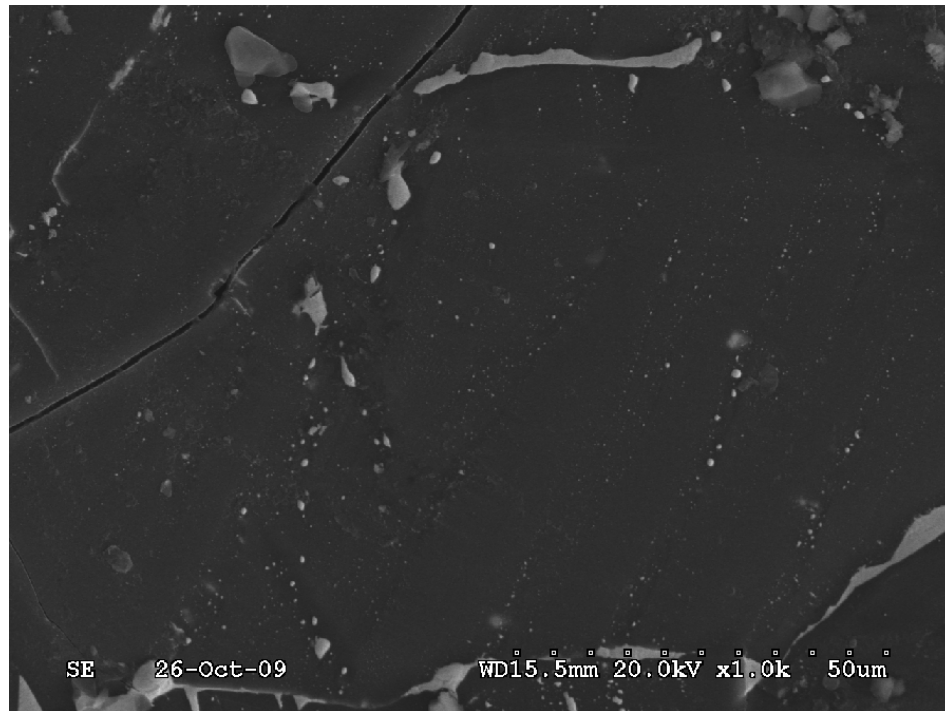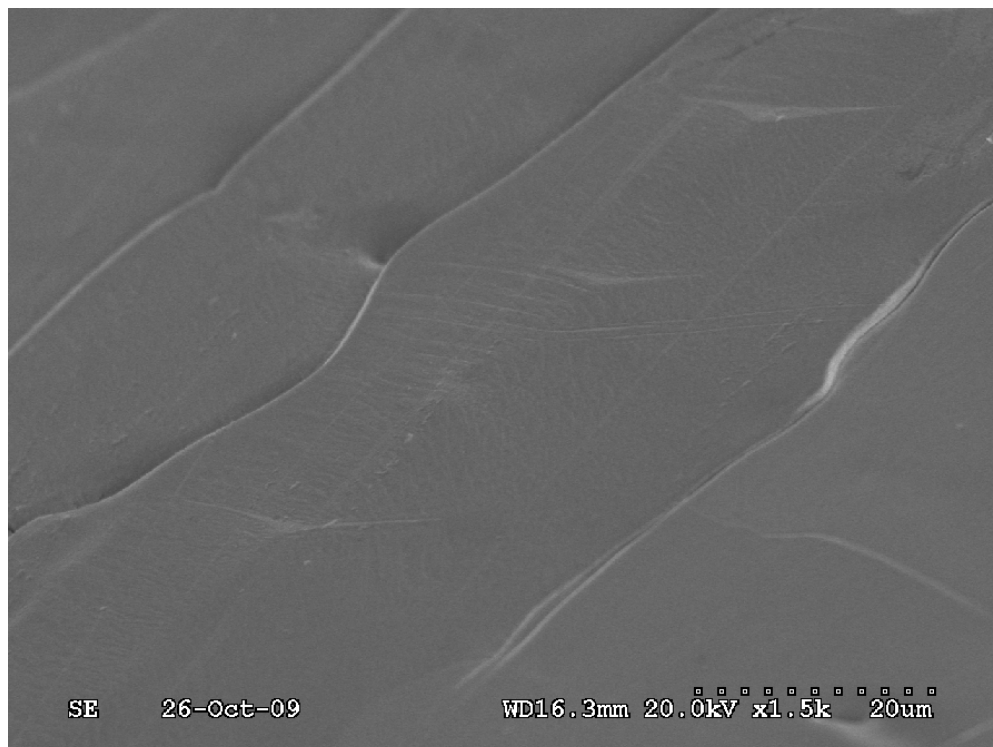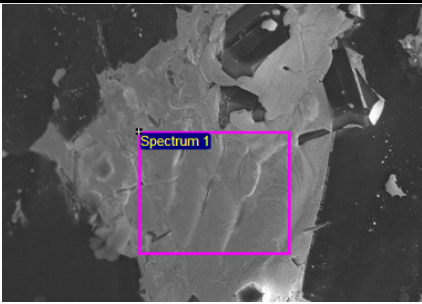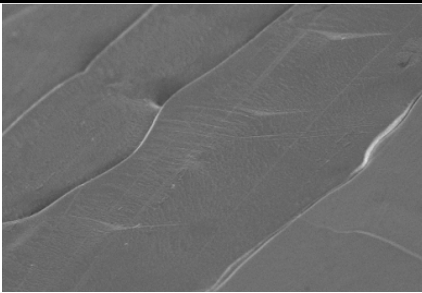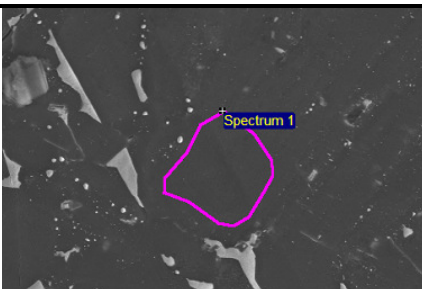

Figure 4.44 SEM image of Pt-B Sample #3: the metal area under 1000× magnification.

Table 4.12 Elemental analysis on different areas of Pt-B Sample #3.

Spot	Element	Atomic%	Detected Area	Note
1	C	54.67		Spot 1 is the metal area in the middle of the boron area; Spot 2 is the metal area relatively far from the boron area;
	N	22.82		
	O	9.78		
	Si	0.62		
	Pt	12.10		
	Totals			
2	C	72.19		Spot 3 is t he boron area.
	O	9.03		
	Si	0.85		
	Pt	17.92		
	Totals			
3	B	99.95		
	Pt	0.05		
	Totals	100		

4.2.2 Conclusion and future work

Compared with the copper-boron system, one disadvantage of solution growth α-B from platinum flux is evident: due to the high melting point of platinum, the experiments have to be conducted at a relatively high temperature (~1800°C) to form a liquid phase of platinum in a short experiment time (5 hours), or have to annealed the sample at low temperature (1200) for a long time (7 days). Thus higher chance of side reaction could be occurred between the melt and its circumstance due to the high operation temperature.

The complexity of the phase diagram of boron-platinum is another disadvantage, based on the results of our experiments, no red crystals were observed, while the production of platinum boride was confirmed by XRD.

In our future work, further characterization (Auger, TEM) will be conducted on our samples. To prevent the contamination from the crucible, the materials of the crucible will be switched from hot pressed boron nitride to pyrolytic boron nitride; the experiments will be run at relatively low temperature (1200°C) for a longer time (e.g. 30 days) to form a uniform platinum-boron solution.

4.3 Preparing Boron Crystals by Vapor Liquid Solid (VLS) Methods

4.3.1 Results of Various Characterization Methods

A series diborane decomposition experiments were conducted on various substrates seeded with metal particles, in the presence of hydrogen. The temperature applied for the VLS experiments were in the range of 800°C to 1000°C; the flow rate of hydrogen was 2 slm, and the mole fraction of diborane was 2%-2.5%. The results of most experiments were similar; the seeded metal particles (platinum, gold) significantly promoted the boron nucleation as seen by clusters of boron at the sites where the metal particles were place. Figure 4.45 to 4.50 illustrated the typical morphology of our samples. Many clusters of boron needles formed on the substrates. The length of the needles varied from several microns to about one hundred microns, and the diameter of the needles (near base) was about 5μm. The result of boron deposition on tantalum was unusual: the tantalum substrate was decomposed during the experiment.

Elemental analysis was conducted on the different areas of a sample which was prepared with silicon substrate seeded with platinum particles. As indicated in Table 4.13, the needle was mainly composed of boron with a negligible amount of silicon which was probably due to the electron beam penetrating the boron needle. Boron was also detected in the board areas, away from the platinum seed particles. Thus the metal particles promoted the formation of the needle clusters.

Raman analysis was also carried out on the samples, and the results are shown in Figure 4.51. This pattern did not match any reported literature. An x-ray diffraction was taken from a sample with a silicon substrate and covered with a thin layer (500nm) of gold; the results are presented in Figure 4.52. In this case, the crystal needles were actually silicon boride. Buddery

and Welch [66] reported that silicon boride can be synthesized at 1000°C~1200°C in an evacuated silica tube by mixing elemental silicon and boron. Thus it was highly possible that the needle clusters are silicon boride.
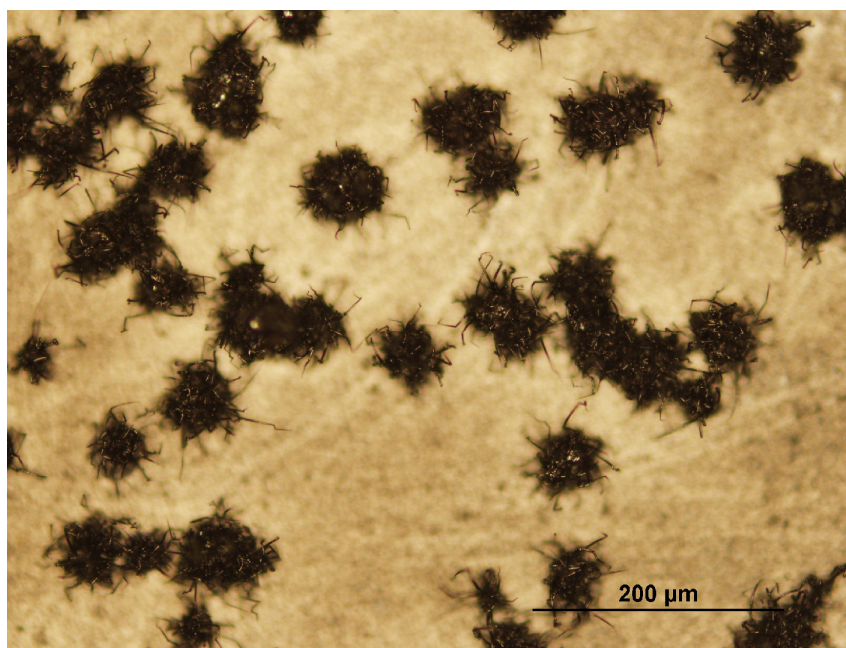
Figure 4.45 Optical micrograph (reflected white light 100×), of clusters of boron needles on a silicon substrate. The clusters tended to grow on the platinum-seeded sites.
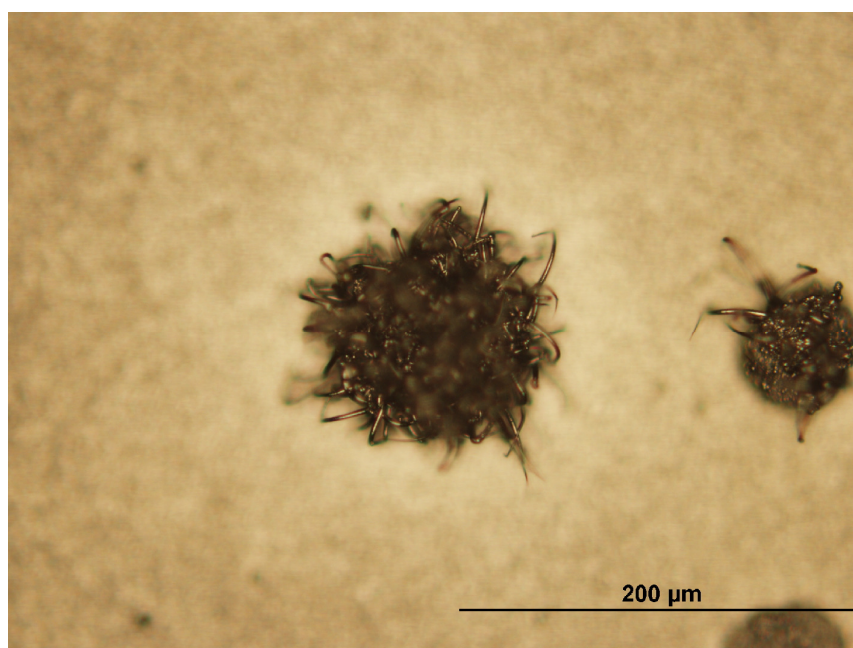
Figure 4.46 Optical micrograph (reflected white light 200×) of clusters of boron needles (the same sample as indicated in Figure 4.45 under higher magnification).
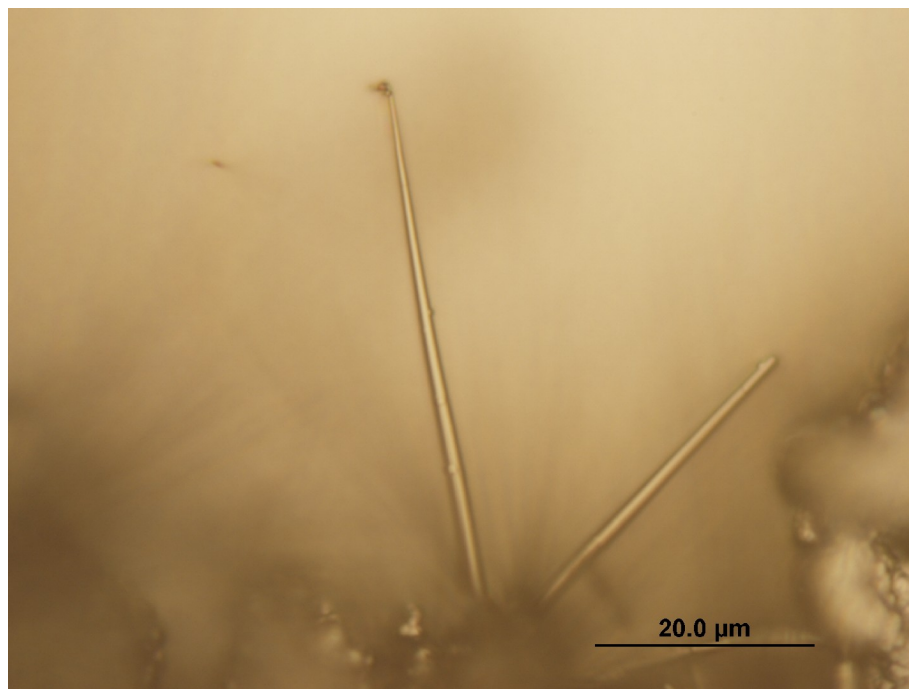
Figure 4.47 Optical micrograph (reflected white light 1000×) of the needle-like boron crystals from the same sample as indicated in Figure 4.45.
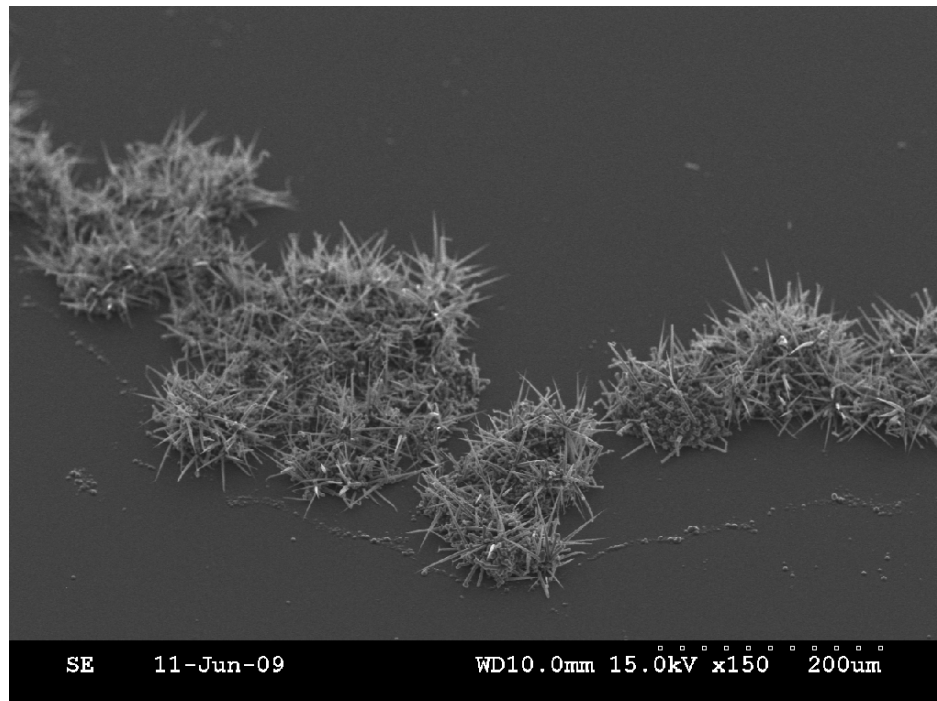
Figure 4.48 SEM image of boron needle clusters on the silicon substrate (the same sample as indicated in Figure 4.45, 150× magnification).
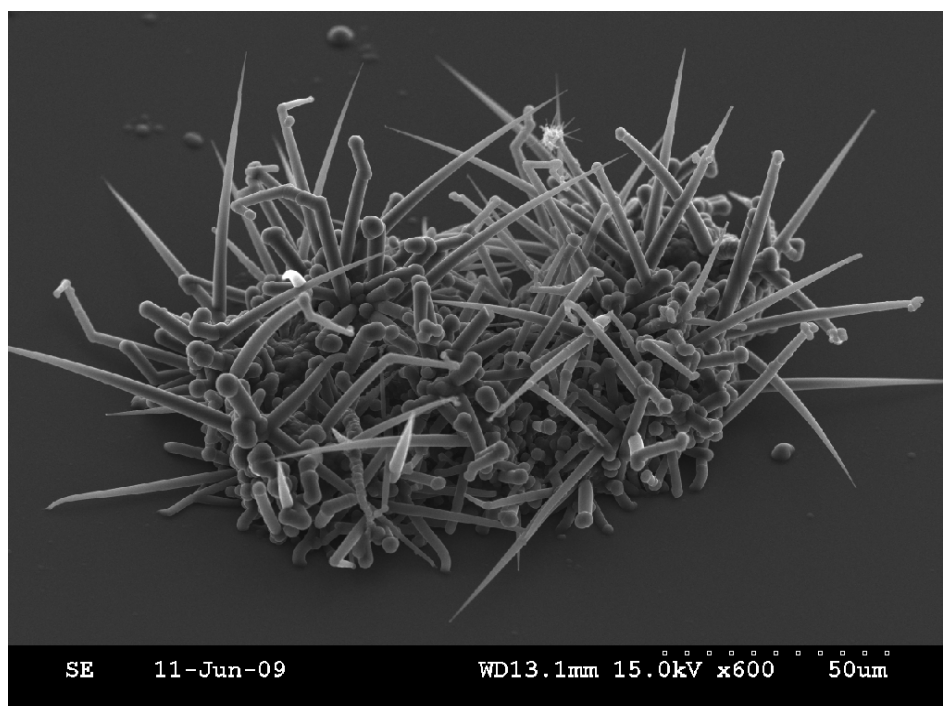
Figure 4.49 SEM image of boron needle clusters on the silicon substrate (the same sample as indicated in Figure 4.45, 600×magnification).
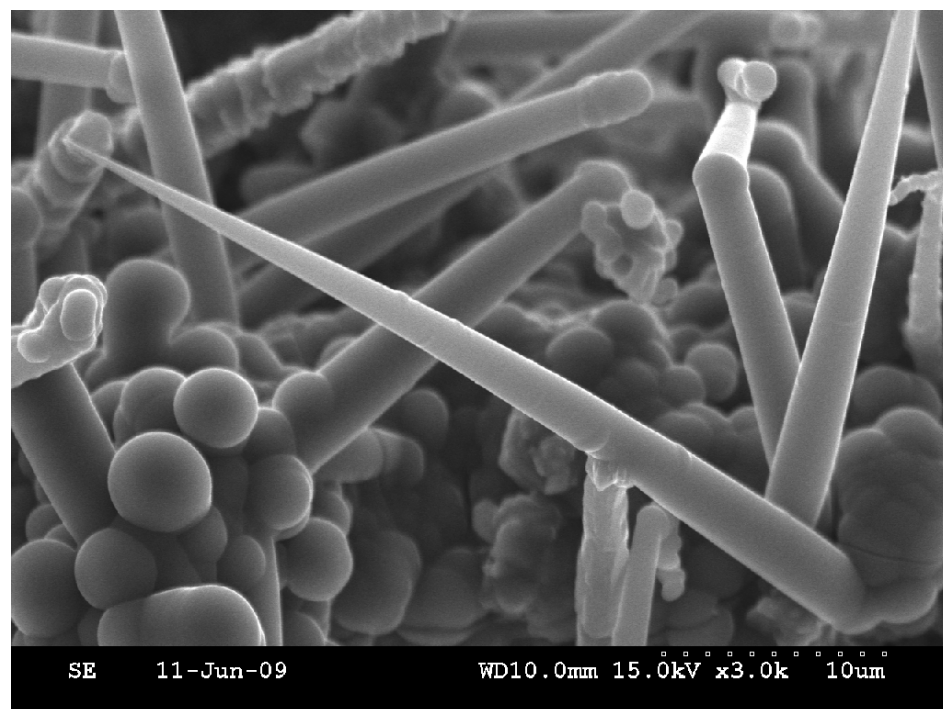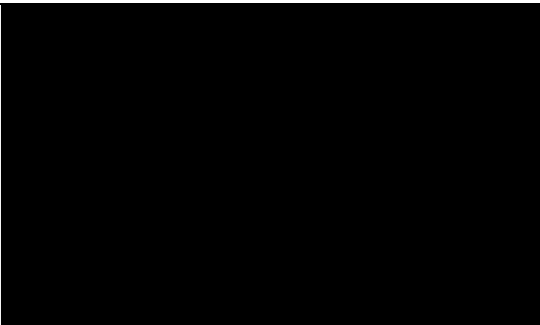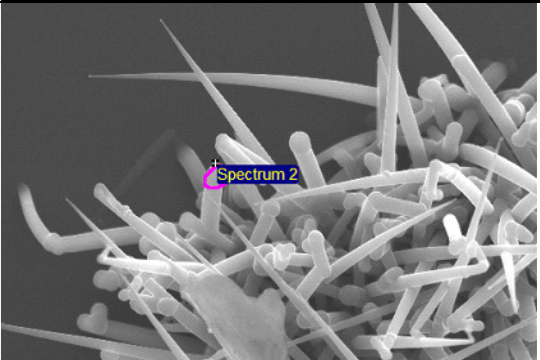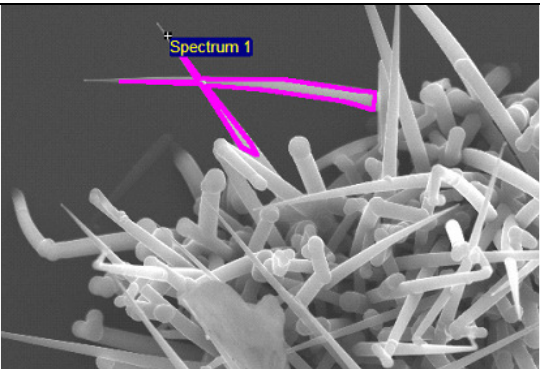
Figure 4.50 SEM image of boron needles under 3000× magnification (the same sample as indicated in Figure 4.45).

Table 4.13 Elemental analysis taken from different areas of a silicon substrate initially seeded with platinum particles, then subjected to boron deposition at 1000°C for 60 minutes.

Element	Atomic%	Detected Area	Note
B	97.2		The board areas without metal particles
Si	2.8		
Totals	100		
B	99.8		The tip of the needle crystal
Si	0.3		
Totals	100		
B	99.5		
Si	0.5		The body of the needle crystal
Totals	100		

Figure 4.51 Raman spectra from a sample prepared with silicon substrate seeded with platinum particles. (Taken from three different positions on the sample).
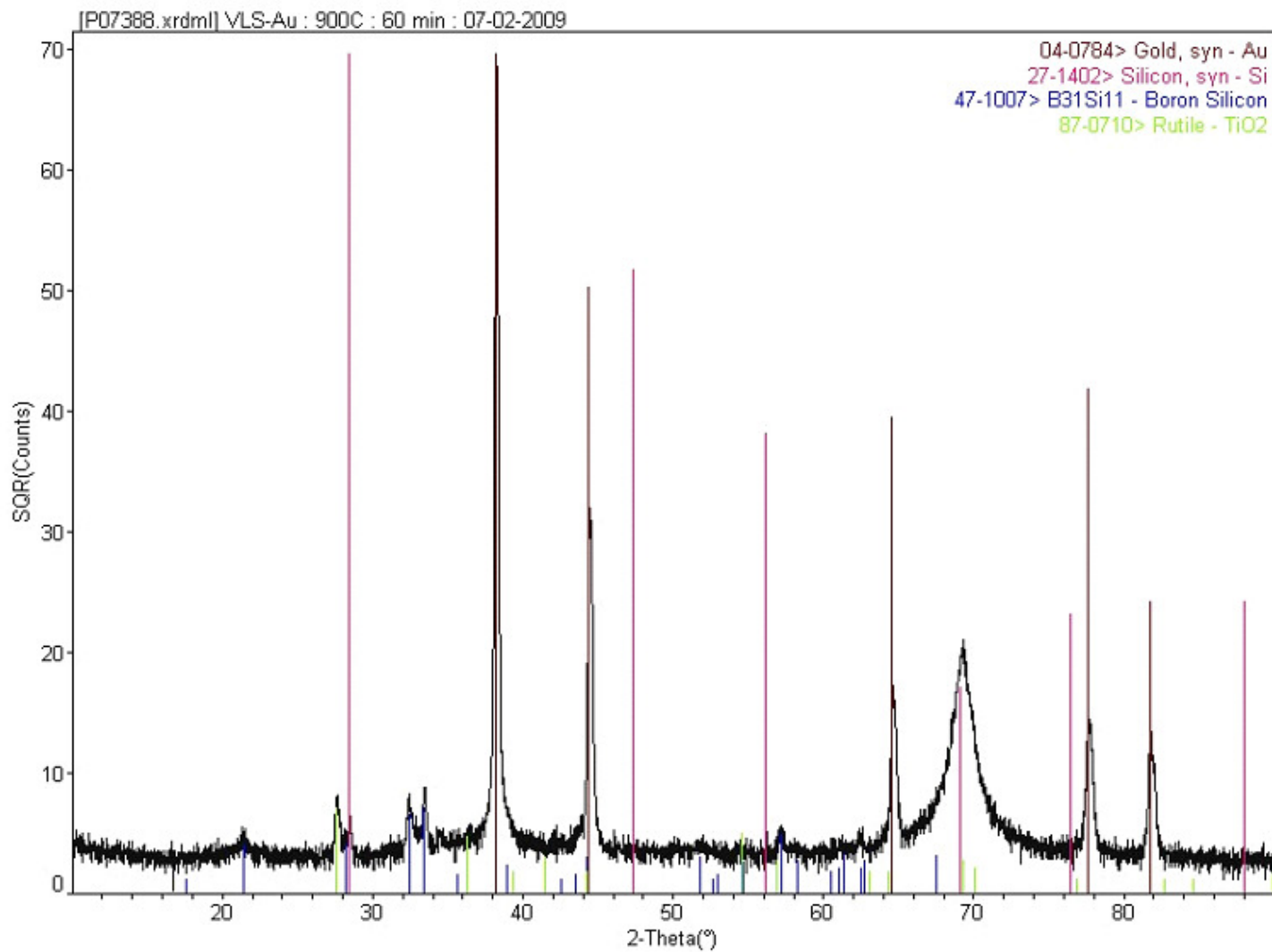
Figure 4.52 X-ray diffraction from a silicon substrate initially covered by a thin layer (500nm) of gold film, then subjected to boron deposition at 1000°C for 60 minutes.

4.3.2 Conclusions and future work

In our experiments, we compared the differences between boron deposition on substrates seeded with metal particle and blank substrate. Clearly the metal seeds promoted the formation of boron "needle crystals".

For the chemical vapor deposition experiments, over the temperature range from 800°C to 1000°C, the temperature did not have a significant impact on the growth rate or needle morphology.

X-ray diffraction analysis suggests the boron reacted with the silicon substrate to form silicon boride. To produce a pure elemental boron crystal, it may be necessary to deposi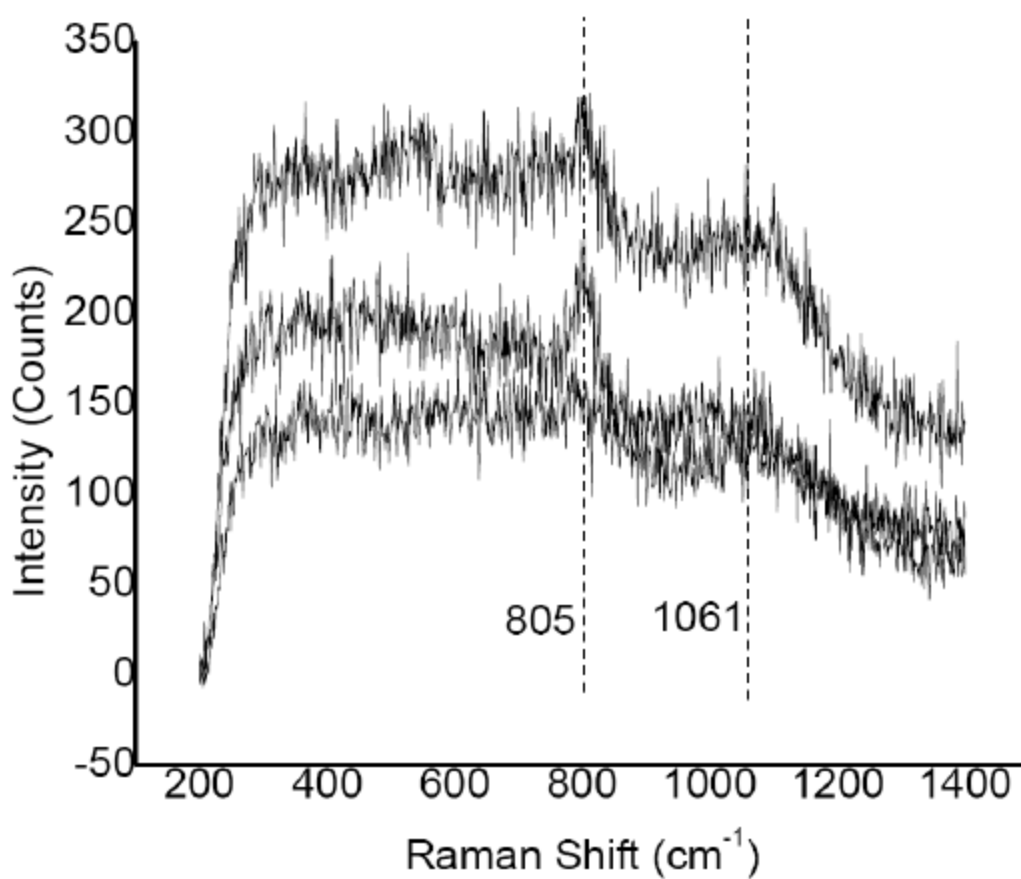t boron for a longer time (e.g. 10 hours) to form a layer of boron compound film first, then let the boron crystals grow on the boride.

In previous studies, tantalum was most frequently used as the substrate in the pyrolysis of boron halide. Some scientists reported that significant reactions of tantalum occurred in the presence of hydrogen and boron trichloride.In our experience it was obvious that tantalum is not suitable as a substrate when diborane and hydrogen are used since tantalum substrate was decomposed during the experiment.

References

1. Dong Li, Young-Nian Xu, and W.Y.Ching, Physical Review B, **45**, 5895 (1992).

2. G.V.Tsagareishvili and F.N.Tavadze, Prog.Crystal Growth and Charac. **16**,341 (1988).

3. McGraw-Hill Encyclopedia of Science and Technology, 10th edition, **3,** 227-228 (2007).

4. N.N. Greenwood and A.Earbsgaw, in *Chemistry of the Elements,* edited by Thomas E. Albrecht-schmitt, (Pergamon Press, Oxford, UK, 1984), p. 16.

5. W.T.M.L. Fernando, L.C. O'Brien, P.F. Bernath, J. Chem. Phys. **93**, 8482 (1990).

6. K.Q. Zhang, B.Guo, V. Braun, M. Dulick, P.F. Bernath, J. Molecular Spectroscopy, **170**, 82 (1995).

7. J. Cueilleron and F.Thevenot, in *Boron and Refractory Boride* edited by V.I.Matkovich (Springer-Verlag, New York, NY, 1977), p. 203

8. E.Yu.Zarechnaya, L.Dubrovinsky, N.Dubrovinskaia, et al., Physical Review Letters, **102**, 1 (2009)

9. David Emin, Physics Today, **40**, 55 (1987).

10. David Emin, Journal of Solid State Chemistry.**179**, 2791 (2006).

11. M. Widom, Physical Review B, **77,** 064113-1 (2008)

12. O.A.Golikova, Chemtronics, **5**, 3 (1991).

13. O.A.Golikova, Phys. Stat. Sol. (a), **101,**277 (1987).

14. T.L.Aselage,.Mat.Res.Soc.Symp.Proc. **97**, 101 (1987).

15. T.Stoto, L.Zuppiroli, J.Pelissier, Radiat.Eff. **90**, 161 (1985).

16. T.Stoto, N.Houssean, L.Zuppiroli, B.Kryger. J.Appl.Phys. **68**, 3198 (1990).

17. M.Carrard, D.Emin, L.Zuppiroli, Phys.Rev.B, **51**, 11270 (1995).

18.B.Morosin,A.Mullendore,D.Emin,G.A.SlackIn:D,Emin,T.L.Aselage,C.L.Beckel,I.A.Howard, C.Wood(Eds.),<u>Boron-rich solids</u>, American Institute of Physics, New York, p.70 (1986).

19. Akira Masago,Koun Shirai, and Hiroshi Katayama-Yoshida, Physical Review B,**73**,104102-1 (2006).

20. F.Perrot, Physical Revies B, **23**, 2004 (1980).

21. F.H.Horn,Appl. Phys. **30**, 1611 (1959).

22. M. Hebbache,Europhysics Letter, **87**,1(2009).

23. David Emin, Journal of Applied Physics, **97**, 013529 (2004).

24.D.S.McGregor, M.D.Hammig, Y.H.Yang, H.K.Gersh, R.T.Klann, Nuclear Instruments and Methods in Physics Research A, **500**, 272 (2003)

25. D.S.McGregor and S.M.Vernon, an unpublished paper available at: http://ww2.mne.ksu.edu./people/personal/mcgregor/bndetector

26. P.Rappaport, Physics Review, **93,** 246 (1954),

27. T.L.Aselage et al, United States Patent. Patent No: **US 6479919 B1**, (2002).

28. A.J.Perry,A.R.Nicoll,K.Phillips,P.R.Sham, Journal of Materials Science, **8**, 1340 (1973).

29. L. V. McCarty, J. S. Kasper, F. H. Horn, B. F. Decker, A. E. Newkirk, Journal of the American Society, **80**, 2592 (1958).

30. L.V.McCarty, D.R.Carpenter, Journal of Electrochemical Society, **107**, 38 (1960).

31. E.Ameberger, W.Dietze, in *Boron-Preparation, Properties and Application*s, edited by Gerhart K.Gaule, (New York, Plenum Press, 1965). **2**, p.1.

32. D.R.Stern and L.Lynds, Journal of the Electrochemical Society.**105**, 676 (1958).

33. A.W.Laubengayer, D.T.Hurd, A.E.Newkirk, and J.L.Hoard, Journal of American Society, **65**, 1924 (1943).

34. E.Ameberger, W.Dietze, in Boron-Preparation and Properties, Edited by Gerhart K. Gaule, (Warszawa: PWN, 1970), **3**, p. 133.

35. R.Naslain, J.Etourneau, P.Haugnmuller, in *Boron-Preparation and Propertie,* Edited by Gerhart K. Gaule (Warszawa: PWN, 1970), **3**, p. 35.

36. C.P.Talley.L.E.Line, Q.D.Overman, in *Boron-synthesis, structure and properties*, edited by J.A. Kohn, W.F. Nye, G.K. Gaule, (New York: Plenum Press, 1960), **1**. p. 94.

37. K.E.Bean, W.E.Medcalf, in *Boron-synthesis, structure and properties*, edited by J.A. Kohn, W.F. Nye, G.K. Gaule, (New York: Plenum Press, 1960).**1**, p. 48.

38. J.A.Ugai and N.E.Soloviev, in *Boron and refractory borides,* edited by V. I. Matkovich, (New York:Springer-Verlag Berlin Heidelberg,1977), p. 227.

39. W.Z.Robb, L.C.Landauer, Abst.Boston Meet.ACS, Division of inorganic chemistry April, p.53, (1959).

40. R.S.Wagner and W.C.Ellis, Applied Physics Letters, **4**, 89(1964).

41. J.P.Sitarik, W.C.Ellis, Journal of Applied Physics, **37**, 2399(1965).

42. Pavel D.Peshev, Bulgarian Chemical Communications, **24**, 235 (1992).

43. F.Wald, Electron Technology, **3**,103(1970).

44. F.Wald and R.W.Stormont, Journal of the less-common metals, **9**, 423 (1965).

45. F.Horn, Journal of the electrochemical society, **106**,905 (1959).

46. J.H.Puddery and A.J.E.Welch, Nature, **167**,362(1951).

47. F.Wald and A.J.Rosenberg.,Transactions of the metallurgical society of AIME, **233**,796 (1965).

48. T.Niemyski, W.Zawadzki. Physics Letters, **2**, 30 (1962).

49. W.Obrowski, Naturwissenschaften, **48**,428 (1961).

50. F.Wald, J.Bullitu, National Technical Information Service, Technical Report AFFDL-TR-73-13 (1973).

51. M.V.Rao, R.N.Anderson,Journal of the Less-Common Metals, **25**,427 (1971).

52. I.Higashi, Y.Takahashi, T.Atoda. **37**,199 (1973).

53. T.Lundstrom and L.E.Tergenius, Journal of the Less-Common Metals, **47**, 23 (1976).

54. F.Lihl, O.Fleichl. Metall, **8**, 11 (1954).

55. K.T.Jacob, Shashank Priya, Yoshio Waseda, Metallurgical and Materials Transactions A, **31**, 2674 (2000).

56. Susan Swapp, University of Wyoming , http://serc.carleton.edu/research_education/geochemsheets/techniques/SEM.html

57. Gorge Mason University, http://www.gmu.edu/departments/SRIF/tutorial/sem/sem.htm

58. Kansas State University, department of Entamology,

http://serc.carleton.edu/research_education/geochemsheets/techniques/SEM.html

59. http://www.kosi.com/Raman_Spectroscopy/rtr-ramantutorial.php?ss=800

60. D.R. Tallant, T.L. Aselage, A.N. Campbell, and D. Emin, *Phys. Rev.* B **40**, 5649   (1989).

61. W. Richter, A. Hausen, and H. Binnenbruch, *Phys. Stat. Sol.* (b) **60**, 461 (1973).

62. www.azom.com/details.asp?ArticleID=3604

63. Barbara L Dutrow, Louisiana State University ,Christine M. Clark, Eastern Michigan
        University
http://serc.carleton.edu/research_education/geochemsheets/techniques/XRD.html

64. C.L. Beckel, M. Yousaf, M.Z. Fuka, S.Y. Raja, and N. Lu, *Phys. Rev.* B **44**, 2535   (1991).

65. N. Vast, S. Baroni, G. Zerah, J.M. Besson, A. Polian, M Grimsditch, and I.C. Chervin, *Phys. Rev. Lett.* **78**, 693 (1997).

66. J. H Buddery, A.J.E Welch, *Nature*, **167**, 362 (1951)